

A Multiscale Analysis Method  
and  
its Application to Mesoscale Rainfall System

Inaugural-Dissertation  
zur  
Erlangung des Doktorgrades  
der Mathematisch-Naturwissenschaftlichen Fakultät  
der Universität zu Köln

vorgelegt von  
Chi Yan Tsui  
aus Hong Kong S.A.R., China

Köln  
2014

Berichtersteller:

Prof. Dr. Y. Shao

Prof. Dr. R. Neggers

Tag der mündlichen Prüfung:

17.10.2014

# Abstract

Heavy rainfall events often occur over southeastern China and the central United States during the summer rainy seasons. The common features of heavy rainfall events in both regions are the low level jets (LLJ) originated from the nearby seas and their associated mesoscale convective systems (MCS). This kind of events has been investigated in terms of synoptic forcing. However, the mechanism of producing rainfall is still unclear as multi-scale interactions are involved.

To better understand the mechanism for the heavy rainfall events, this study develops a multi-scale analysis method and applies it to a rainfall event in southeastern China. A conceptual model for the heavy rainfall system (HRS), is proposed. The HRS consists of a LLJ and an upper level jet (ULJ), MCS and cumulus. The three components are presented based on the observations and analysis in previous studies. These components represent respectively large, middle and small scale motions. Governing equation sets of these three scales are derived by using successive filtering. Cross-scale terms in the resultant equations represent the interactions between the scales.

The proposed mechanism can then be explained by use of three simplified equations, corresponding to the jets (large scale), MCS (middle scale) and cumulus (small scale). The simplified equations are obtained through dimensional analysis and only the terms essential to the MCS are retained. With these equations, it is found that an ageostrophic circulation developed between the jets. LLJ's ageostrophy in the exit region is associated with the vertical mesoscale momentum flux divergence and the deceleration of the jet. Upward momentum transport originated from the cyclonic side of the LLJ reaches the upper atmosphere on the cyclonic side of the ULJ. This momentum transport constitutes the upward branch of the ageostrophic circulation. The downward branch of this circulation is formed by the downward momentum transport from the anti-cyclonic side of the ULJ due to its ageostrophy and it contributes to the momentum flux divergence near the anti-cyclonic side of the LLJ. The mesoscale momentum flux divergence can intensify the jet stream in the entrance region of LLJ. As a result, a closed mesoscale ageostrophic dynamic circulation is formed between the large-scale jets sustaining the LLJ, which in turn keeps supplying large scale moisture for the MCS circulation and small-scale cumuli.

The dynamic circulation can also be strengthened by the thermodynamic processes that occur on meso- to small scales. At the LLJ level, at the location of MCS, the ascent is enhanced due to the increase of buoyancy. The buoyancy is associated with the mesoscale heat flux divergence, and this heat flux divergence is associated with the corresponding counterpart of latent heat. The related mesoscale condensation is contributed by small scale cumulus moisture flux divergence and the MCS itself. A reverse process occurs in the downward branch of the circulation with evaporation. As a result, the whole circulation is strengthened.

A numerical experiment with the Weather Research and Forecasting Model (WRF) was used to verify the aforementioned hypothesis. A heavy rainfall event on 13 June 2008 over Southeastern China was simulated. The model results from the parent and two nested domains with resolutions corresponding to large, middle and small scales were used in this event. To investigate the significance of the terms in the simplified equations, the quantities related to the jets, MCS and cumulus were computed and the terms related to the essential interactions were evaluated. Overall, the analysis results were consistent with the proposed mechanism. An ageostrophic circulation was found between LLJ and ULJ. The ascents were enhanced due to mesoscale latent heat flux divergence, and thus the circulation was strengthened. This mesoscale latent heat flux divergence was contributed by the condensation on the corresponding scale. Cumulus moisture tended to condense on mesoscale and so the small scale latent heat accumulated on mesoscale. The cumulus heat which was vertically transported on mesoscale was insignificant to the mesoscale heat flux divergence.

To sum up, HRS is a collaboration of sub-systems with scales from global to micro. In summer seasons, ULJ migrates southward to the exit region of the LLJ. When the exit regions of both jets are close to each other, the circulation associated with the jets' ageostrophy is triggered. Momentum is transported on mesoscale between the jets, and the LLJ is intensified (weakened) in its entrance (exit) region. The associated ascending motion is enhanced by the mesoscale heat flux divergence above the LLJ level, where the MCS and heavy precipitation are located. Large scale moisture is transported horizontally by LLJ, and vertically transport occurs mainly on small cumulus scale below the jet level and on mesoscale above the jet level.

## Zusammenfassung

Starkregenereignisse treten oft über Südostchina und den mittleren Vereinigten Staaten während der Sommerregenzeit auf. In beiden Regionen beinhalten die Starkregenereignisse einen „low level jet“ (LLJ), herrührend von der nahe gelegenen See, und das damit verbundene mesoskalige konvektive System (MCS). Diese Art von Ereignissen wurde oft auf synoptische Antriebe untersucht. Der Prozess der Regenerzeugung ist jedoch noch immer unverstanden da multiskalige Wechselwirkungen involviert sind.

Um den Mechanismus der Starkregenereignisse besser zu verstehen, wird in dieser Arbeit eine multiskalige Analyseverfahren entwickelt und auf ein Regenereignis in Südostchina angewendet. Ein Begriffsmodell für das Starkregensystem (engl. heavy rainfall system, HRS) wird vorgeschlagen. Das HRS besteht aus einem LLJ und einem „upper level jet“ (ULJ), MCS und Cumulus. Die drei Komponenten werden basierend auf frühere Beobachtungen und Studien vorgestellt und repräsentieren jeweils groß-, mittel- und kleinskalige Bewegungen. Beschreibende Gleichungssysteme dieser drei Skalen wurden durch sukzessive Filterung hergeleitet. Gemischtskalige Terme in den resultierenden Gleichungen repräsentieren die Wechselwirkungen zwischen den Skalen.

Der vorgeschlagene Mechanismus kann somit durch drei vereinfachte Gleichungen beschrieben werden, welche den (großskaligen) Jets, (mittelskaligen) MCS und (kleinskaligen) Cumulus entsprechen. Die Gleichungen wurden dabei durch eine Dimensionsanalyse vereinfacht, und nur die für das MCS wichtigen Terme blieben erhalten. Mit diesen Gleichungen konnte die Entwicklung einer ageostrophischen Zirkulation zwischen den Jets gezeigt werden. Die LLJ-Ageostrophie in der Auslaufsregion ist mit der vertikalen mesoskaligen Impulsflussdivergenz und der Verlangsamung des Jets verbunden. Aufwärts gerichteter Impulstransport rührt von der zyklonischen Seite des LLJ her und erreicht die obere Atmosphäre auf der zyklonalen Seite des ULJ. Dieser Impulstransport bildet den aufwärts gerichteten Zweig der ageostrophischen Zirkulation. Der abwärts gerichtete Zweig wird aufgrund der Ageostrophie von der antizyklonalen Seite des ULJ durch den abwärts gerichteten Impulstransport gebildet und dieser trägt zu der Impulsflussdivergenz nahe der antizyklonalen Seite des LLJ bei. Als Konsequenz wird eine geschlossene mesoskalige ageostrophische dynamische Zirkulation zwischen den großskaligen Jets gebildet, die den LLJ erhält. Der LLJ wiederum stellt im Gegenzug Feuchte von der großen Skalen für die MCS Zirkulation und kleinskaligen Kumuli bereit.

Die dynamische Zirkulation kann auch durch thermodynamische Prozesse verstärkt werden, welche auf Meso- bis kleinen Skalen auftreten. Auf dem LLJ-Niveau, am Ort des MCS, wird der Aufstieg durch die Zunahme des Auftriebs verstärkt. Der Auftrieb wurde mit der mesoskaligen Wärmeflussdivergenz assoziiert, und diese Wärmeflussdivergenz wurde mit dem entsprechendem Gegenstück der latenten Wärme in Zusammenhang gebracht. Die entsprechende mesoskalige Kondensationsrate wird durch die kleinskalige Kumulusfeuchteflussdivergenz und dem MCS selbst beigesteuert. Ein Umkehrprozess tritt am abwärts gerichteten Zweig der Zirkulation mit Verdunstung auf. Als Resultat wird die gesamte Zirkulation verstärkt.

Ein numerisches Experiment mit dem „Weather Research and Forecasting Model“ (WRF) wurde benutzt um die oben genannte Hypothese zu verifizieren. Dazu wurde ein Starkregenereignis am 13. Juni 2008 über Südostchina simuliert. Die Modellergebnisse der Ausgangsdomäne und zweier genesteter Domänen wurden mit Auflösungen entsprechend der großen, mittleren und kleinen Skala verwendet. Um die Signifikanz der Terme in den vereinfachten Gleichungen zu untersuchen, wurden die einzelnen Größen der Jets, MCS und Cumulus berechnet und die Terme der grundlegenden Wechselwirkungen bestimmt. Insgesamt sind die Analyseergebnisse konsistent mit dem vorgeschlagenen Mechanismus. Es wurde eine ageostrophische Zirkulation zwischen dem LLJ und dem ULJ gefunden. Der Aufstieg wurde durch die mesoskalige Latente-Wärme-Flussdivergenz beschleunigt und damit die Zirkulation verstärkt. Diese mesoskalige Latente-Wärme-Flussdivergenz wurde durch Kondensation auf den entsprechenden Skalen erreicht. Cumulusfeuchte kondensierte tendenziell auf der Mesoskala und führte somit zur Akkumulation der kleinskaligen latenten Wärme auf der Mesoskala. Die Cumuluswärme, die auf der Mesoskala vertikal transportiert wurde, war für die mesoskalige Wärmeflussdivergenz nicht signifikant.

Zusammengefasst ist das HRS ein Zusammenschluss von Untersystemen mit globaler bis mikroskopischer Skala. In den Sommermonaten wandert der ULJ südwärts bis zur Auslaufregion des LLJ. Wenn die Auslaufregionen beider Jets nahe beieinander liegen, wird die Zirkulation, die mit der Ageostrophie der Jets zusammenhängt, angeregt. Impuls zwischen den Jets wird auf der Mesoskala transportiert und der LLJ wird in seinem Einzugs- (Auslauf-) Gebiet verstärkt (geschwächt). Die assoziierte aufsteigende Bewegung wird durch die mesoskalige Wärmeflussdivergenz oberhalb des LLJ-Niveaus angeregt, wo sich das MCS und der Starkregen befinden. Horizontaler Transport großskaliger Feuchte wird durch den LLJ realisiert. Vertikaler Transport tritt hauptsächlich auf kleinen Cumuluskalen unterhalb des Jet-Niveaus und auf Mesoskalen oberhalb des Jets auf.

# Table of Contents

<b>1</b>	<b>Introduction.....</b>	<b>1</b>
<b>2</b>	<b>Research Motivation and Review .....</b>	<b>3</b>
2.1	Research Motivation .....	4
2.2	Rainfall System .....	5
2.2.1	Upper level jet and its associated precipitation.....	5
2.2.2	Low level jet .....	7
2.2.3	Mesoscale Convective System.....	8
2.3	Hypothesis of Heavy Rainfall System .....	10
2.4	The Current Issues in Multiscale Analysis.....	12
<b>3</b>	<b>Derivation of Multiscale Equations.....</b>	<b>15</b>
3.1	Total Derivative for Multiscale .....	16
3.1.1	Single value on different scales .....	16
3.1.2	Derivation of general equation.....	19
3.2	Equation Set for Heavy Rainfall System.....	22
3.2.1	Horizontal momentum equation.....	23
3.2.2	Vertical momentum equation.....	29
3.2.3	Conservation of heat .....	33
3.2.4	Conservation of moisture .....	36
3.2.5	Continuity equation.....	39
3.2.6	Equation of state .....	40
<b>4</b>	<b>Theory on Heavy Rainfall System .....</b>	<b>41</b>
4.1	Dynamics Simplification.....	43
4.1.1	Simplification of large scale equation.....	43
4.1.2	Simplification of small scale equation .....	46
4.1.3	Simplification of middle scale equation.....	46
4.2	Thermodynamics Simplification .....	54
4.2.1	Simplification of large scale equation.....	54
4.2.2	Simplification of small scale equation .....	55
4.2.3	Simplification of middle scale equation.....	58
4.3	Physical Interpretation of the Multiscale Heavy Rainfall .....	62
4.3.1	Dynamic circulation.....	63
4.3.2	Thermodynamic circulation .....	65

<b>5</b>	<b>Numerical Experiment for MCS Diagnosis .....</b>	<b>69</b>
5.1	Background.....	70
5.2	Experiment Design .....	70
5.3	Result Analysis .....	72
5.3.1	General pattern .....	72
5.3.2	Diagnosis on the event .....	74
5.4	Conclusions and Discussion .....	91
5.4.1	Evaluation of the dynamic circulation .....	91
5.4.2	Evaluation of thermodynamic circulation .....	92
5.4.3	Evaluation of the MCS.....	93
5.4.4	Conclusion.....	97
<b>6</b>	<b>Summary and Outlook.....</b>	<b>99</b>
<b>7</b>	<b>Appendix .....</b>	<b>105</b>
<b>8</b>	<b>List of Abbreviations .....</b>	<b>110</b>
<b>9</b>	<b>List of Parameters / Constants .....</b>	<b>110</b>
<b>10</b>	<b>List of Symbols.....</b>	<b>111</b>
<b>11</b>	<b>List of Equations .....</b>	<b>117</b>
<b>12</b>	<b>Reference .....</b>	<b>125</b>
<b>13</b>	<b>Acknowledgements .....</b>	<b>129</b>
<b>14</b>	<b>Erklärung .....</b>	<b>131</b>
<b>15</b>	<b>Lebenslauf .....</b>	<b>133</b>



# 1 Introduction

In rainy seasons, heavy rainfall events often occur over southeastern China and central United States. The striking common feature of the heavy rainfall events in both regions is a low level jet (LLJ) which originates from the South China Sea and the Gulf of Mexico, respectively. Apart from the LLJ, some other common features are shared by both cases, such as the southerly characteristics of the LLJs, occurrence of the events in the mid-latitudes, the presence of mesoscale structures etc. These phenomena are often analyzed by using synoptic charts (e.g. Chen et al. 1993), described in term of large scale forcing due to the LLJ existence, the scale of the associated moisture transport and the scale of area where the instability develops.

In this study, this kind of events is considered as an outcome of a system consisting of several components in distinctive scales, which will be referred to as a heavy rainfall system (HRS). As it involves multiscale interactions, the mechanism of producing rainfall is complex and still unclear. The importance of mesoscale convective system (MCS) is hidden when synoptic and micro (cumulus) scales are the study focus. It remains hidden when the events are simulated and the effect of convections are parameterized. A multiscale analysis technique therefore is developed in this study. The interactions between the distinctive scales can be evaluated by taking the advantage of high resolution numerical simulation.

The objectives of this study are:

1. To build a conceptual model of heavy rainfall system;
2. To develop a multiscale analysis method;
3. To establish a simplified equation set with focus on mesoscale, which is specific to heavy rainfall system;
4. To compute the essential interactions among the scales using the simulation result of a heavy rainfall event in Southeastern China, and to explain the mechanism of the involved system;
5. To evaluate the reliability of the proposed mechanism; and
6. To visualize the heavy rainfall system of the event.

This thesis is divided into 6 chapters, including this one. In Chapter 2, the research motivation and relevant literature review will be given and a conceptual model is built. In Chapter 3, equation sets on three distinctive scales, namely, large, middle and small, are derived. In Chapter 4, the equation sets for the three representative scales are simplified to show the bare essential cross-scale interactions. Based on these equation sets, a mechanism of heavy rainfall system is then proposed. In Chapter 5, the analysis method is applied to a numerical simulation of a heavy rainfall event over southeastern China. In the last chapter, the whole work is summarized, conclusion and outlook are also given.

## **2 Research Motivation and Review**

In this chapter, we describe the motivation of the study and the scientific challenges. The chapter consists of four parts. The first part describes the research motivation. In the second part, relevant studies on the components of HRS will be reviewed in order to investigate the interactions among the components. In the third part, a conceptual model of HRS is introduced. The model is constructed based on observations in China and the United States. A hypothesis for the mechanism of HRS is proposed. At last, the difficulties in dealing with multi-scale problems will be outlined.

## 2.1 Research Motivation

During the summer months in the northern hemisphere, LLJs often occur and are accompanied with severe weather conditions. In central United States, LLJ originated from the Gulf of Mexico is associated with the heavy precipitation in the Great Plains. The temperature and moisture fluxes on 24 June 1998 estimated by Wu et al. (1998) showed that LLJ originated from the Gulf of Mexico contributes to positive advections of the quantities in the inland region. Another event, which occurred in 12 June 2008 over southeastern China, showed that heavy rainfall was associated with a southwesterly LLJ [Wu et al. (2011)]. Both events have several features in common:

- 1) Both events happened in summer at mid-latitudes;
- 2) Accompanying the LLJ, a upper level jet (ULJ) in an almost orthogonal alignment existed [Figure 3(c) in Wu et al. (1998) and Figure 10(a) in Wu et al. (2011)];
- 3) The role of LLJ is important, as it was responsible for the transport of moisture;
- 4) Topographical conditions of the coastal regions in both cases are similar. They favour the moisture transport of LLJ from wet to dry region; and
- 5) Both LLJs are southwesterly.

According to the diagnoses of the two events, the HRS is triggered when the ULJ and the LLJ occur at specific positions. By its occurrence in the summer season, it can be deduced that HRS is established once LLJ and ULJ get closer, when ULJ migrates southward while LLJ is persistent and stationary in coastal region during summer seasons.

Precipitation occurs through moist convection, which usually arises as either microscale cumulus, or MCS, or both. Cumuli contribute somewhat to the rainfall. However, the scale of cumulus is too small compared to that of the rainfall area. In contrast, the MCS can explain the scale of the rainfall area. According to observation, for example, the coastal region along the entire southeastern China was effected as stated by Wu et al. (2008). Also, the origin of MCS is the splitting or dying cells of cumuli and the development of MCS is associated with LLJ. By studying the mesoscale convective complex (MCC) over US, Augustine et al. (1991) concluded that the development of MCC is associated with the warm moist air transported by LLJ. Meanwhile, by analyzing the rainfall episodes over Eastern China, Chen et al. (2014) stated that LLJ helps to sustain the conditional unstable layer in rainfall region, and the moisture transported enhances the instability.

As a whole, it can be argued that a HRS consists of at least three components: Jets (ULJ and LLJ), MCS (e.g. MCC), and cumulus. The geometry of these three components trigger the occurrence of heavy rainfall in certain location. As these components are of different scales, a multi-scale analysis method is needed to be developed to establish a hypothesis on the mechanism of this kind of HRS. This is also the main objective of this study.

## **2.2 Rainfall System**

Before proposing the mechanism for HRS, the interactions among the components will be reviewed to interpret the HRS concept.

### **2.2.1 Upper level jet and its associated precipitation**

When looking at the zonally averaged wind field in northern hemisphere, we can find a belt of westerly flow in upper troposphere sweeping along the midlatitudes. Within the belt, there are noticeable narrow maxima located in northern America and east Asia. These narrow streaks, known as jet streaks, are the signature of the ULJs. These jets are permanent feature on synoptic charts, but they shift southward and become weaker during the northern hemispheric summer. Figure 2.1 shows the monthly averaged wind speed for June 2008 at the 200 hPa level in the northern hemisphere. It can be seen that there are two prominent jet streaks embedded in the wind belt, one located over the Eurasia continent (60°E) and one over east Asia (150°E). For the east Asian jet, Kuang et al. (2007) found that its seasonal variation depends on meridional temperature difference. It retreats southward and weakens during the summer season, but appears to be stationary during June – July but with a rapid zonal displacement.

Early in 1952, an event of drought in the United States was documented in two monthly diagnostic reports written by Klein (1952) and Hawkins Jr (1952). Summarizing their findings, they found the drought was associated with the retardation of a polar front due to the strengthening of the westerly jet. This ULJ, in which the wind speed was more than twice as that at 200 hPa, prevented the southward penetration of cold polar air mass. As a result, the forced ascending convective motions were weakened and rainfall reduced. Furthermore, anti-cyclonic flow in the area to the south of the jet, where the central and eastern US located, also suppressed the lifting motions, and took moisture out of the States. On the basis of their diagnoses, Hawkins Jr (1952) attributed the breaking of the drought to the release of moisture in the cyclonic area with the

penetration of the front. Despite their simplicity, these reports give a clue on what the framework of a HRS should consist of. Although the ULJ and its influence are not a complete story, they tell that (westerly) ULJ itself is an essential component in a HRS. The position and the strength of the jet determine the location and intensity of the rainfall.

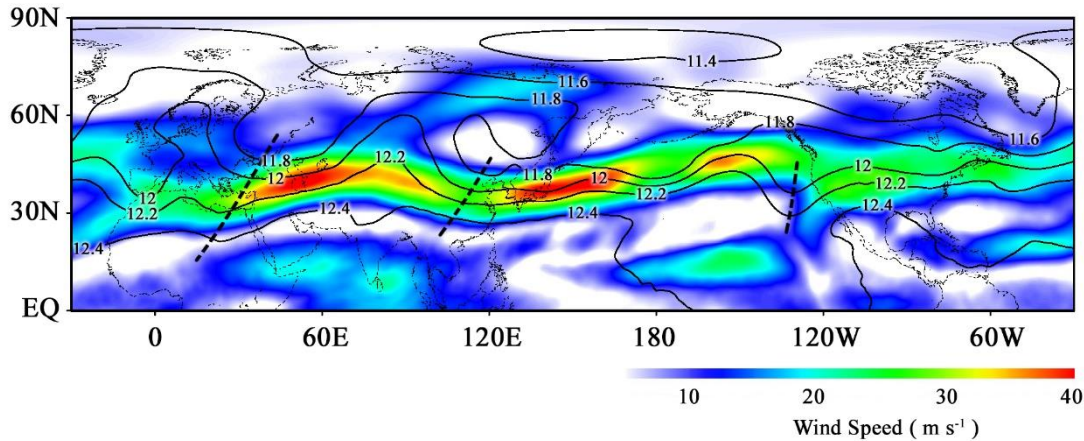


Figure 2.1 ULJs in northern hemisphere in June 2008. Obtained by averaging wind field at 200 hPa level using NCEP FNL Reanalysis data. Wind speed is colour shaded ( $\text{m s}^{-1}$ ), geopotential height in contour (km) and heavy dashed line indicates the axis of trough. Note that all the ULJs are found in the downstream of the troughs.

An idealized structure of the westerly ULJ was introduced by Blackmon (1977), as shown in Figure 2.2. It suggests that ULJ is maintained by a thermal-direct and a thermal-indirect circulation, in the upstream and downstream sections, respectively. The flow accelerates in the upstream section of the jet stream, with a poleward ageostrophic circulation transverse to the jet, while it decelerates downstream with an equatorward ageostrophic transverse circulation. Furthermore, in the exit region, a maximum of convergence of eddy flux of westerly momentum is found to the north of jet stream level, and underneath there is a maximum of eddy heat flux. Through the analysis of the stream function and velocity potential distribution, in the meaning of rotational and divergent circulations, Chen et al. (1988) concluded that the jet is maintained by the balance between kinetic energy associated with ageostrophic flow and the divergence of kinetic energy flux.

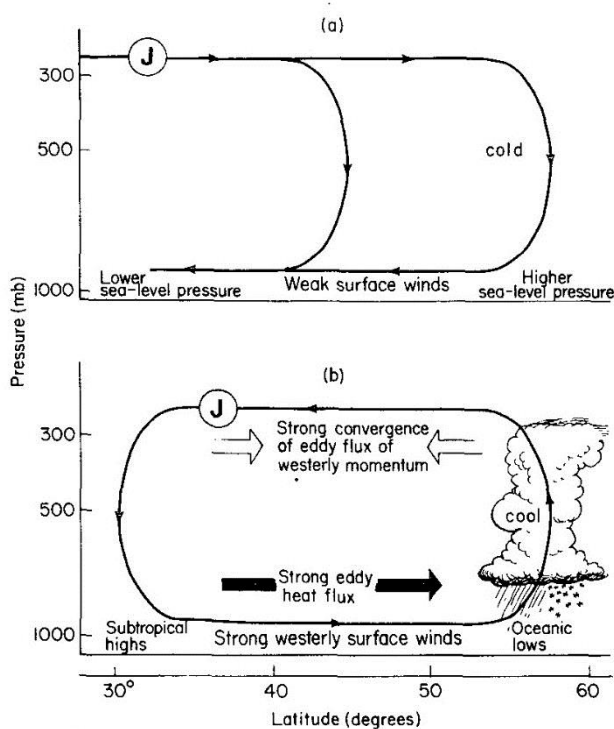


Figure 2.2

Ideal model of ULJ.

(a) Transverse, thermal-directed circulation in the entrance region of a westerly ULJ.

(b) Transverse, thermal-indirected circulation in the exit region of westerly ULJ

[Adopted from Blackmon (1977), Figure 15]

## 2.2.2 Low level jet

When looking on the time-averaged wind field in the lower troposphere in the northern hemisphere, one can observe there are significant meridional variations. A series of jets are located along the coasts of continents over the world and orientate southwesterly in common. The most noticeable jets are located over the Gulf of Mexico in southern US and South China Sea in east Asia. These two LLJs are the typical cases for studying the relationship between the synoptic scale environment and mesoscale convective systems. The southeast Asia LLJ plays an important role during the East Asian Summer Monsoon period. The LLJ, just like ULJ, can be sustained by an ageostrophic circulation [Bonner (1968)]. It also acts as a moisture conveyor belt for the heavy precipitation over southeastern China. Despite the different mechanisms for heavy precipitation in the rainy seasons in different places, numerous studies have presented convincing evidences coincidentally to show that LLJ transports moisture for the development of deep convections associated with storms and heavy precipitations, particularly in the rainy seasons. In Japan, Matsumoto (1972) found that precipitation prefers to occur on the cyclonic side of a LLJ, and the moisture tongue coincides with the jet streak. Similar findings are shown by Matsumoto et al. (1972) and Akiyama (1973). In Northern Taiwan, Chen et al. (1988a, 1988b, 2004) statistically proved that heavy rainfall is closely related to the LLJ's occurrence.

LLJs can be recognized on a synoptic chart by locating the horizontal wind maxima at

vertical levels between 850 – 600 hPa. From the observation, positive vorticity always occurs on the left side of the jet axis while negative on the right side (e.g. Chen et al. 1997). Meanwhile, they are categorized in terms of life cycle, jet streak height and magnitude of wind shears. For example, the “formal” LLJs, which possess a significant diurnal cycle, was distinguished from nocturnal LLJs (Stensrud 1996) and barrier jets (Chen et al. 2004). Obviously, they are distinguished according to the formation mechanisms. In this study, the LLJ in the rainfall system is the formal one which carries the characteristics defined by Stensrud (1996) and Chen et al. (2004):

1. Related to synoptic scale forcing,
2. Significant vertical and horizontal wind shear,
3. Transports warm and moist air from lower latitudes (towards frontal area), and
4. Helps to establish a convectively unstable environment.

To maintain the function of a moisture conveyer belt, the LLJ has to be sustained and thus intensification is needed in its entrance region. One of the intensification mechanisms is associated with ULJ, which is studied by Uccellini et al. (1979). The study proposed that the intensification of the LLJ is the result of its coupling with ULJ. The LLJ which is embedded in the lower branch of an indirect circulation between the jets, is intensified due to the increase of isallobaric wind component. This study later was verified by a numerical experiment carried out by Sortais (1993). The experiment confirmed the coupling of the ULJ and LLJ and demonstrated the formation of a pre-frontal rain band along the cyclonic side of the LLJ. Note that the formation of LLJs is beyond the scope of this study, but the importance and contribution to the HRS. Only the behavior of LLJ and its influences on mesoscale motion over south China are the concerns of this study.

### **2.2.3 Mesoscale Convective System**

The study of mesoscale motions has been started since van der Hoven (1957) found a “gap” (i.e. relative low variance) in energy spectra. The gap appears as a large valley separating the microscale from the macroscale peaks, with scales ranging from a few minutes to few hours temporally, or on the order of 1 to 100 km spatially. These scales of lacking variation are of typical mesoscale processes. Progressive studies on the role of mesoscale motion in spectrum have been done for decades and well-summarized by Atkinson (1981). Mesoscale processes in terms of temporal and spatial scale has been classified by Orlanski (1975). Recent study by Hamilton et al. (2008), using a GCM with high resolution, showed that the upper tropospheric kinetic energy spectrum,



synonym of wind speed variance spectrum in this case, is associated with the space-time variability of rainfall. While with more energy on scales with wave number larger than 10, it comes with higher variability of rainfall, and the authors suggested that there may be a significant role of direct latent heat forcing of mesoscale motions in shaping the energy curve in the mesoscale portion.

Mesoscale systems sometimes exist as clouds in different shapes. They can be recognized in terms of their orientation or appearance. Organized MCSs are often observed in the frontal area. Squall line is one of the examples. Figure 2.3 shows the conceptual structure of a squall line proposed by Biggerstaff et al. (1991). Other systems which appear in circular (irregular) shapes are termed as MCC [Maddox (1980)]. The kinematic and thermodynamic circulation of organized MCS has been well documented. For example, Houze et al. (1989) and Biggerstaff et al. (1991) have proposed isolated structures of organized MCS by doppler-radar and rawinsonde data, respectively.

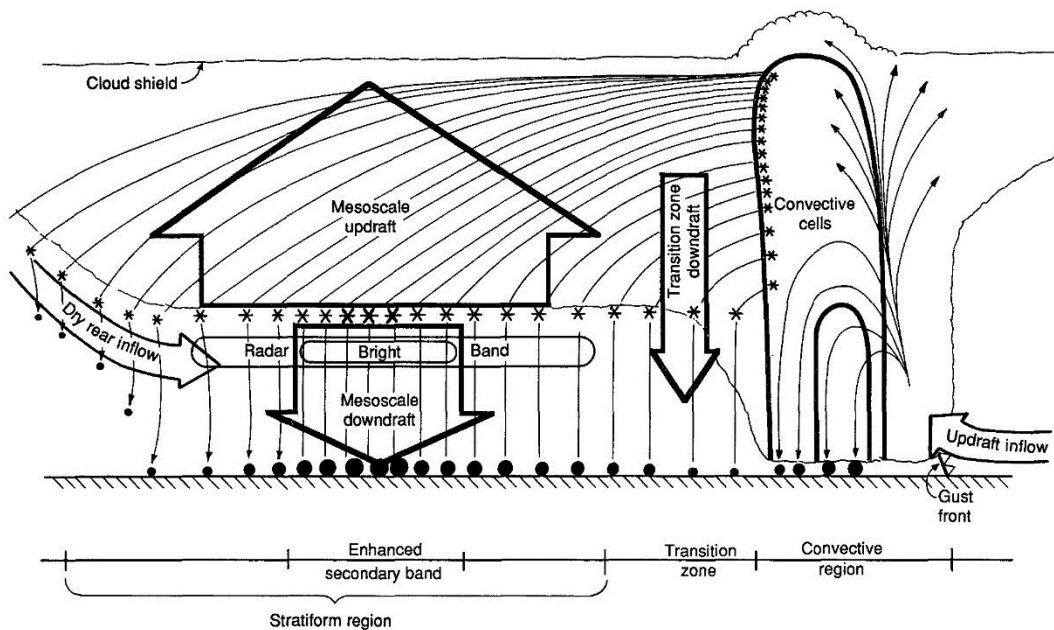


Figure 2.3 A conceptual two-dimensional model for a squall line. Hydrometeor produced by convective cells tends to be transported to the stratiform region. Note that in the stratiform region there is a mesoscale updraft due to the condensation of hydrometeor, while downdraft underneath due to evaporation of precipitation.

[Adopted from Figure 18 of Biggerstaff et al. (1991)]

For those MCS (or MCC) in irregular shape, they are formed loosely in group of cells in an environment with weaker wind shear compared to organized MCS [Emanuel (1994)]. Its lifetime varies from hours to days, and the distribution of updraft region is determined by the nature of the MCCs themselves. Since MCC are regular in properties and features, Maddox (1980) has defined MCC by its size and lifetime using IR temperature instead of its orientations.

Mesoscale motion plays an important role in maintaining the upper jet stream. The close relationship of mean zonal (synoptic) flow and eddy circulation has been deeply revealed by Grotjahn (1993). In short, the synoptic flow is continuous along the latitude circle, while the flow accelerates due to its ageostrophy and constitutes the ascending branch of Hadley cell, another secondary circulation must exist to constrain the flow from “speeding” infinitely. It means that, to preserve the flow continuity, the flow does decelerate. The deceleration is accomplished by the “eddy” motions associated with mid-latitude cells, or “Ferrel cell”. Hence, most ULJs observed are often southwesterly rather than strictly westerly. Severe rainfall or storms are frequently observed on the cyclonic side of the ULJ where the flow decelerates. By temporal filtering, Holopainen (1984) has statistically proved that eddy motion dominates in the storm track region and the energy tends to be drawn from the mean flow to the “synoptic-scale” eddies. This provides an evidence that mesoscale motions are crucial in maintaining ULJs and responsible for the transport of moisture and heat.

Beside the effect on ULJ, MCS also intensifies LLJ. To adjust the geostrophic balance, Chen et al. (1998) showed that a secondary equatorward cross-jet circulation was developed in the exit region of ULJ. Mesoscale convection is found in the pre-frontal region. To feed the air required for the convection in the lower troposphere, a poleward cross-jet circulation was induced beneath the ULJ. LLJ therefore was developed and intensified by the meso-inflow.

### **2.3 Hypothesis of Heavy Rainfall System**

Based on the interactions among the HRS components, a mechanism of HRS is proposed here. The three components, i.e. LLJ and ULJ, MCS, and cumulus are presented schematically in Figure 2.4. The LLJ is assumed to be southerly, while ULJ westerly. MCS is located only on the cyclonic side of both jets, while cumuli are located on the cyclonic side of the LLJ.

The forcing of the large scale jets is geostrophic. When the ULJ migrates southward and is close enough to the LLJ, the jets' ageostrophy could be associated with mesoscale ascent and moisture transport. This phenomena is evidenced by the observations / studies aforementioned. The mesoscale ascent constitutes the upward branch of the ageostrophic circulation where condensation takes place. The latent heat released enhances the instability, which therefore foster the occurrence of heavy precipitation. The downward branch of the circulation is also considered. The mesoscale downdraft intensifies the LLJ in its entrance region, which in turn sustain the moisture transport for the HRS.

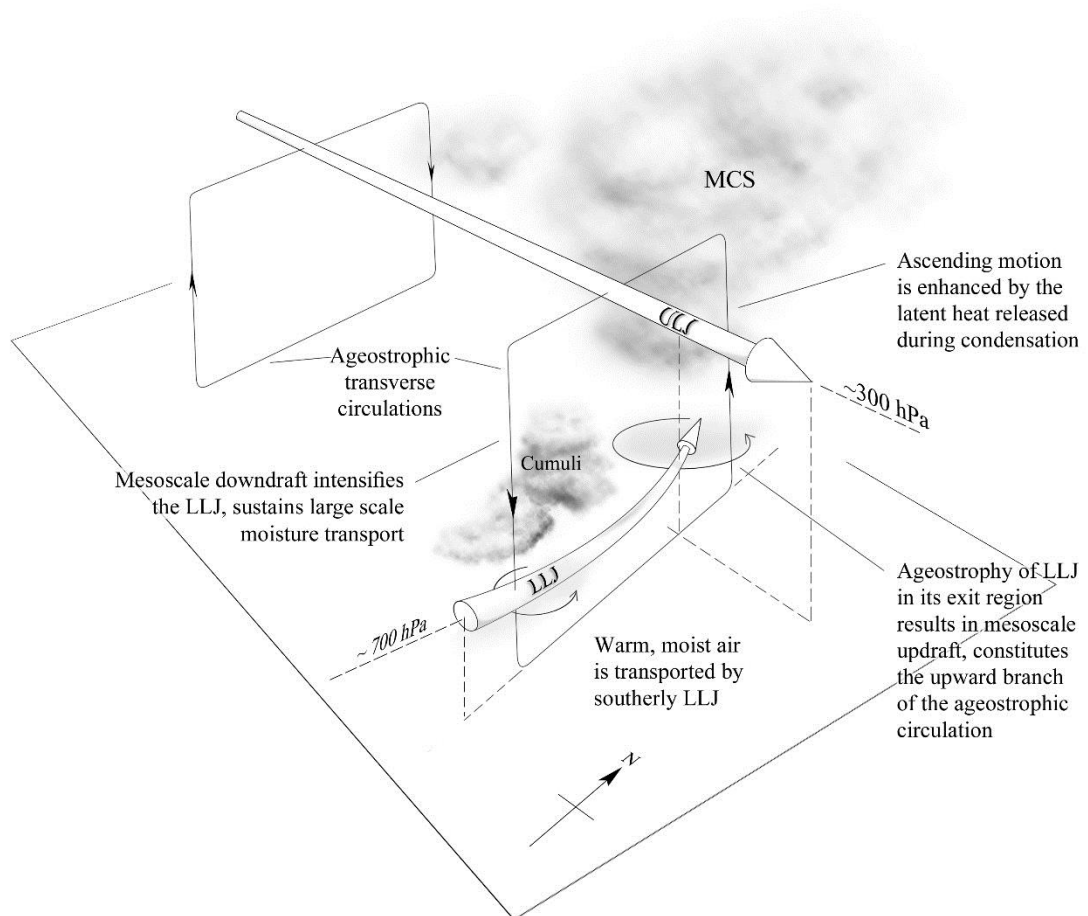


Figure 2.4 A hypothesis on heavy rainfall system mechanism. The dashed lines visualize the relative levels of the jets. Vortexes represent the positive vorticity regions on the jets' cyclonic sides.

The MCS tends to occur in the region with the highest positive vorticity, because positive vorticity with convergence means the presence of upward motion. Note that the MCS also favours cumuli. As mentioned before, MCS is generated by the splitting or dying cells of cumuli in an instable region. Accordingly, cumulus can be formed on the LLJ's cyclonic side, with the positive vorticity decreasing.

In such geometry, the HRS can be maintained in a steady state by the ageostrophy of the jets, and a continuous supply of moisture can be achieved. However, more detailed investigations are needed to get a clearer picture and plot the whole story.

## **2.4 The Current Issues in Multiscale Analysis**

The HRS consists of components in three distinctive scales. These three scales, namely, large, middle and small scales, interact with each other to form a complex sustaining system. These threefold relationships behave in a complicated manner. What makes the situation more challenging is the distinctness of the scales. As shown in Figure 2.5, each component falls on different scale. According to the figure, by the definition given by the Committee of Atmospheric Science of the National Academy (CAS), baroclinic wave (associated with ULJ) is of climatological-synoptic scale, LLJ and squall line (a kind of MCS) are of synoptic-mesoscale [but also can be of meso- $\beta$ -scale proposed by Orlanski (1975)]. Deep convection (a form of cumulus) is of micro-scale. As a whole, the borders of between components' scales obscure the processes in term of space and time, i.e. process with a given spatial scale may be of another temporal scale. In order to distinguish the scale of the components clearly, the scales should be well-defined in the new analysis technique, so that the interaction between components can be estimated. In this study, only spatial scale will be used to avoid confusion.

The heat and moisture transport in the threefold relationship is one of the focuses. However, the existing parameterizations are capable of dealing with one (spatial) sub-scale only, but not two. So, this barrier has to be broken through in the new technique. Although parameterization is a typical strategy to deal with such kind of "sub-scale" problems, only the contribution of the sub-scale motions on the large scale is estimated by the parameterization but not the sub-scale motions themselves.

$L_s \backslash T_s$	1 MONTH $(\beta  L_R )^{-1}$	1 DAY $(f)^{-1}$	1 HOUR $(\frac{g}{\theta} \frac{d\theta}{dz})^{-1/2}$	MINUTE $(\frac{g}{H})^{-1/2} (\frac{L}{U})$	1 SEC	
10,000 Km	STANDING WAVES	ULTRA-LONG WAVES	TIDAL WAVES			MACRO $\alpha$ SCALE
2,000 Km		BAROCLINIC WAVES				MACRO $\beta$ SCALE
200 Km		FRONTS & HURRICANES				MESO $\alpha$ SCALE
20 Km			NOCTURNAL LOW LEVEL JET SQUALL LINES INERTIAL WAVES CLOUD CLUSTERS MTN. & LAKE DISTURBANCES			MESO $\beta$ SCALE
2 Km				THUNDERSTORMS I.G.W. C.A.T. URBAN EFFECTS		MESO $\gamma$ SCALE
200 m				TORNADOES DEEP CONVECTION SHORT GRAVITY WAVES		MICRO $\alpha$ SCALE
20 m				DUST DEVILS THERMALS WAKES		MICRO $\beta$ SCALE
					PLUMES ROUGHNESS TURBULENCE	MICRO $\gamma$ SCALE
C.A.S.	CLIMATOLOGICAL SCALE	SYNOPTIC PLANETARY SCALE	MESO SCALE	MICRO-SCALE		PROPOSED DEFINITION

Figure 2.5 Scale definition of different processes in term of temporal and spatial coverages. [Adopted from Figure 6 of Atkinson (1981), p. 19]

In reality, however, mesoscale convective systems play important role. For example, Zipser (1977) observed the presence of mesoscale downdrafts out of cumulus clusters at the rear part of a squall line. The horizontal scale of these downdrafts was of several hundred kilometers. In these downdraft, convections due to cumuli were suppressed. The observations suggested that, the scales of these meso-structures fall between the synoptic scale and micro- $\alpha$  scale (or “convective” scale), and their mechanism differs from that of cumulus. To complete the picture, one of the solutions was the development of mesoscale parameterization. In this aspect, based on the findings of Zipser et al. (1969, 1977), Leary et al. (1979) proposed a mesoscale parameterization by introducing

an idealized mesoscale system on a larger-scale environment. The idealized system consists of a convective region and an anvil region. Apart from a detrainment to the environment, there is also an entrainment into the anvil region from the convective region. The contribution from convective cumuli is assumed to be included in this idealized model. When the area of anvil region was deducted, the parameterization scheme is simply restored to typical mass-flux approach. However, with this idealized model, the control parameters in the flow of water and heat budgets were based on studied cases, i.e. empirical values, as well as the dimensions of the model itself. Unlike the cumulus parameterization which is initialized by CAPE extent, this parameterization is “compulsory”. The above parameterization tells the importance of mesoscale structure to the large scale environment.

The sub-scale terms that used by parameterization are produced by performing Reynolds Averaging on the large scale governing equations. Two types of are formed, i.e. the averaged and the covariance terms. The averaged term represents the large scale advection while the covariance the effect of sub-scale motion. That is, when performing Reynolds Averaging on the equation, it resolves the motion into averaged and sub-scale only, but not more. Moreover, Reynolds Averaging gives no restriction on the sub-scale. Hence, in principle all the scales which are smaller than that of average can be regarded as “fluctuation” in the averaging and hence reflected by the covariance terms altogether. In the atmosphere, there is no obvious gap among the processes on large, meso-, and convective scales. As a result, Reynolds Averaging is unable to separate the multi-scale process, thereby the definition of ‘sub-scale’ in all parameterization processes are subjective. This problem has been realized by Arakawa (2004) that the definition of “sub-scale” or “sub-grid” varies upon applications. He stated that “... *I have avoided to use the words large-scale processes and small scale processes. This is because those words are not well defined when there is no gap in the spectrum of atmospheric processes ... avoided the words grid scale and sub-grid scale because the concept of parameterization is not unique to a numerical model ...* “. All facts above point out that the traditional strategy is not sufficient enough in dealing with “sub-grid” processes and hence it is not possible to estimate the contribution of the intermediate scale process in a multi-scale system.

In this study, a multi-scale analysis technique is developed. Instead of estimating the large-scale averaged values, synoptic, meso- and convective structures will be resolved with the help of high computation power. The essential interactions between each scale will be clearly illustrated, in order to show the how the jets and cumuli interact with the mesoscale convective system.

### **3 Derivation of Multiscale Equations**

In this section, the governing equations for the HRS are derived. Based on the HRS, each governing equation is required to be derived on three scales in order to describe the components on the corresponding scales.

In the first part, an arbitrary quantity is first decomposed to  $n$  scales, then the general form of total derivative, which is presented in all governing equations, is established for these  $n$  scales by using Reynolds (spatial) Averaging. In the second part, the three scales, i.e. large, middle and small scales, are defined respect to the HRS, and the corresponding governing equations are developed, the corresponding continuity equation and equation of state are also given.

## 3.1 Total Derivative for Multiscale

### 3.1.1 Single value on different scales

Before dealing with specific scales of interest, an expression of a quantity on  $n$ -th scale is needed to be defined. An arbitrary quantity,  $\chi$ , can be decomposed as

$$\chi = \chi^{L1} + \chi^{H1} \quad (3.1)$$

where  $\chi^{L1}$  is the *low-pass* signal of  $\chi$  with a window size of the 1st scale, and  $\chi^{H1}$  is the corresponding *high-pass* signal. In case of Reynolds averaging,  $\chi$  is decomposed to a mean and a perturbation. Then,  $\chi^{L1}$  is processed in the same manner as  $\chi$ , but with a window size of the 2nd scale. This process is shown schematically in Figure 3.1.

For the  $n$ -th scale, we have

$$\chi^{L(n-1)} = \chi^{Ln} + \chi^{Hn} \quad (3.2)$$

This equation states that the low-pass quantity  $\chi^{L(n-1)}$  on  $(n-1)$ -th scale is composed of a low-pass signal  $\chi^{Ln}$  on  $n$ -th scale which acts as a “background”, and a high-pass signal  $\chi^{H(n-1)}$  which is the perturbation with respect to  $\chi^{Ln}$ . If the filtering is simply spatial averaging, the following relationship is satisfied for two dimensional space

$$\chi^{Ln} = \frac{1}{ab} \sum_{i=1}^a \sum_{j=1}^b \chi_{ij}^{L(n-1)}$$

where  $i$  and  $j$  are the indices in the directions of  $x$  and  $y$ , respectively.  $a$  and  $b$  are two positive integers. This implies that the averaged area for the  $n$ -th scale must be  $a \times b$  times that for  $(n-1)$ -th scale. Note that  $a$  and  $b$  can be different on different stage of filtering. Figure 3.2 shows an example on the first 2 stages.  $\chi^{L1}$  is obtained by averaging 4  $\chi$  values, as shown in (a). Then, similarly,  $\chi^{L2}$  is obtained by 4  $\chi^{L1}$  values.



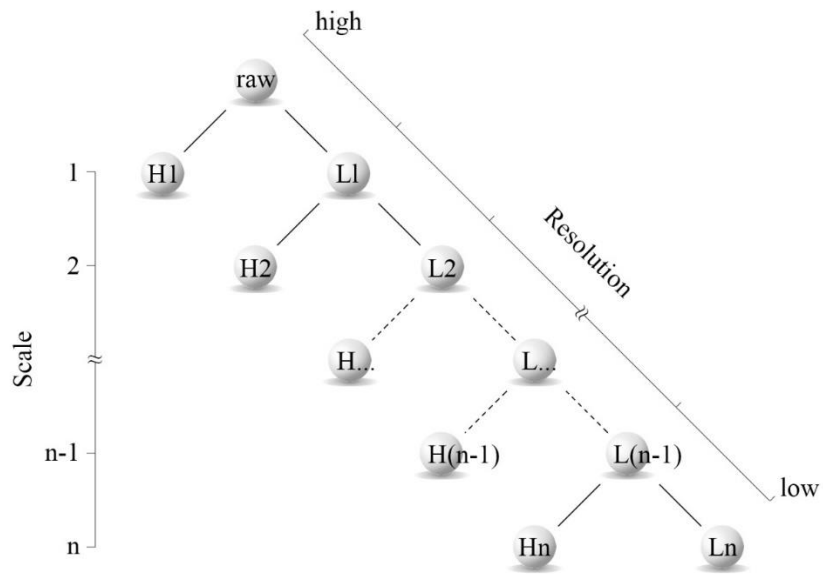


Figure 3.1 Schematic diagram showing how filtering processes on low-pass signals continuously. Note that the resolution of the low-pass signals decreases during the progress.

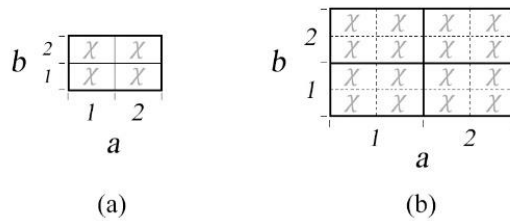


Figure 3.2 Stages of the averaging. Each fine grid represents an area consisted of a quantity  $\chi$ , thick grid the averaging area.  
 (a) Average on the 1st scale  $\chi^{L1}$  when  $a = b = 2$ .  
 (b) Progressive average  $\overline{\chi^{L1L2}}$  when  $a = 2$  and  $b = 2$ , which is an average of 4  $\chi^{L1}$  values.

Likewise, this relationship can be extended to volumetric averaging in 3-dimensional space, i.e.

$$\chi^{Ln} = \frac{1}{abc} \sum_{i=1}^a \sum_{j=1}^b \sum_{k=1}^c \chi_{ijk}^{L(n-1)}$$

where  $k$  and  $c$  resemble  $i$  ( $j$ ) and  $a$  ( $b$ ), but in the vertical direction.

The quantity  $\chi$  can now be expressed in term of  $n$  scales

$$\chi = \chi^{Ln} + \sum_1^n \chi^{Hn} \quad (3.3)$$

It states that  $\chi$  can be considered as a summation of all high-pass signals and a low-pass signal on the largest scale, as shown in Figure 3.1. A quantity with the highest resolution is now considered to be composed of signals with various resolutions. In other words, the signal can be decomposed into infinite components with distinctive resolutions (or frequencies).

### 3.1.2 Derivation of general equation

In order to develop a multi-scale equation system, it is important to examine first the decomposition of the total derivative of a quantity, as it is an essential term in all prognostic equations. If  $\chi$  is conserved, then

$$\frac{\partial \chi}{\partial t} = -\frac{\partial u \chi}{\partial x} - \frac{\partial v \chi}{\partial y} - \frac{\partial w \chi}{\partial z} \quad (3.4)$$

where  $u$ ,  $v$ ,  $w$  are the zonal, meridional, and vertical wind velocities, respectively.

As Eq. (3.1), with  $u$ ,  $v$ , and  $w$  expanded in the same way, it gives

$$\begin{aligned} \frac{\partial(\chi^{L1} + \chi^{H1})}{\partial t} = & -\frac{\partial(u^{L1} + u^{H1})(\chi^{L1} + \chi^{H1})}{\partial x} - \frac{\partial(v^{L1} + v^{H1})(\chi^{L1} + \chi^{H1})}{\partial y} \\ & - \frac{\partial(w^{L1} + w^{H1})(\chi^{L1} + \chi^{H1})}{\partial z} \end{aligned} \quad (3.5)$$

Take an average of the equation above over the 1st scale, the resultant equation is given by

$$\frac{\partial \chi^{L1}}{\partial t} = -\overline{\nabla_h} \cdot \mathbf{v}_h^{L1} \chi^{L1} - \overline{\nabla_h} \cdot \overline{\mathbf{v}_h^{H1} \chi^{H1} L1} - \frac{\partial w^{L1} \chi^{L1}}{\partial z} - \frac{\partial \overline{w^{H1} \chi^{H1} L1}}{\partial z} \quad (3.6)$$

where  $\overline{\nabla_h}$  and  $\mathbf{v}_h$  are horizontal del operator and velocity (vector), respectively, with  $\mathbf{v}_h = \mathbf{u} + \mathbf{v}$

By subtracting (3.6) from (3.5), the tendency of  $\chi^{H1}$  is given by

$$\begin{aligned} \frac{\partial \chi^{H1}}{\partial t} = & -\overline{\nabla_h} \cdot \mathbf{v}_h^{L1} \chi^{H1} - \overline{\nabla_h} \cdot \mathbf{v}_h^{H1} \chi^{L1} - \overline{\nabla_h} \cdot \mathbf{v}_h^{H1} \chi^{H1} + \overline{\nabla_h} \cdot \overline{\mathbf{v}_h^{H1} \chi^{H1} L1} \\ & - \frac{\partial w^{L1} \chi^{H1}}{\partial z} - \frac{\partial w^{H1} \chi^{L1}}{\partial z} - \frac{\partial w^{H1} \chi^{H1}}{\partial z} + \frac{\partial \overline{w^{H1} \chi^{H1} L1}}{\partial z} \end{aligned} \quad (3.7)$$

Eq. (3.6) describes the tendency of  $\chi$  when it is averaged over the 1st scale, while Eq. (3.7) the tendency of  $\chi$ 's perturbation relative to the 1st scale. Following the procedure above, the equations for Scale n can be given as

$$\frac{\partial \chi^{Ln}}{\partial t} = \underbrace{-\vec{\nabla}_h \cdot \mathbf{v}_h^{Ln} \chi^{Ln}}_{\text{I}} - \underbrace{\vec{\nabla}_h \cdot \overline{\sum_1^n \mathbf{v}_h^{Hn} \chi^{Hn Ln}}}_{\text{II}} - \underbrace{\frac{\partial (w^{Ln} \chi^{Ln})}{\partial z}}_{\text{III}} - \underbrace{\frac{\partial (\overline{\sum_1^n w^{Hn} \chi^{Hn Ln}})}{\partial z}}_{\text{IV}} \quad (3.8)$$

where

- Term I represents the storage of average  $\chi$  on Scale n
- Term II the flux divergence associated with horizontal advection due to the motion on the same scale
- Term III the flux divergences associated with perturbations on scales smaller than Scale n
- Term IV, V are the vertical counterpart of II and III, respectively.

Eq. ( 3.8) reveals that the temporal change of a quantity  $\chi$  on Scale n depends on local advectons, as well as the divergence of sub-grid flux divergences.

And the relevant high-pass equation is given as

$$\begin{aligned} \frac{\partial \chi^{Hn}}{\partial t} = & \underbrace{-\vec{\nabla} \cdot \mathbf{v}_h^{Ln} \chi^{Hn}}_{\text{I}} - \underbrace{\vec{\nabla} \cdot \mathbf{v}_h^{Hn} \bar{\chi}^{Ln}}_{\text{II}} - \underbrace{\vec{\nabla} \cdot \mathbf{v}_h^{Hn} \chi^{Hn}}_{\text{III}} \\ & - \underbrace{\vec{\nabla} \cdot \overline{\sum_1^n \mathbf{v}_h^{H(n-1)} \chi^{H(n-1)}}^{L(n-1)}}_{\text{IV}} + \underbrace{\vec{\nabla} \cdot \overline{\sum_1^n \mathbf{v}_h^{Hn} \chi^{Hn Ln}}}_{\text{V}} \\ & - \underbrace{\frac{\partial (v_h^{Ln} \chi^{Hn})}{\partial z}}_{\text{VI}} - \underbrace{\frac{\partial (v_h^{Hn} \chi^{Ln})}{\partial z}}_{\text{VII}} - \underbrace{\frac{\partial (v_h^{Hn} \chi^{Hn})}{\partial z}}_{\text{VIII}} \\ & - \underbrace{\frac{\partial \overline{\sum_1^n w^{H(n-1)} \chi^{H(n-1)}}^{L(n-1)}}{\partial z}}_{\text{IX}} + \underbrace{\frac{\partial \overline{\sum_1^n w^{Hn} \chi^{Hn Ln}}}{\partial z}}_{\text{X}} \end{aligned} \quad (3.9)$$

where

- Term I describes the storage of  $\chi$ 's perturbation relative to Scale n
- Term II flux divergence associated with the advection of  $\chi^{Hn}$  itself brought by the horizontal mean flow  $v_h^{Ln}$
- Term III flux divergence associated with the advection of  $\chi^{Ln}$  brought by the perturbative motion  $v_h^{Hn}$
- Term IV flux divergence due to the perturbations relative to Scale n
- Term V total contribution of all perturbation flux divergences up to Scale n-1

Term VI as Term III in Eq. ( 3.8), but with opposite sign. It reveals the linkage between mean and perturbation on Scale n  
 Term VII – XI are the vertical counterpart of Term II – VI, respectively

Eq. ( 3.9) implies that the temporal change of  $\chi$ 's perturbation on Scale n is attributed to several factors. First, the change is associated with its corresponding averaged motion related to Terms II, III, VII and VIII. In other words, the perturbative quantities ( $\chi^{Hn}$ ,  $\mathbf{v}_h^{Hn}$ , ...) interact with the averaged quantities ( $\chi^{Ln}$ ,  $\mathbf{v}_h^{Ln}$ , ...). Several scenarios can be made for these interactions and will be discussed in the later sections. Second, it depends on the advections on its own scale, i.e. Terms IV and IX. Third, the sum of the sub-grid flux divergences, Terms V and X, which consists of the high-pass divergences of all scales *smaller than* Scale n and averaged over Scale n-1, contribute to the change. Finally, Terms VI and XI, which are the total of averaged effects of all sub-grid flux divergences over Scale n, have the opposite sign to the Term III and V in Eq. ( 3.8). This is not surprising because Eq. ( 3.8) states that Terms III and V contribute to the temporal change of  $\chi^{Ln}$ , as a result, equal amounts should be taken from the change of  $\chi^{Hn}$  in order to maintain the conservation of  $\chi$ . Overall, Eq. ( 3.8) shows how an arbitrary quantity  $\chi$  is deposited with respect to the n scales. On this basis, the interactions among the interested scales will be studied.

### 3.2 Equation Set for Heavy Rainfall System

Beginning with the basic governing equations, and using the outcome from the previous section, equations for three scales, which are the most relevant to the HRS, are developed.

The equations for  $n$ -th scale in the previous section now reaches the 3th scale, i.e. three scales are covered, namely large, middle and small, with superscripts of  $l$ ,  $m$ , and  $s$ , respectively. For each scale, the corresponding low-pass and high-pass signals are given with superscripts  $L$  and  $H$ , respectively. For example,  $u^{Ll}$  represents the low-pass signal ( $L$ ) of zonal wind velocity on large scale ( $l$ ), while  $u^{Hl}$  high-pass signal ( $H$ ) on the corresponding scale ( $l$ ).

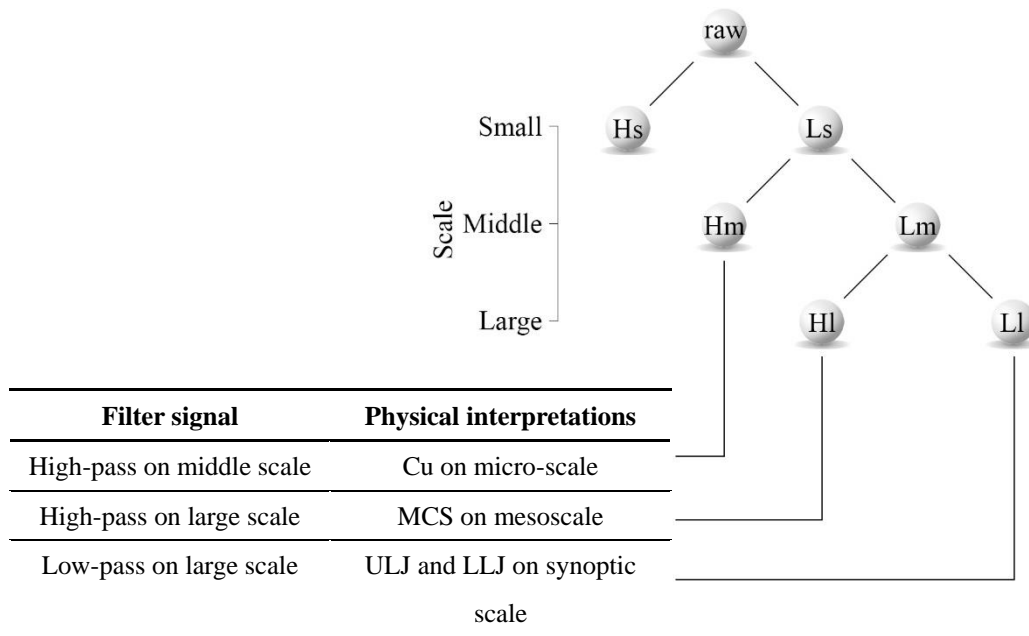


Figure 3.3 A quantity on three representative scales. Signals are assigned to the components in the heavy rainfall system.

As illustrated in Figure 3.3, the components of the heavy rainfall system are assigned to the specific signals. Generally, sub-scale effects are represented by the perturbation on the corresponding mean (average).  $Hl$  is the MCS signal on the large scale mean  $Ll$ ; while  $Hm$  (cumulus) on middle scale mean  $Lm$ .  $Hl$  has a higher resolution than  $Ll$  and is identical to that of  $Lm$ . The situation of  $Hm$  is similar accordingly. In addition, although  $Ls$  and  $Lm$  are not used to describe HRS, they are essential for the computation of  $Hm$  and  $Hl$ , respectively. Based on these notations, the equations for the HRS's components can be developed.

Seven basic equations are needed to describe the dynamics of the atmosphere. These include

- A. Momentum equations (Newton’s second law in 3 dimensions)
- B. Temperature equation (Conservation of energy)
- C. Moisture equation (Conservation of moisture)
- D. Continuity equation (Conservation of mass)
- E. Equation of state

Hereafter, these 7 equations will be termed as an “equation set” for simplicity. Despite the wide coverage in its frequency spectrum, the rainfall system can be simplified to one which composed of only small, middle, and large scales. The motions on each scale are represented by one equation set. It follows that there are 3 equation sets for the representation of the rainfall system. In this sub-chapter, the derivation of equations respect to these 3 scales are given.

### 3.2.1 Horizontal momentum equation

The momentum equation in  $x$ -direction is

$$\underbrace{\frac{\partial u}{\partial t}}_I + \underbrace{\overline{\mathbf{V}}_h \cdot \mathbf{v}_h u}_{II} + \underbrace{\frac{\partial wu}{\partial z}}_{III} = \underbrace{fv}_{IV} - \underbrace{\frac{1}{\rho} \frac{\partial p}{\partial x}}_V + \underbrace{\nu \nabla^2 u}_{VI} \quad (3.10.1)$$

where  $u$  is zonal wind speed;  
 $v$  meridional wind speed;  
 $f$  Coriolis parameter;  
 $\rho$  air density;  
 $p$  pressure; and  
 $\nu$  the kinematic viscosity.

Term I in Eq. ( 3.10.1) is the tendency terms, Term II and III the advection terms in flux form, Term IV the Coriolis term, Term V the pressure gradient forces, and Term VI the viscosity terms representing the influence of viscous stress and is often omitted so as in this study because they are small and only significant on the molecular scale.

A1 Small scale equations

As discussed before,  $u$  can be decomposed as

$$u = u^{Ls} + u^{Hs}$$

Expanding  $u$  in Eq. ( 3.10.1), with viscosity terms omitted, gives

$$\begin{aligned} \frac{\partial(u^{Ls}+u^{Hs})}{\partial t} + \overline{\nabla_h} \cdot (\mathbf{v}_h^{Ls} + \mathbf{v}_h^{Hs})(u^{Ls} + u^{Hs}) + \frac{\partial(w^{Ls}+w^{Hs})(u^{Ls}+u^{Hs})}{\partial z} \\ = f(v^{Ls} + v^{Hs}) - \frac{1}{\rho^{Ls}} \frac{\partial(p^{Ls}+p^{Hs})}{\partial x} \end{aligned} \quad ( 3.11.1 )$$

The equation above describes the full temporal change of horizontal momentum on small scale. The equation is filtered necessarily in order to obtain the equations for the mean momentum and the corresponding perturbation.

Using the outcome of Eq. ( 3.6), and substituting  $\chi$  with  $u$ , the equations for the mean horizontal momentum on small scale are

$$\begin{aligned} \frac{\partial u^{Ls}}{\partial t} = \underbrace{-\overline{\nabla_h} \cdot \mathbf{v}_h^{Ls} u^{Ls}}_{\text{I}} - \underbrace{\overline{\nabla_h} \cdot \mathbf{v}_h^{Hs} u^{Hs}}_{\text{II}} \underbrace{u^{Ls}}_{\text{III}} \\ - \underbrace{\frac{\partial w^{Ls} u^{Ls}}{\partial z}}_{\text{IV}} - \underbrace{\frac{\partial \overline{w^{Hs} u^{Hs}}}{\partial z}}_{\text{V}} + \underbrace{f v^{Ls}}_{\text{VI}} - \underbrace{\frac{1}{\rho^{Ls}} \frac{\partial p^{Ls}}{\partial x}}_{\text{VII}} \end{aligned} \quad ( 3.12.1 )$$

All symbols are as defined before. As these equations are specific to the motions over a small scale. All the terms now have physical meanings related to the small scale mean. Note that the Coriolis term and pressure gradient forces are processed for small scale as follows

Term VI reveals the Coriolis forces, by averaging  $f(v^{Ls} + v^{Hs})$  and  $f(u^{Ls} + u^{Hs})$  over  $Ls$

Term VII the pressure gradient force in zonal / meridional direction, by

$$\text{averaging } \frac{\partial p^{Ls}}{\partial x} + \frac{\partial p^{Hs}}{\partial x} \text{ and } \frac{\partial p^{Ls}}{\partial y} + \frac{\partial p^{Hs}}{\partial y} \text{ over } Ls$$



Accordingly, the perturbation equations for the small scale (i.e. the turbulence equation) is analogous to Eq. ( 3.7)

$$\begin{aligned}
 \frac{\partial u^{Hs}}{\partial t} = & \underbrace{-\overline{\mathbf{v}_h} \cdot \mathbf{v}_h^{Ls} u^{Hs}}_{\text{I}} - \underbrace{\overline{\mathbf{v}_h} \cdot \mathbf{v}_h^{Hs} u^{Ls}}_{\text{II}} - \underbrace{\overline{\mathbf{v}_h} \cdot \mathbf{v}_h^{Hs} u^{Hs}}_{\text{III}} + \underbrace{\overline{\mathbf{v}_h} \cdot \overline{\mathbf{v}_h^{Hs} u^{Hs}}^{Ls}}_{\text{IV}} \\
 & - \underbrace{\frac{\partial w^{Ls} u^{Hs}}{\partial z}}_{\text{VI}} - \underbrace{\frac{\partial w^{Hs} u^{Ls}}{\partial z}}_{\text{VII}} - \underbrace{\frac{\partial w^{Hs} u^{Hs}}{\partial z}}_{\text{VIII}} + \underbrace{\frac{\partial \overline{w^{Hs} u^{Hs}}^{Ls}}{\partial z}}_{\text{IX}} + \underbrace{f v^{Hs}}_{\text{X}} - \underbrace{\frac{1}{\rho^{Ls}} \frac{\partial p^{Hs}}{\partial x}}_{\text{XI}}
 \end{aligned}
 \tag{ 3.13.1 }$$

Term X describes the fluctuation of Coriolis forces on small scale  
 Term XI the perturbation of pressure gradient forces on small scale

Eq. ( 3.12.1) implies that the temporal changes of mean momentums is contributed by the advection of mean motions, averaged advection due to turbulence, Coriolis force and pressure gradient force.

Unlike that of the mean momentum, the temporal change of turbulence, i.e. Term I in Eq. ( 3.13.1), is contributed by the interaction with the corresponding mean motions, advection of the turbulence itself (as well as the averaged counterpart), and the perturbation of Coriolis force and pressure gradient force. The interaction of turbulence and the mean motion will be discussed in detail later. Note that the averaged advection due to turbulence are always in opposite to their counterparts in the corresponding mean equations.

Due to their similarity, the equation corresponding to meridional component  $v$  is not shown here. Hereafter, zonal component  $u$  will be used only as an example to show the derivation of the equations which involve horizontal components. The corresponding meridional equations can be found with codes following the respective zonal equations documented on the List of Equations of this thesis.

A2 Middle scale equations

Similar for middle scale, we have

$$\begin{aligned}
 \frac{\partial u^{Lm}}{\partial t} = & \underbrace{-\overline{\nabla}_h \cdot \mathbf{v}_h^{Lm} u^{Lm}}_{\text{I}} - \underbrace{\overline{\nabla}_h \cdot \mathbf{v}_h^{Hm} u^{Hm Lm}}_{\text{II}} - \underbrace{\overline{\nabla}_h \cdot \mathbf{v}_h^{Hs} u^{Hs Lm}}_{\text{III}} \\
 & - \underbrace{\frac{\partial(\overline{w^{Lm} u^{Lm}})}{\partial z}}_{\text{IV}} - \underbrace{\frac{\partial(\overline{w^{Hm} u^{Hm Lm}})}{\partial z}}_{\text{V}} - \underbrace{\frac{\partial(\overline{w^{Hs} u^{Hs Lm}})}{\partial z}}_{\text{VI}} \\
 & + f v^{Lm} - \frac{1}{\rho^{Lm}} \frac{\partial p^{Lm}}{\partial x} \\
 & \underbrace{\phantom{+ f v^{Lm}}}_{\text{VII}} \quad \underbrace{\phantom{- \frac{1}{\rho^{Lm}} \frac{\partial p^{Lm}}{\partial x}}}_{\text{VIII}} \quad \underbrace{\phantom{- \frac{1}{\rho^{Lm}} \frac{\partial p^{Lm}}{\partial x}}}_{\text{IX}}
 \end{aligned} \tag{3.14.1}$$

where all terms are analogous to the corresponding terms in the equation for small scale mean [Eq. (3.12.1)], except that

Term IV represents the advection of turbulence momentum on middle scale

Term VII as Term IV, but for vertical

And,

$$\begin{aligned}
 \frac{\partial u^{Hm}}{\partial t} = & \underbrace{-\overline{\nabla}_h \cdot \mathbf{v}_h^{Lm} u^{Hm}}_{\text{I}} - \underbrace{\overline{\nabla}_h \cdot \mathbf{v}_h^{Hm} u^{Lm}}_{\text{II}} - \underbrace{\overline{\nabla}_h \cdot \mathbf{v}_h^{Hm} u^{Hm}}_{\text{III}} \\
 & - \underbrace{\overline{\nabla}_h \cdot \mathbf{v}_h^{Hs} u^{Hs Ls}}_{\text{IV}} + \underbrace{\overline{\nabla}_h \cdot \mathbf{v}_h^{Hm} u^{Hm Lm}}_{\text{V}} + \underbrace{\overline{\nabla}_h \cdot \mathbf{v}_h^{Hs} u^{Hs Lm}}_{\text{VI}} \\
 & - \underbrace{\frac{\partial(\overline{w^{Lm} u^{Hm}})}{\partial z}}_{\text{VII}} - \underbrace{\frac{\partial(\overline{w^{Hm} u^{Lm}})}{\partial z}}_{\text{VIII}} - \underbrace{\frac{\partial(\overline{w^{Hm} u^{Hm}})}{\partial z}}_{\text{IX}} \\
 & - \underbrace{\frac{\partial(\overline{w^{Hs} u^{Hs Ls}})}{\partial z}}_{\text{X}} + \underbrace{\frac{\partial(\overline{w^{Hm} u^{Hm Lm}})}{\partial z}}_{\text{XI}} + \underbrace{\frac{\partial(\overline{w^{Hs} u^{Hs Lm}})}{\partial z}}_{\text{XII}} \\
 & + f v^{Hm} - \frac{1}{\rho^{Lm}} \frac{\partial p^{Hm}}{\partial x} \\
 & \underbrace{\phantom{+ f v^{Hm}}}_{\text{XIII}} \quad \underbrace{\phantom{- \frac{1}{\rho^{Lm}} \frac{\partial p^{Hm}}{\partial x}}}_{\text{XIV}} \quad \underbrace{\phantom{- \frac{1}{\rho^{Lm}} \frac{\partial p^{Hm}}{\partial x}}}_{\text{XV}}
 \end{aligned} \tag{3.15.1}$$

All the terms are analogous to the corresponding terms in the equation for middle scale perturbation [Eq. ( 3.13.1)]. It is noteworthy to state that the advection due to turbulence on small scale (Term V and XI) are also factors in the temporal change.

A3 Large scale equations

Likewise,

$$\begin{aligned}
 \frac{\partial u^{Ll}}{\partial t} = & \underbrace{-\vec{\nabla}_h \cdot \mathbf{v}_h^{Ll} \bar{u}^{Ll}}_{\text{I}} - \underbrace{\vec{\nabla}_h \cdot \overline{\mathbf{v}_h^{Hl} u^{Hl}}^{Ll}}_{\text{II}} - \underbrace{\vec{\nabla}_h \cdot \overline{\mathbf{v}_h^{Hm} u^{Hm}}^{Ll}}_{\text{III}} - \underbrace{\vec{\nabla}_h \cdot \overline{\mathbf{v}_h^{Hs} u^{Hs}}^{Ll}}_{\text{IV}} \\
 & - \underbrace{\frac{\partial(\overline{w^{Ll} u^{Ll}})}{\partial z}}_{\text{V}} - \underbrace{\frac{\partial(\overline{w^{Hl} u^{Hl}}^{Ll})}{\partial z}}_{\text{VI}} - \underbrace{\frac{\partial(\overline{w^{Hm} u^{Hm}}^{Ll})}{\partial z}}_{\text{VII}} - \underbrace{\frac{\partial(\overline{w^{Hs} u^{Hs}}^{Ll})}{\partial z}}_{\text{VIII}} \\
 & + \underbrace{f v^{Ll}}_{\text{IX}} - \underbrace{\frac{1}{\rho^{Ll}} \frac{\partial p^{Ll}}{\partial x}}_{\text{X}} \quad \text{XI}
 \end{aligned} \tag{3.16.1}$$

- Term IV shows that the advection of cumulus on large scale
- Term V advection of turbulence on large scale
- Term VIII as IV, but in vertical direction
- Term IX as V, but in vertical direction

And,

$$\begin{aligned}
 \frac{\partial u^{Hl}}{\partial t} = & \underbrace{-\overline{\nabla}_h \cdot \mathbf{v}_h^{Ll} u^{Hl}}_{\text{I}} - \underbrace{\overline{\nabla}_h \cdot \mathbf{v}_h^{Hl} u^{Ll}}_{\text{II}} - \underbrace{\overline{\nabla}_h \cdot \mathbf{v}_h^{Hl} u^{Hl}}_{\text{III}} \\
 & - \underbrace{\overline{\nabla}_h \cdot \overline{\mathbf{v}_h^{Hm} u^{Hm}{}^{Lm}}}_{\text{V}} - \underbrace{\overline{\nabla}_h \cdot \overline{\mathbf{v}_h^{Hs} u^{Hs}{}^{Lm}}}_{\text{VI}} \\
 & + \underbrace{\overline{\nabla}_h \cdot \overline{\mathbf{v}_h^{Hl} u^{Hl}{}^{Ll}}}_{\text{VII}} + \underbrace{\overline{\nabla}_h \cdot \overline{\mathbf{v}_h^{Hm} u^{Hm}{}^{Ll}}}_{\text{VIII}} + \underbrace{\overline{\nabla}_h \cdot \overline{\mathbf{v}_h^{Hs} u^{Hs}{}^{Ll}}}_{\text{IX}} \\
 & - \underbrace{\frac{\partial(w^{Ll} u^{Hl})}{\partial z}}_{\text{X}} - \underbrace{\frac{\partial(w^{Hl} u^{Ll})}{\partial z}}_{\text{XI}} - \underbrace{\frac{\partial(w^{Hl} u^{Hl})}{\partial z}}_{\text{XII}} \\
 & - \underbrace{\frac{\partial \overline{w^{Hm} u^{Hm}{}^{Lm}}}{\partial z}}_{\text{XIII}} - \underbrace{\frac{\partial \overline{w^{Hs} u^{Hs}{}^{Lm}}}{\partial z}}_{\text{XIV}} \\
 & + \underbrace{\frac{\partial \overline{w^{Hl} u^{Hl}{}^{Ll}}}{\partial z}}_{\text{XV}} + \underbrace{\frac{\partial \overline{w^{Hm} u^{Hm}{}^{Ll}}}{\partial z}}_{\text{XVI}} + \underbrace{\frac{\partial \overline{w^{Hs} u^{Hs}{}^{Ll}}}{\partial z}}_{\text{XVII}} \\
 & + f v^{Hl} - \frac{1}{\rho^{Ll}} \frac{\partial p^{Hl}}{\partial x} \\
 & \underbrace{\hspace{10em}}_{\text{XVIII}} \quad \underbrace{\hspace{10em}}_{\text{XIX}}
 \end{aligned} \tag{3.17.1}$$

- Term V describes the advection of cumulus on middle scale
- Term VI as V, but for the advection of turbulence
- Term XIII the vertical form of V
- Term XIV the vertical form of VI

### 3.2.2 Vertical momentum equation

The derivation of multi-scale vertical momentum equations is identical to those of horizontal, except the addition of a buoyancy term which is crucial in vertical motions.

#### B1 Small scale equations

Starts with the vertical momentum equation

$$\frac{\partial w}{\partial t} = -\vec{\nabla} \cdot \mathbf{v}_h w - \frac{\partial w^2}{\partial z} - \frac{1}{\rho} \frac{\partial p}{\partial z} - g \quad (3.18)$$

where  $w$  is vertical wind speed,  
 $\rho$  is air density, and  
 $g$  is the acceleration due to gravity

and

$$\begin{aligned} w &= w^{Ls} + w^{Hs} \\ \rho &= \rho^{Ls} + \rho^{Hs} \end{aligned}$$

Expanding Eq. (3.18) and multiplying with a factor of  $\rho^{Ls} + \rho^{Hs}$ , then divided by  $\rho^{Ls}$ , it gives

$$\begin{aligned} \left(1 + \frac{\rho^{Hs}}{\rho^{Ls}}\right) \frac{\partial(w^{Ls} + w^{Hs})}{\partial t} = & \\ - \left(1 + \frac{\rho^{Hs}}{\rho^{Ls}}\right) \vec{\nabla} \cdot (\mathbf{v}_h^{Ls} w^{Ls} + \mathbf{v}_h^{Ls} w^{Hs} + \mathbf{v}_h^{Hs} w^{Ls} + \mathbf{v}_h^{Hs} w^{Hs}) & \\ - \left(1 + \frac{\rho^{Hs}}{\rho^{Ls}}\right) \frac{\partial(w^{Ls} w^{Ls} + w^{Ls} w^{Hs} + w^{Hs} w^{Ls} + w^{Hs} w^{Hs})}{\partial z} & \\ - \frac{1}{\rho^{Ls}} \frac{\partial(p^{Ls} + p^{Hs})}{\partial z} - \left(1 + \frac{\rho^{Hs}}{\rho^{Ls}}\right) g & \end{aligned}$$

Assuming that the density's perturbation  $\frac{\rho^{Hs}}{\rho^{Ls}}$  is negligible, hence all the terms with the factor of  $\frac{\rho^{Hs}}{\rho^{Ls}}$  vanish. However, the term  $\left(1 + \frac{\rho^{Hs}}{\rho^{Ls}}\right) g$  retains because its order is comparable with other advection terms associated with the mean motions.

This gives a full equation describing the small scale vertical motion.

$$\begin{aligned} \frac{\partial w^{Ls+w^{Hs}}}{\partial t} = & -\vec{\nabla} \cdot (\mathbf{v}_h^{Ls} w^{Ls} + \mathbf{v}_h^{Ls} w^{Hs} + \mathbf{v}_h^{Hs} w^{Ls} + \mathbf{v}_h^{Hs} w^{Hs}) \\ & - \frac{\partial(w^{Ls} w^{Ls} + w^{Ls} w^{Hs} + w^{Hs} w^{Ls} + w^{Hs} w^{Hs})}{\partial z} \\ & - \frac{1}{\rho^{Ls}} \frac{\partial(p^{Ls} + p^{Hs})}{\partial z} - \left(1 + \frac{\rho^{Hs}}{\rho^{Ls}}\right) g \end{aligned} \quad (3.19)$$

Using the outcome of Eq. (3.7), the equation of vertical momentum perturbation for small scale is given as follow

$$\begin{aligned} \frac{\partial w^{Hs}}{\partial t} = & \underbrace{-\vec{\nabla}_h \cdot \mathbf{v}_h^{Ls} w^{Hs}}_{\text{I}} - \underbrace{\vec{\nabla}_h \cdot \mathbf{v}_h^{Hs} w^{Ls}}_{\text{II}} - \underbrace{\vec{\nabla}_h \cdot \mathbf{v}_h^{Hs} w^{Hs}}_{\text{III}} + \underbrace{\vec{\nabla}_h \cdot \overline{\mathbf{v}_h^{Hs} w^{Hs}}^{Ls}}_{\text{IV}} \\ & - \underbrace{\frac{\partial w^{Ls} w^{Hs}}{\partial z}}_{\text{VI}} - \underbrace{\frac{\partial w^{Hs} w^{Ls}}{\partial z}}_{\text{VII}} - \underbrace{\frac{\partial w^{Hs} w^{Hs}}{\partial z}}_{\text{VIII}} + \underbrace{\frac{\partial \overline{w^{Hs} w^{Hs}}^{Ls}}{\partial z}}_{\text{IX}} \\ & - \underbrace{\frac{1}{\rho^{Ls}} \frac{\partial p^{Hs}}{\partial z}}_{\text{X}} - \underbrace{\frac{\rho^{Hs}}{\rho^{Ls}} g}_{\text{XI}} \end{aligned} \quad (3.20)$$

All terms above are analogous to the corresponding equations for horizontal momentum on small scale, except

Term XI describes the buoyancy effect due to the perturbation in density

B2 Middle scale equations

Similarly, we have

$$\begin{aligned}
 \frac{\partial w^{Hm}}{\partial t} = & \underbrace{-\overline{\nabla}_h \cdot \overline{\mathbf{v}}_h^{Lm} w^{Hm}}_{\text{I}} - \underbrace{\overline{\nabla}_h \cdot \mathbf{v}_h^{Hm} \overline{w}^{Lm}}_{\text{II}} - \underbrace{\overline{\nabla}_h \cdot \mathbf{v}_h^{Hm} w^{Hm}}_{\text{III}} \\
 & - \underbrace{\overline{\nabla}_h \cdot \overline{\mathbf{v}}_h^{Hs} \overline{w}^{Hs^{Ls}}}_{\text{V}} + \underbrace{\overline{\nabla}_h \cdot \mathbf{v}_h^{Hm} \overline{w}^{Hm^{Lm}}}_{\text{VI}} + \underbrace{\overline{\nabla}_h \cdot \overline{\mathbf{v}}_h^{Hs} \overline{w}^{Hs^{Lm}}}_{\text{VII}} \\
 & - \underbrace{\frac{\partial(\overline{w}^{Lm} w^{Hm})}{\partial z}}_{\text{VIII}} - \underbrace{\frac{\partial(w^{Hm} \overline{w}^{Lm})}{\partial z}}_{\text{IX}} - \underbrace{\frac{\partial(w^{Hm} w^{Hm})}{\partial z}}_{\text{X}} \\
 & - \underbrace{\frac{\partial \overline{w}^{Hs} \overline{w}^{Hs^{Ls}}}{\partial z}}_{\text{XI}} + \underbrace{\frac{\partial \overline{w}^{Hm} \overline{w}^{Hm^{Lm}}}{\partial z}}_{\text{XII}} + \underbrace{\frac{\partial \overline{w}^{Hs} \overline{w}^{Hs^{Lm}}}{\partial z}}_{\text{XIII}} \\
 & - \underbrace{\frac{1}{\rho^{Lm}} \frac{\partial p^{Hm}}{\partial z}}_{\text{XIV}} - \underbrace{\frac{\rho^{Hm}}{\rho^{Lm}} \mathbf{g}}_{\text{XV}}
 \end{aligned} \tag{3.21}$$

## B3 Large scale equations

Likewise,

$$\begin{aligned}
 \frac{\partial w^{Ll}}{\partial t} = & \underbrace{-\vec{\nabla}_h \cdot \mathbf{v}_h^{Ll} w^{Ll}}_{\text{I}} - \underbrace{\vec{\nabla}_h \cdot \overline{\mathbf{v}_h^{Hl} w^{HlLl}}}_{\text{II}} - \underbrace{\vec{\nabla}_h \cdot \overline{\mathbf{v}_h^{Hm} w^{HmLl}}}_{\text{III}} - \underbrace{\vec{\nabla}_h \cdot \overline{\mathbf{v}_h^{Hs} w^{HsLl}}}_{\text{IV}} \\
 & - \underbrace{\frac{\partial(\overline{w^{Ll} w^{Ll}})}{\partial z}}_{\text{VI}} - \underbrace{\frac{\partial(\overline{w^{Hl} w^{HlLl}})}{\partial z}}_{\text{VII}} - \underbrace{\frac{\partial(\overline{w^{Hm} w^{HmLl}})}{\partial z}}_{\text{VIII}} - \underbrace{\frac{\partial(\overline{w^{Hs} w^{HsLl}})}{\partial z}}_{\text{IX}} \\
 & - \underbrace{\frac{1}{\rho^{Ll}} \frac{\partial p^{Ll}}{\partial z}}_{\text{X}} - \underbrace{g}_{\text{XI}}
 \end{aligned} \tag{3.22}$$

$$\begin{aligned}
 \frac{\partial w^{Hl}}{\partial t} = & \underbrace{-\vec{\nabla}_h \cdot \mathbf{v}_h^{Ll} w^{Hl}}_{\text{I}} - \underbrace{\vec{\nabla}_h \cdot \mathbf{v}_h^{Hl} w^{Ll}}_{\text{II}} - \underbrace{\vec{\nabla}_h \cdot \mathbf{v}_h^{Hl} w^{Hl}}_{\text{III}} \\
 & - \underbrace{\vec{\nabla}_h \cdot \overline{\mathbf{v}_h^{Hm} w^{HmLm}}}_{\text{V}} - \underbrace{\vec{\nabla}_h \cdot \overline{\mathbf{v}_h^{Hs} w^{HsLm}}}_{\text{VI}} \\
 & + \underbrace{\vec{\nabla}_h \cdot \overline{\mathbf{v}_h^{Hl} w^{HlLl}}}_{\text{VII}} + \underbrace{\vec{\nabla}_h \cdot \overline{\mathbf{v}_h^{Hm} w^{HmLl}}}_{\text{VIII}} + \underbrace{\vec{\nabla}_h \cdot \overline{\mathbf{v}_h^{Hs} w^{HsLl}}}_{\text{IX}} \\
 & - \underbrace{\frac{\partial(\overline{w^{Ll} w^{Hl}})}{\partial z}}_{\text{X}} - \underbrace{\frac{\partial(\overline{w^{Hl} w^{Ll}})}{\partial z}}_{\text{XI}} - \underbrace{\frac{\partial(\overline{w^{Hl} w^{Hl}})}{\partial z}}_{\text{XII}} \\
 & - \underbrace{\frac{\partial(\overline{w^{Hm} w^{HmLm}})}{\partial z}}_{\text{XIII}} - \underbrace{\frac{\partial(\overline{w^{Hs} w^{HsLm}})}{\partial z}}_{\text{XIV}} \\
 & + \underbrace{\frac{\partial(\overline{w^{Hl} w^{HlLl}})}{\partial z}}_{\text{XV}} + \underbrace{\frac{\partial(\overline{w^{Hm} w^{HmLl}})}{\partial z}}_{\text{XVI}} + \underbrace{\frac{\partial(\overline{w^{Hs} w^{HsLl}})}{\partial z}}_{\text{XVII}} \\
 & - \underbrace{\frac{1}{\rho^{Ll}} \frac{\partial p^{Hl}}{\partial z}}_{\text{XVIII}} - \underbrace{\frac{\rho^{Hl}}{\rho^{Ll}} g}_{\text{XIX}}
 \end{aligned} \tag{3.23}$$



### 3.2.3 Conservation of heat

Following the previous routine, the equations regarding the conservation of heat can be derived as below

*C1 Small scale equations*

$$\begin{aligned}
 \frac{\partial \theta^{Ls}}{\partial t} = & \underbrace{-\overline{\nabla}_h \cdot \mathbf{v}_h^{Ls} \theta^{Ls}}_{\text{I}} - \underbrace{\overline{\nabla}_h \cdot \mathbf{v}_h^{Hs} \theta^{Hs}}_{\text{II}} \\
 & - \underbrace{\frac{\partial \overline{w^{Ls} \theta^{Ls}}}{\partial z}}_{\text{IV}} - \underbrace{\frac{\partial \overline{w^{Hs} \theta^{Hs}}}{\partial z}}_{\text{V}} - \underbrace{\frac{1}{\rho^{Ls} C_p} (\nabla \cdot Q^{Ls})}_{\text{VI}} - \underbrace{\frac{L_p e^{Ls}}{\rho^{Ls} C_p}}_{\text{VII}}
 \end{aligned} \tag{3.24}$$

The filtering related to the terms with  $\theta$  are analogous to those in the momentum equations aforementioned. Term VI describes the spatial change of energy due to net radiation, where  $C_p$  is the specific heat capacity approximately equals to that for dry air  $C_{pd} = 1004.67 \text{ J kg}^{-1} \text{ K}^{-1}$ , by  $C_p = C_{pd}(1 + 0.84q)$ .  $Q [\text{J m}^{-2} \text{ s}^{-1}]$  is the net radiation rate which is directional dependent, with  $\nabla$  a three dimensional del operator. Term VII shows the contribution associated with the phase change of hydrometeors.  $L_v [\text{J kg}^{-1}]$  is the latent heat of water depending on phase change,  $e [\text{kg m}^3 \text{ s}^{-1}]$  net condensation / evaporation rate.

$$\begin{aligned}
 \frac{\partial \theta^{Hs}}{\partial t} = & \underbrace{-\overline{\nabla}_h \cdot \mathbf{v}_h^{Ls} \theta^{Hs}}_{\text{I}} - \underbrace{\overline{\nabla}_h \cdot \mathbf{v}_h^{Hs} \theta^{Ls}}_{\text{II}} - \underbrace{\overline{\nabla}_h \cdot \mathbf{v}_h^{Hs} \theta^{Hs}}_{\text{III}} + \underbrace{\overline{\nabla}_h \cdot \mathbf{v}_h^{Hs} \theta^{Hs}}_{\text{IV}} \\
 & - \underbrace{\frac{\partial \overline{w^{Ls} \theta^{Hs}}}{\partial z}}_{\text{VI}} - \underbrace{\frac{\partial \overline{w^{Hs} \theta^{Ls}}}{\partial z}}_{\text{VII}} - \underbrace{\frac{\partial \overline{w^{Hs} \theta^{Hs}}}{\partial z}}_{\text{VIII}} + \underbrace{\frac{\partial \overline{w^{Hs} \theta^{Hs}}}{\partial z}}_{\text{IX}} \\
 & - \underbrace{\frac{1}{\rho^{Ls} C_p} (\nabla \cdot Q^{Hs})}_{\text{X}} - \underbrace{\frac{L_p e^{Hs}}{\rho^{Ls} C_p}}_{\text{XI}}
 \end{aligned} \tag{3.25}$$

Term X reveals the contribution due to the perturbation of net radiation on small scale, while Term XI reflects the effect by the phase change of hydrometeors due to the perturbation of net evaporation rate. The rest of the terms are analogous to the corresponding equations.

## C2 Middle scale equation

Similarly, we have

$$\begin{aligned}
 \frac{\partial \theta^{Lm}}{\partial t} &= \underbrace{-\vec{\nabla}_h \cdot \mathbf{v}_h^{Lm} \theta^{Lm}}_{\text{I}} - \underbrace{\vec{\nabla}_h \cdot \overline{\mathbf{v}_h^{Hm} \theta^{Hm} Lm}}_{\text{II}} - \underbrace{\vec{\nabla}_h \cdot \overline{\mathbf{v}_h^{Hs} \theta^{Hs} Lm}}_{\text{III}} \\
 &\quad - \underbrace{\frac{\partial(\overline{w^{Lm} \theta^{Lm}})}{\partial z}}_{\text{V}} - \underbrace{\frac{\partial(\overline{w^{Hm} \theta^{Hm} Lm})}{\partial z}}_{\text{VI}} - \underbrace{\frac{\partial(\overline{w^{Hs} \theta^{Hs} Lm})}{\partial z}}_{\text{VII}} \\
 &\quad - \underbrace{\frac{1}{\rho^{Lm} C_p} (\nabla \cdot Q^{Lm})}_{\text{VIII}} - \underbrace{\frac{L_v e^{Lm}}{\rho^{Lm} C_p}}_{\text{IX}}
 \end{aligned} \tag{3.26}$$

And

$$\begin{aligned}
 \frac{\partial \theta^{Hm}}{\partial t} &= \underbrace{-\vec{\nabla}_h \cdot \mathbf{v}_h^{Lm} \theta^{Hm}}_{\text{I}} - \underbrace{\vec{\nabla}_h \cdot \mathbf{v}_h^{Hm} \theta^{Lm}}_{\text{II}} - \underbrace{\vec{\nabla}_h \cdot \mathbf{v}_h^{Hm} \theta^{Hm}}_{\text{III}} \\
 &\quad - \underbrace{\vec{\nabla}_h \cdot \overline{\mathbf{v}_h^{Hs} \theta^{Hs} Ls}}_{\text{V}} + \underbrace{\vec{\nabla}_h \cdot \overline{\mathbf{v}_h^{Hm} \theta^{Hm} Lm}}_{\text{VI}} + \underbrace{\vec{\nabla}_h \cdot \overline{\mathbf{v}_h^{Hs} \theta^{Hs} Lm}}_{\text{VII}} \\
 &\quad - \underbrace{\frac{\partial(\overline{w^{Lm} \theta^{Hm}})}{\partial z}}_{\text{VIII}} - \underbrace{\frac{\partial(\overline{w^{Hm} \theta^{Lm}})}{\partial z}}_{\text{IX}} - \underbrace{\frac{\partial(\overline{w^{Hm} \theta^{Hm}})}{\partial z}}_{\text{X}} \\
 &\quad - \underbrace{\frac{\partial \overline{w^{Hs} \theta^{Hs} Ls}}{\partial z}}_{\text{XI}} + \underbrace{\frac{\partial \overline{w^{Hm} \theta^{Hm} Lm}}{\partial z}}_{\text{XII}} + \underbrace{\frac{\partial \overline{w^{Hs} \theta^{Hs} Lm}}{\partial z}}_{\text{XIII}} \\
 &\quad - \underbrace{\frac{1}{\rho^{Lm} C_p} (\nabla \cdot Q^{Hm})}_{\text{XIV}} - \underbrace{\frac{L_v e^{Hm}}{\rho^{Lm} C_p}}_{\text{XV}}
 \end{aligned} \tag{3.27}$$

## C3 Large scale equation

Following the routine, we have

$$\begin{aligned}
 \frac{\partial \theta^{Ll}}{\partial t} = & \underbrace{-\overline{\nabla}_h \cdot \mathbf{v}_h^{Ll} \theta^{Ll}}_{\text{I}} - \underbrace{\overline{\nabla}_h \cdot \mathbf{v}_h^{Hl} \theta^{Hl}}_{\text{II}} - \underbrace{\overline{\nabla}_h \cdot \mathbf{v}_h^{Hm} \theta^{Hm}}_{\text{III}} - \underbrace{\overline{\nabla}_h \cdot \mathbf{v}_h^{Hs} \theta^{Hs}}_{\text{IV}} \\
 & - \underbrace{\frac{\partial(\overline{w^{Ll} \theta^{Ll}})}{\partial z}}_{\text{VI}} - \underbrace{\frac{\partial(\overline{w^{Hl} \theta^{Hl}})}{\partial z}}_{\text{VII}} - \underbrace{\frac{\partial(\overline{w^{Hm} \theta^{Hm}})}{\partial z}}_{\text{VIII}} - \underbrace{\frac{\partial(\overline{w^{Hs} \theta^{Hs}})}{\partial z}}_{\text{IX}} \\
 & - \underbrace{\frac{1}{\rho^{Ll} C_p} (\nabla \cdot Q^{Ll})}_{\text{X}} - \underbrace{\frac{L_v e^{Ll}}{\rho^{Ll} C_p}}_{\text{XI}}
 \end{aligned} \tag{3.28}$$

$$\begin{aligned}
 \frac{\partial \theta^{Hl}}{\partial t} = & \underbrace{-\overline{\nabla}_h \cdot \mathbf{v}_h^{Ll} \theta^{Hl}}_{\text{I}} - \underbrace{\overline{\nabla}_h \cdot \mathbf{v}_h^{Hl} \theta^{Ll}}_{\text{II}} - \underbrace{\overline{\nabla}_h \cdot \mathbf{v}_h^{Hl} \theta^{Hl}}_{\text{III}} \\
 & - \underbrace{\overline{\nabla}_h \cdot \mathbf{v}_h^{Hm} \theta^{Hm}^{Lm}}_{\text{V}} - \underbrace{\overline{\nabla}_h \cdot \mathbf{v}_h^{Hs} \theta^{Hs}^{Lm}}_{\text{VI}} \\
 & + \underbrace{\overline{\nabla}_h \cdot \mathbf{v}_h^{Hl} \theta^{Hl}^{Ll}}_{\text{VII}} + \underbrace{\overline{\nabla}_h \cdot \mathbf{v}_h^{Hm} \theta^{Hm}^{Ll}}_{\text{VIII}} + \underbrace{\overline{\nabla}_h \cdot \mathbf{v}_h^{Hs} \theta^{Hs}^{Ll}}_{\text{IX}} \\
 & - \underbrace{\frac{\partial(\overline{w^{Ll} \theta^{Hl}})}{\partial z}}_{\text{X}} - \underbrace{\frac{\partial(\overline{w^{Hl} \theta^{Ll}})}{\partial z}}_{\text{XI}} - \underbrace{\frac{\partial(\overline{w^{Hl} \theta^{Hl}})}{\partial z}}_{\text{XII}} \\
 & - \underbrace{\frac{\partial(\overline{w^{Hm} \theta^{Hm}^{Lm}})}{\partial z}}_{\text{XIII}} - \underbrace{\frac{\partial(\overline{w^{Hs} \theta^{Hs}^{Lm}})}{\partial z}}_{\text{XIV}} \\
 & + \underbrace{\frac{\partial(\overline{w^{Hl} \theta^{Hl}^{Ll}})}{\partial z}}_{\text{XV}} + \underbrace{\frac{\partial(\overline{w^{Hm} \theta^{Hm}^{Ll}})}{\partial z}}_{\text{XVI}} + \underbrace{\frac{\partial(\overline{w^{Hs} \theta^{Hs}^{Ll}})}{\partial z}}_{\text{XVII}} \\
 & - \underbrace{\frac{1}{\rho^{Ll} C_p} (\nabla \cdot Q^{Hl})}_{\text{XVIII}} - \underbrace{\frac{L_v e^{Hl}}{\rho^{Ll} C_p}}_{\text{XIX}}
 \end{aligned} \tag{3.29}$$

### 3.2.4 Conservation of moisture

The derivation of these equations is identical to those in the previous part by taking  $\theta$  as  $q$ .

*D1 Small scale equation*

$$\begin{aligned}
 \frac{\partial q^{Ls}}{\partial t} = & \underbrace{-\vec{\nabla}_h \cdot \mathbf{v}_h^{Ls} q^{Ls}}_{\text{I}} - \underbrace{\vec{\nabla}_h \cdot \overline{\mathbf{v}_h^{Hs} q^{Hs}}^{Ls}}_{\text{III}} \\
 & - \underbrace{\frac{\partial w^{Ls} q^{Ls}}{\partial z}}_{\text{IV}} - \underbrace{\frac{\partial \overline{w^{Hs} q^{Hs}}^{Ls}}{\partial z}}_{\text{V}} - \underbrace{\frac{S^{Ls}}{\rho^{Ls}}}_{\text{VI}} - \underbrace{\frac{e^{Ls}}{\rho^{Ls}}}_{\text{VII}}
 \end{aligned} \tag{3.30}$$

$$\begin{aligned}
 \frac{\partial q^{Hs}}{\partial t} = & \underbrace{-\vec{\nabla}_h \cdot \mathbf{v}_h^{Ls} q^{Hs}}_{\text{I}} - \underbrace{\vec{\nabla}_h \cdot \mathbf{v}_h^{Hs} q^{Ls}}_{\text{II}} - \underbrace{\vec{\nabla}_h \cdot \mathbf{v}_h^{Hs} q^{Hs}}_{\text{III}} + \underbrace{\vec{\nabla}_h \cdot \overline{\mathbf{v}_h^{Hs} q^{Hs}}^{Ls}}_{\text{V}} \\
 & - \underbrace{\frac{\partial \overline{w^{Ls} q^{Hs}}}{\partial z}}_{\text{VI}} - \underbrace{\frac{\partial w^{Hs} \overline{q}^{Ls}}{\partial z}}_{\text{VII}} - \underbrace{\frac{\partial w^{Hs} q^{Hs}}{\partial z}}_{\text{VIII}} + \underbrace{\frac{\partial \overline{w^{Hs} q^{Hs}}^{Ls}}{\partial z}}_{\text{IX}} \\
 & - \underbrace{\frac{S^{Hs}}{\rho^{Ls}}}_{\text{X}} - \underbrace{\frac{e^{Hs}}{\rho^{Ls}}}_{\text{XI}}
 \end{aligned} \tag{3.31}$$

where  $S^{Ls}$  is the net moisture source term. Term VI in Eq. ( 3.30) is the contribution due to a net moisture source, and Term VII due to a net evaporation. Terms X and XI in Eq. ( 3.31) are similar to the two terms just mentioned, but for the corresponding perturbations of net moisture source and net evaporation, respectively.

## D2 Middle scale equation

$$\begin{aligned}
 \frac{\partial q^{Lm}}{\partial t} &= \underbrace{-\overline{\nabla}_h \cdot \mathbf{v}_h^{Lm} q^{Lm}}_{\text{I}} - \underbrace{\overline{\nabla}_h \cdot \mathbf{v}_h^{Hm} q^{Hm Lm}}_{\text{II}} - \underbrace{\overline{\nabla}_h \cdot \mathbf{v}_h^{Hs} q^{Hs Lm}}_{\text{III}} \\
 &\quad - \underbrace{\frac{\partial(\overline{w}^{Lm} \overline{q}^{Lm})}{\partial z}}_{\text{V}} - \underbrace{\frac{\partial(\overline{w}^{Hm} \overline{q}^{Hm Lm})}{\partial z}}_{\text{VI}} - \underbrace{\frac{\partial(\overline{w}^{Hs} \overline{q}^{Hs Lm})}{\partial z}}_{\text{VII}} \\
 &\quad - \underbrace{\frac{s^{Lm}}{\rho^{Lm}}}_{\text{VIII}} - \underbrace{\frac{e^{Lm}}{\rho^{Lm}}}_{\text{IX}}
 \end{aligned} \tag{3.32}$$

$$\begin{aligned}
 \frac{\partial q^{Hm}}{\partial t} &= \underbrace{-\overline{\nabla}_h \cdot \mathbf{v}_h^{Lm} q^{Hm}}_{\text{I}} - \underbrace{\overline{\nabla}_h \cdot \mathbf{v}_h^{Hm} q^{Lm}}_{\text{II}} - \underbrace{\overline{\nabla}_h \cdot \mathbf{v}_h^{Hm} q^{Hm}}_{\text{III}} \\
 &\quad - \underbrace{\overline{\nabla}_h \cdot \mathbf{v}_h^{Hs} q^{Hs Ls}}_{\text{V}} + \underbrace{\overline{\nabla}_h \cdot \mathbf{v}_h^{Hm} q^{Hm Lm}}_{\text{VI}} + \underbrace{\overline{\nabla}_h \cdot \mathbf{v}_h^{Hs} q^{Hs Lm}}_{\text{VII}} \\
 &\quad - \underbrace{\frac{\partial(\overline{w}^{Lm} \overline{q}^{Hm})}{\partial z}}_{\text{VIII}} - \underbrace{\frac{\partial(\overline{w}^{Hm} \overline{q}^{Lm})}{\partial z}}_{\text{IX}} - \underbrace{\frac{\partial(\overline{w}^{Hm} \overline{q}^{Hm})}{\partial z}}_{\text{X}} \\
 &\quad - \underbrace{\frac{\partial \overline{w}^{Hs} \overline{q}^{Hs Ls}}{\partial z}}_{\text{XI}} + \underbrace{\frac{\partial \overline{w}^{Hm} \overline{q}^{Hm Lm}}{\partial z}}_{\text{XII}} + \underbrace{\frac{\partial \overline{w}^{Hs} \overline{q}^{Hs Lm}}{\partial z}}_{\text{XIII}} \\
 &\quad - \underbrace{\frac{s^{Hm}}{\rho^{Ls}}}_{\text{XIV}} - \underbrace{\frac{e^{Hm}}{\rho^{Lm}}}_{\text{XV}}
 \end{aligned} \tag{3.33}$$

## D3 Large scale equation

$$\begin{aligned}
 \frac{\partial q^{Ll}}{\partial t} = & \underbrace{-\bar{\nabla}_h \cdot \mathbf{v}_h^{Ll} q^{Ll}}_{\text{I}} - \underbrace{\bar{\nabla}_h \cdot \mathbf{v}_h^{Hl} q^{Hl^{Ll}}}_{\text{II}} - \underbrace{\bar{\nabla}_h \cdot \mathbf{v}_h^{Hm} q^{Hm^{Ll}}}_{\text{III}} - \underbrace{\bar{\nabla}_h \cdot \mathbf{v}_h^{Hs} q^{Hs^{Ll}}}_{\text{IV}} \\
 & - \underbrace{\frac{\partial(\bar{w}^{Ll} q^{Ll})}{\partial z}}_{\text{VI}} - \underbrace{\frac{\partial(\bar{w}^{Hl} q^{Hl^{Ll}})}{\partial z}}_{\text{VII}} - \underbrace{\frac{\partial(\bar{w}^{Hm} q^{Hm^{Ll}})}{\partial z}}_{\text{VIII}} - \underbrace{\frac{\partial(\bar{w}^{Hs} q^{Hs^{Ll}})}{\partial z}}_{\text{IX}} \\
 & - \underbrace{\frac{S^{Ll}}{\rho^{Ll}}}_{\text{X}} - \underbrace{\frac{e^{Ll}}{\rho^{Ll}}}_{\text{XI}}
 \end{aligned} \tag{3.34}$$

$$\begin{aligned}
 \frac{\partial q^{Hl}}{\partial t} = & \underbrace{-\bar{\nabla}_h \cdot \mathbf{v}_h^{Ll} q^{Hl}}_{\text{I}} - \underbrace{\bar{\nabla}_h \cdot \mathbf{v}_h^{Hl} q^{Ll}}_{\text{II}} - \underbrace{\bar{\nabla}_h \cdot \mathbf{v}_h^{Hl} q^{Hl}}_{\text{III}} \\
 & - \underbrace{\bar{\nabla}_h \cdot \mathbf{v}_h^{Hm} q^{Hm^{Lm}}}_{\text{V}} - \underbrace{\bar{\nabla}_h \cdot \mathbf{v}_h^{Hs} q^{Hs^{Lm}}}_{\text{VI}} \\
 & + \underbrace{\bar{\nabla}_h \cdot \mathbf{v}_h^{Hl} q^{Hl^{Ll}}}_{\text{VII}} + \underbrace{\bar{\nabla}_h \cdot \mathbf{v}_h^{Hm} q^{Hm^{Ll}}}_{\text{VIII}} + \underbrace{\bar{\nabla}_h \cdot \mathbf{v}_h^{Hs} q^{Hs^{Ll}}}_{\text{IX}} \\
 & - \underbrace{\frac{\partial(\bar{w}^{Ll} q^{Hl})}{\partial z}}_{\text{X}} - \underbrace{\frac{\partial(\bar{w}^{Hl} \bar{q}^{Ll})}{\partial z}}_{\text{XI}} - \underbrace{\frac{\partial(\bar{w}^{Hl} q^{Hl})}{\partial z}}_{\text{XII}} \\
 & - \underbrace{\frac{\partial \bar{w}^{Hm} q^{Hm^{Lm}}}{\partial z}}_{\text{XIII}} - \underbrace{\frac{\partial \bar{w}^{Hs} q^{Hs^{Lm}}}{\partial z}}_{\text{XIV}} \\
 & + \underbrace{\frac{\partial \bar{w}^{Hl} q^{Hl^{Ll}}}{\partial z}}_{\text{XV}} + \underbrace{\frac{\partial \bar{w}^{Hm} q^{Hm^{Ll}}}{\partial z}}_{\text{XVI}} + \underbrace{\frac{\partial \bar{w}^{Hs} q^{Hs^{Ll}}}{\partial z}}_{\text{XVII}} \\
 & - \underbrace{\frac{S^{Hl}}{\rho^{Ls}}}_{\text{XVIII}} - \underbrace{\frac{e^{Hl}}{\rho^{Ll}}}_{\text{XIX}}
 \end{aligned} \tag{3.35}$$

So far all the prognostic equations are derived. The rest of the governing equations are processed as follow.

### 3.2.5 Continuity equation

Mass continuity can be expressed as

$$\frac{\partial \rho}{\partial t} = -\frac{\partial \rho u}{\partial x} - \frac{\partial \rho v}{\partial y} - \frac{\partial \rho w}{\partial z}$$

In this study, the air is assumed to be incompressible, and so the equation is simplified to

$$0 = \frac{\partial \rho u}{\partial x} + \frac{\partial \rho v}{\partial y} + \frac{\partial \rho w}{\partial z}$$

After spatial averaging, the continuity equations on the three scales regards to the HRS, are given as follows:

*E1 Small scale equation*

$$0 = \frac{\partial u^{Hs}}{\partial x} + \frac{\partial v^{Hs}}{\partial y} + \frac{\partial w^{Hs}}{\partial z}$$

*E2 Middle scale equations*

$$0 = \frac{\partial u^{Hm}}{\partial x} + \frac{\partial v^{Hm}}{\partial y} + \frac{\partial w^{Hm}}{\partial z}$$

*E3 Large scale equation*

$$0 = \frac{\partial u^{Ll}}{\partial x} + \frac{\partial v^{Ll}}{\partial y} + \frac{\partial w^{Ll}}{\partial z}$$

$$0 = \frac{\partial u^{Hl}}{\partial x} + \frac{\partial v^{Hl}}{\partial y} + \frac{\partial w^{Hl}}{\partial z}$$

### 3.2.6 Equation of state

The last governing equation is equation of state which states that

$$\frac{p}{R} = \rho_m T_v$$

where  $p$  is pressure,  
 $R$  gas constant for dry air,  
 $\rho_m$  density of moist air, and  
 $T_v$  virtual temperature

For simplicity,  $\rho_m$  will be assumed to be the density of dry air  $\rho$  in this study.

*F1 Small scale equation*

$$p^{Hs} = R \left( \rho^{Ls} T_v^{Hs} + \rho^{Hs} T_v^{Ls} + \rho^{Hs} T_v^{Hs} - \overline{\rho^{Hs} T_v^{Hs} Ls} \right)$$

Similar to the prognostic equations, the averaged product of perturbations  $\overline{\rho^{Hs} T_v^{Hs} Ls}$  also contributes to the pressure perturbation  $p^{Hs}$ .

*F2 Middle scale equation*

$$p^{Hm} = R \left( \rho^{Lm} T_v^{Hm} + \rho^{Hm} T_v^{Lm} + \rho^{Hm} T_v^{Hm} + \overline{\rho^{Hs} T_v^{Hs} Ls} - \overline{\rho^{Hm} T_v^{Hm} Lm} - \overline{\rho^{Hs} T_v^{Hs} Lm} \right)$$

*F3 Large scale equations*

$$p^{Ll} = R \left( \rho^{Ll} T_v^{Ll} + \overline{\rho^{Hl} T_v^{Hl} Ll} + \overline{\rho^{Hm} T_v^{Hm} Ll} + \overline{\rho^{Hs} T_v^{Hs} Ll} \right)$$

$$p^{Hl} = R \left( \rho^{Ll} T_v^{Hl} + \rho^{Hl} T_v^{Ll} + \rho^{Hl} T_v^{Hl} + \overline{\rho^{Hm} T_v^{Hm} Lm} + \overline{\rho^{Hs} T_v^{Hs} Lm} - \overline{\rho^{Hl} T_v^{Hl} Ll} - \overline{\rho^{Hm} T_v^{Hm} Ll} - \overline{\rho^{Hs} T_v^{Hs} Ll} \right)$$



## 4 Theory on Heavy Rainfall System

In the previous chapter, full sets of seven governing equations are developed for the three scales. These equation sets will be used to study the interactions of the flows on large (i.e. Jets), middle (i.e. MCS), and small (i.e. cumuli) scales. It is not possible to solve these equations analytically because of their complexities and non-linear characteristics. Obviously, numerical method is a more feasible approach to tackle the problem. However, scale diversity of the equation sets leads to the difficulty on performing analysis since they carry too much information. Therefore, simplification is a must in order to understand the essential interactions among the scales. In this chapter, the equation sets for the three scales are simplified to establish the crucial linkages between them. To facilitate description, the equation set for the large scale hereafter will be simply called “L equation”; that for MCS for the middle scale “M equation”; that for cumulus “S equation”. The aim of the simplification is to show the bare essential interactions, not for detailed diagnosis. The effects of over-simplification will be discussed in the corresponding discussion parts, when they are significant in the relevant balances. The simplification is focused on the rainfall system assumed to be in a steady state. Thus, the system shows no prognostic characteristics and the tendency terms (Term I) in all equations are omitted.

This chapter is divided into dynamic and thermodynamic sections. The dynamic section deals with the momentum equations, while the thermodynamic section potential temperature (heat) and moisture. There are three parts in each section:

- a) The first part is the simplification of the L equation, in order to show the characteristics of the jets in the simplest form.
- b) The second part is the simplification of the S equation. The circulation associated with cumulus and the compatibility to the existing parameterization are considered. Feedbacks to large scale and MCS are also discussed.
- c) The third part is the simplification of the M equation and it is also the focus of this study. With respect to the mesoscale system, the linkages to jets and cumuli are shown to explain the role of MCS in HRS.

At last, the results from the simplifications will be composed to show how MCS interacts with all three scales from both dynamic and thermodynamic perspectives.

## 4.1 Dynamics Simplification

### 4.1.1 Simplification of large scale equation

In this section, dynamic equations will be simplified. Hereafter, superscript  $L$ ,  $M$ , and  $S$  will be used, which refer to jets (large scale mean  $Ll$ ), MCS (perturbation  $Hl$  on large scale) and cumulus (small scale  $Ls$ ).

#### a) Upper level jet

ULJ is a large-scale system as shown in Figure 2.1. In most cases, we are interested in the zonal component of ULJ and thus it is convenient to assume ULJ as a purely westerly flow in concept. Therefore, in the upper troposphere, Eq. (3.16.1) can be used to delineate the circulation associated with ULJ. The simplification can be made step by step regarding the physical interpretations and the significance of those motions on smaller scales. For large scale circulations such as ULJ, the influences of smaller scales such as turbulence can be omitted.

#### 1 Turbulence terms

The effect of turbulence can be neglected because of its small scale and the fact that ULJ exists in the upper troposphere. As a result, turbulent flux divergences contribute little to the large scale zonal momentum on large scale and Term V and IX in Eq. (3.16.1) can be neglected.

#### 2 Cumulus terms

It is a good assumption that the large scale mean momentum is independent of cumulus dynamics. One of the reasons is that cumulus updrafts hardly reach the level of ULJ, provided that the cloud tops of most cumulus (congestus) reach  $\sim 4 - 6$  km even in tropical region [Redelsperger et al. (2002)], though it is possible for the deepest convection to penetrate the upper troposphere. Another reason is that the proportion of convective region to the large scale area is small. Anthes (1977) has estimated the magnitude of horizontal eddy (here referred as the cumulus scale) heat flux, and found that the value is insignificant compared to that of the vertical eddy flux. The result of his estimation is also valid on the horizontal momentum eddy flux which perturbations of horizontal momentum are even smaller or closed to that of potential temperature. The last reason, which was also mentioned by Anthes (1977), is that the value of flux *divergence* is further decreased by a high resolution which is equivalent to a small grid size in simulation. Based on these 3 factors, Term IV and VIII are neglected.

### 3 MCS terms

As mentioned in Section 2, the dynamics of ULJ is maintained by “eddy” circulations in the exit region, so it is reasonable to interpret that this kind of “eddies” is actually implying to a type of circulation on a smaller adjacent scale. As MCS often accompanies in the ULJ’s exit region (also LLJ’s), it is plausible to deduce that these eddies are the vertical flux divergences arisen from MCS and has a significant effect in the jet dynamics when considering in large area. In other words, horizontal momentum associated with MCS is transported vertically between the jets. The horizontal “meso-momentum” transported by the ascent constitutes the upward branch of an ageostrophic circulation associated with the jets. To complete this transverse circulation, the meso-momentum is transported downward on the anti-cyclonic side and leads to the enhancement of LLJ.

As MCS scale is closer to the large scale compared to the cumulus scale, the last factor mentioned in the previous part becomes more significant. Moreover, vertical MCS momentum transport is more important than the horizontal transport for the maintenance of ULJ. As a result, Term III is omitted and VII is preserved. Note that Term VII coexists in both MCS and large scale equations, and it means a linkage between the ULJ and the MCS. In simple, the vertical transport of MCS momentum on a large area is responsible for the transfer of momentum between LLJ and ULJ. The details of this term will be discussed later.

### 4 Large scale real force terms

For the large scale real motion itself, the relevant terms are simplified on the basis of ULJ’s characteristics. The horizontal dynamic forcing of ULJ is dominant by Coriolis force (Term X) and pressure gradient force (Term XI) according to its scale and feature. In the case of a ULJ in steady state, the tendency term (Term I), as well as the large scale advective terms (Term II and VI), vanish. The forcing of the jet flow then is ageostrophic which is counterbalanced by Term VII.

The resultant large scale equation for ULJ is given as

$$\frac{\partial(\overline{w^M u^M})}{\partial z} = f v^L - \frac{1}{\rho} \frac{\partial p^L}{\partial x} \quad (4.1)$$

VII                  X                  XI

This equation implies that the vertical transport of mesoscale horizontal momentum associated with MCS in a large area contributes to the ageostrophic circulation associated with ULJ. In steady state, a balance exists between these three forces. Note that the air density is assumed to be independent of scale now. In other words, the air in the multiscale system is incompressible.

b) Low Level Jet

The scale of LLJs is always an argument since it covers the border between synoptic and mesoscale, as shown in Figure 2.5. In the conceptual model, LLJ is categorized as large scale system because the (spatial) scale of the interested LLJ is comparably larger than that of MCS. LLJ is a similar regime as ULJ that can be observed in the lower troposphere, and it carries also ageostrophic characteristics in the streak region. In most cases LLJs are found to be southwesterly beneath the westerly ULJ over central US and southeastern China. With its prominent southerly characteristics, LLJ is assumed to be purely southerly for simplicity, and hence Eq. (3.16.2) is used to describe the dynamics of LLJ.

In analogy to Eq. (4.1), the simplified equation for LLJ is

$$-f u^L - \frac{1}{\rho} \frac{\partial p^L}{\partial y} = \frac{\partial (\overline{w^M v^M})}{\partial z} \quad (4.2)$$

X      XI    VII

It also states that ageostrophic circulation associated with the LLJ is counterbalanced by the vertical transport of horizontal MCS momentum. LLJ decelerates in its exit region, and the large scale horizontal momentum converts to that on mesoscale and transported vertically by the mean of MCS (see Figure 4.6). In its entrance region, LLJ accelerates due to the descent of mesoscale momentum on its anti-cyclonic side, i.e. a reverse process described in Eq. (4.2). In short, vertical mesoscale flux divergence determines the LLJ's dynamics. More details will be discussed in the last section.

c) Vertical Momentum

As both ULJ and LLJ belong to large scale regime, which exist in stable environment, it is reasonable to assume that the jets are hydrostatic, i.e.  $w^L \approx 0 \text{ m s}^{-1}$ . In other words, all the advection terms in Eq. (3.22) are ignored and only real forces are retained.

The simplified equation is given as

$$\frac{1}{\rho} \frac{\partial p^L}{\partial z} = -g \quad (4.3)$$

X      XI

This equation is simply hydrostatic equation which states the balance between vertical pressure gradient force (Term X) and gravitational force (Term XI).

### 4.1.2 Simplification of small scale equation

In the dynamics of cumulus, the vertical motion dominates and the horizontal motion is often ignored. This leads to the abandonments of Eq. ( 3.15.1) and (3.15.2). Most cumulus parameterization schemes in present assumed the cumulus dynamics in steady state. It implies that the cumulus vertical momentum remains unchanged with time [Term I in Eq. ( 3.21) equals to 0], and it gives Eq. ( 4.4). This assumption is preserved in our model and so the theory can be compatible to the existing parameterization schemes.

$$\frac{\partial w^S}{\partial t} = 0 \quad (4.4)$$

One point has to be clarified is that though the time rate of vertical momentum is assumed to be unchanged, the updraft and downdraft still exist in cumulus for the transport of thermodynamic quantities.

### 4.1.3 Simplification of middle scale equation

As emphasized before, the influence of the jets and cumuli to MCS is the focus of this study. It is crucial to establish an applicable equation which clearly depicts the interactions between the jets, cumuli and MCS, with respect to the MCS itself.

#### A Horizontal momentum

The routine in the previous section is used to simplify Eq. ( 3.17.1) and (3.17.2).

#### A1 Turbulence terms

Due to its insignificance on mesoscale, all the turbulent terms vanish, i.e. Term VI, IX, XIV and XVII.

### A2 Cumulus terms

Same as their insignificance on large scale, horizontal cumulus flux divergence are also assumed to be insignificance on MCS's scale, as cumulus hardly reaches the level of MCS anvil region, and so the small scale momentum hardly be transported on MCS level. In this case, all the related flux divergences are omitted, i.e. Term V, VIII, XIII and XVI.

### A3 MCS terms

The MCS dynamics resembles to cumulus dynamics and also assumed to be in steady state. As vertical motion dominates in MCS, horizontal mesoscale momentum flux divergence, i.e. Term IV, is neglected. As mentioned, vertical transport of mesoscale momentum is important because it is associated with the jets' ageostrophy, therefore the relevant Term XII is retained. Although the corresponding effect on large scale, which is reflected by Term XV, is important, this equation is with respect to mesoscale, hence this effect is not the concern in this middle scale equation. In fact its contribution is insignificance and it will be investigated in the corresponding discussion part. In the same manner, its horizontal counterpart, Term VII, is also neglected.

### A4 Terms associated with Jets and MCS

The interaction between the jets and the MCS is the most prominent one in the dynamic issue. As precipitation is often be found on the cyclonic side of ULJ and LLJ, so there must be a kinematic interaction between the jets and the MCS. This interaction tells how the MCS motions is associated to the large scale motion arises from the jets. Quantitatively, the possible term(s) which links the motion on large and middle scales are Terms II, III X and XI. However, it is difficult to determine the linkage by the terms themselves.

As mentioned the vertical mesoscale momentum flux divergences are responsible for the transport between the jets, these terms must be related to mesoscale vertical motion. Consider the lifting of air in which vorticity and divergence are needed. Expanding Eq. (3.17.1) and (3.17.2) by chain rule, differentiate the equations with respect to  $y$  and  $x$ , respectively, then subtract the resultant equations. It gives the vorticity equation for MCS. The full derivation is documented in Appendix A, while its essences can be represented as follow

$$\frac{\partial \zeta^M}{\partial t} = \underbrace{-\overline{\mathbf{v}}_h \cdot \mathbf{v}_h^L \zeta^M}_{A} - \underbrace{\overline{\mathbf{v}}_h \cdot \mathbf{v}_h^M \zeta^L}_{B} - \underbrace{2\zeta^M D^L}_{C} - \underbrace{2\zeta^L D^M}_{D} - \underbrace{\frac{\partial}{\partial x} \frac{\partial w^M v^M}{\partial z}}_{E} - \underbrace{\frac{\partial}{\partial y} \frac{\partial w^M u^M}{\partial z}}_{F}$$

where  $\zeta^M = \frac{\partial v^M}{\partial x} - \frac{\partial u^M}{\partial y}$ ,  $D^M = \frac{\partial u^M}{\partial x} + \frac{\partial v^M}{\partial y}$  are the vorticity and divergence associated with MCS, respectively. Accordingly,  $\zeta^L = \frac{\partial v^L}{\partial x} - \frac{\partial u^L}{\partial y}$ ,  $D^L = \frac{\partial u^L}{\partial x} + \frac{\partial v^L}{\partial y}$  are the counterparts on large scale, respectively.

It states that the mesoscale vorticity following the flow increases with time due to 6 main factors:

- A) Mesoscale vorticity itself is advected by large mean flow;
- B) Large scale vorticity is advected by middle flow;
- C) Mesoscale vorticity is concentrated by large scale convergence;
- D) Large scale vorticity is concentrated by mesoscale convergence;
- E) Zonal gradient of vertical flux divergence of mesoscale meridional momentum; and
- F) Meridional gradient of vertical flux divergence of mesoscale zonal momentum.

Note that the essences on the basis of the interaction between the large and middle scales. Irrelevant and insignificant terms are ignored. As we are considering the interaction at a steady state, the equation above can be rewritten as

$$\begin{matrix} \vec{\nabla}_h \cdot \mathbf{v}_h^L \zeta^M & + & \vec{\nabla}_h \cdot \mathbf{v}_h^M \zeta^L & = & -2\zeta^M D^L & - & 2\zeta^L D^M & - & \frac{\partial}{\partial x} \frac{\partial w^M v^M}{\partial z} & - & \frac{\partial}{\partial y} \frac{\partial w^M u^M}{\partial z} \end{matrix} \quad (4.5)$$

A                      B                      C                      D                      E                      F

It states that the advection of vorticities on meso- and large scale is balanced by the divergence effects and the gradient of mesoscale vertical flux divergences. In the case of the HRS, Term C and D are the source of mesoscale vorticity. Term C refers to the concentration of MCS vorticity by the convergence associated with jets. It is a reliable source as the precipitation region located beneath the ULJ which aligned downstream of an upper level trough (see Figure 2.1). The advection of (large scale) positive vorticity associated with the ULJ results in the upper level divergence. In response to the divergence, low level convergence on large scale is developed in the region. This convergence concentrates the mesoscale vorticities on a large area, as shown in Figure 4.1(a). Term D represents a similar effect, but with the scales replaced by each other. The positive vorticity associated with LLJ on its cyclonic side is concentrated by the mesoscale divergence [Figure 4.1(b)]. This is a process that large scale vorticity converts to mesoscale vorticities.



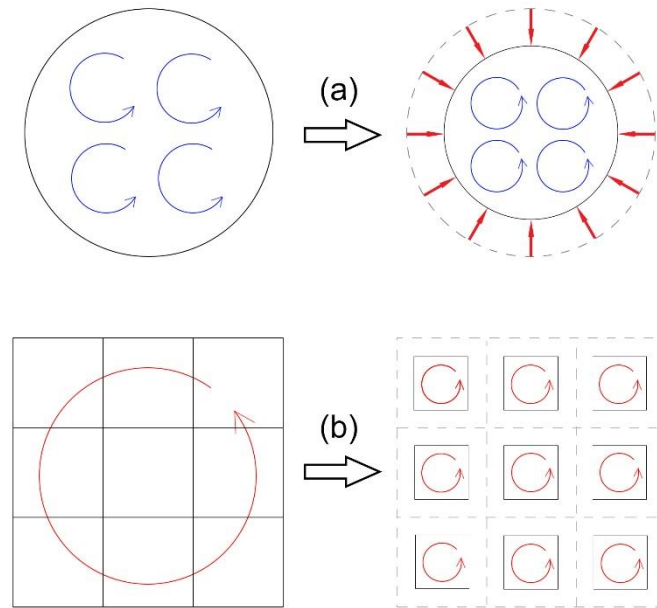


Figure 4.1 Schematic diagram showing the increase of mesoscale vorticity.  
 (a) Mesoscale vorticity increase due to large scale convergence.  
 (b) Large scale vorticity is “splitted” and converts to mesoscale vorticities due to mesoscale convergence.

Term E and F represent the contribution to the increase of mesoscale vorticity due to the horizontal gradient of vertical mesoscale flux divergence. The demonstration of Term E is shown in Figure 4.2. In the entrance region of LLJ, the zonal gradient of the flux divergence from Quarter 1 to 2 is negative, contributes to positive advection process of the vorticity, i.e. positive vorticity is advected from the cyclonic side to the anti-cyclonic side. Respect to large scale, when the averaged value of the flux divergence on large scale remains positive, say in Quarter 1, then the jet accelerates due to its ageostrophy described by Eq. (4.2). This process describes how the mesoscale flux divergence intensifies the LLJ in the entrance region through the advection of mesoscale vorticity in order to maintain the jet as well as the transport of moisture.

The contribution in the exit region can be explained in an opposite sense. The positive gradient of the flux divergence leads to the negative advection of mesoscale vorticity, i.e. positive vorticity is advected away from Quarter 3 to the west, or can be considered as negative vorticity which is advected from Quarter 4 to the east. Accordingly, when the averaged value of the flux divergence on Area 3 remains negative, according to Eq. (4.2), the jet decelerates.

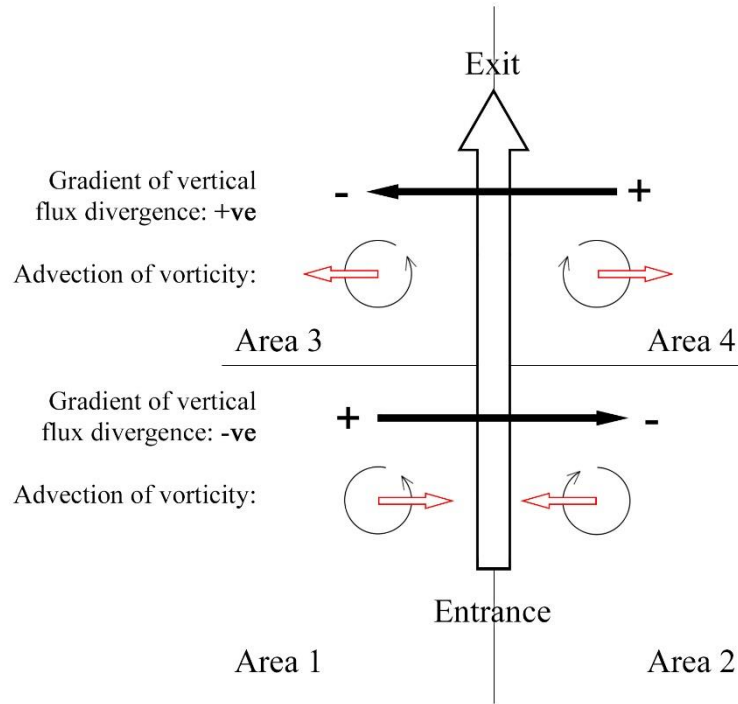


Figure 4.2 Effect of Term E on the jet dynamics. Big opened arrow represents LLJ. Sign “+” and “-“ represent the values of  $\frac{\partial w^M v^M}{\partial z}$ , while solid black arrow indicates the gradient of it. Opened red arrow represents advection direction of the corresponding vorticity.

To sum up, when the interaction between large and middle scale is in a steady state, the advection of vorticity (Term A and B) is balanced by the enhancement of vorticity due to divergence effect among the two scales (Term C and D), and the horizontal advection of vertical flux divergence of mesoscale horizontal momentum (Term E and F).

Term A, B, C and D are the product of horizontal derivatives of Term II and III in Eq. ( 3.17.1) and (3.17.2) with respect to orthogonal directions, while Term E and F are the product of Term XV from both equations). Therefore, it can be implied that the spatial change of the horizontal interactions between large and middle flows results in the enhancement of vorticity in the area.

Back to the simplification of Eq. ( 3.17.1) and (3.17.2), Term II and Term III describe the interaction between middle and large scale flows. As it is responsible for the transport between ULJ and LLJ, Term XII must be included in the simplification which involved mesoscale vertical transport. Noted that Term X and XI are ignored. For Term X, due to the hydrostatics assumed on large scale, therefore it vanishes as  $w^{ll}$  is close to zero. For Term XI, following the derivation of Term II and III, it is not difficult to

realize that it is responsible for the tilting of horizontal vorticities, which is not the main concern in the mechanism of heavy rainfall system, and hence it is omitted. Term XVIII and XIX are the effect of Coriolis force and pressure gradient force, respectively, compared to the scale of MCS, both are omitted.

If the interaction is assumed in a dynamic equilibrium that the advections of the two scales in space remain unchanged, the dynamic process between middle and large flow can be simplified as

$$\underbrace{\overline{\nabla}_h \cdot \mathbf{v}_h^L u^M}_{\text{II}} + \underbrace{\overline{\nabla}_h \cdot \mathbf{v}_h^M u^L}_{\text{III}} = \underbrace{\frac{\partial w^M u^M}{\partial z}}_{\text{XII}} \quad (4.6.1)$$

These two equations imply that, in steady state, the horizontal momentum of MCS interacts with jet motions. These interaction are presented in the enhancement of MCS's vorticity which is responsible for the acceleration (deceleration) of the LLJ in its entrance (exit) region and contributes to mesoscale vertical flux divergence. Note that the equations above are independent of cumulus dynamics.

## B Vertical momentum

The simplification of vertical momentum equation for MCS [Eq. ( 3.23)] is similar to that of horizontal.

### B1 Turbulence and cumulus terms

Following the routine in previous section, Term VI, IX, XIV, and XVII which associated with turbulence aspect; Term V, VIII, XIII, and XVI which associated with cumulus aspect, are neglected.

### B2 MCS term

In middle scale, the horizontal momentum flux divergence of MCS, i.e. Term IV, are omitted. For the same reason mentioned in previous section, vertical momentum flux divergence Term XII is retained and its counterparts on large scale, Term VII and XV, are neglected.

*B3 Terms associated with large scale and MCS*

Term II, III, X and XI are not necessary to be retained because the vertical component do not contribute to horizontal mesoscale vorticity which is not a sufficient precursor for precipitation.

Term XVIII and XIX are the real forces exerted by buoyancy and pressure gradient, respectively. To keep the simplicity, pressure gradient force is ignored, though it contributes to the ascent to an extent. Compare to pressure gradient force, the buoyancy term is a more dominant factor.

Applying Boussinesq Approximation on Term XIX, the resultant equation is written as

$$\frac{\partial w^M w^M}{\partial z} = \frac{\theta^M}{\theta^L} g \quad (4.7)$$

XV      XIX

This equation implies that, the vertical momentum flux divergence of MCS, i.e. the vertical transport of vertical mesoscale momentum, is supported by the buoyancy of the air mass associated with MCS itself. In other words, MCS's vertical motion is enhanced by the density departure in MCS scale.

**C Vertical Transport of horizontal momentum**

To delineate the transport of mesoscale horizontal momentum flux divergence by the corresponding ascent, Eq. ( 3.17.1) and ( 3.23) are used to construct a zonal momentum flux divergence equation. Multiple the equations by  $w^M$  and  $u^M$ , respectively, then sum the equations up, we have

$$\frac{\partial w^M (w^M u^M)}{\partial z} = u^M \frac{\theta^M}{\theta^L} g \quad (4.8)$$

A                  B

where all the horizontal terms and non-linear terms are ignored since only vertical contribution is concerned. The full derivation is shown in Appendix B.

Likewise, the equation for meridional momentum constructed from (3.17.2) and (3.23) are

$$\frac{\partial w^M(w^M v^M)}{\partial z} = v^M \frac{\theta^M}{\theta^L} g \quad (4.9)$$

A                      B

The two equations above state that the vertical transport of vertical flux divergence of horizontal MCS momentum increases when the corresponding horizontal momentum is transported by the buoyancy. When the rainfall system reaches a steady state, the transport of horizontal momentum is intensified by the buoyancy associated with the vertical motion. The details regarding the origin of mesoscale buoyancy forcing will be discussed in the next section.

## 4.2 Thermodynamics Simplification

### 4.2.1 Simplification of large scale equation

The simplification of Eq. ( 3.28) and ( 3.34) are similar to the previous section, with more attention is paid on the compatibility to the parameterization scheme in present. In this section, the heat issue described by Eq. ( 3.28) is used as an example for the simplification, and the outcome can be applied to the moisture issue described by Eq. ( 3.34).

#### 1 Cumulus and turbulence terms

In all the aspects except large scale itself, the cumulus parameterization schemes proposed by Awakara et al. (1974) and Tiedtke (1989) focused on the contribution of cumulus vertical transport of heat and moisture to the large scale forcing [Term VIII in Eq. ( 3.28) and ( 3.34)], while that arisen from horizontal transports are ignored due to their insignificance. In addition, all the effects due to turbulence are out of the consideration. On this basis, Terms IV, V, and IX, which have been mentioned above, are neglected. Therefore, only Term VIII is retained.

#### 2 MCS terms

As MCS carries convection property as cumulus does, horizontal transport associated with MCS are be treated in the same way as the cumulus counterpart on the basis of those parameterization schemes aforementioned. As a result, Term III is omitted. The vertical transport term, Term VII, which is associated with MCS vertical heat transport, is retained.

#### 3 Large scale terms

Term II explains the horizontal transport of moisture by a mean flow. As described in Section 2, the main feature of LLJ is the transport of moisture from sources, so it should be related to a horizontal moisture flux divergence on a large scale. It is not hard to see that Term II is describing the relevant phenomenon, hence it is retained. In the conceptual model, heat and moisture are transported by the vertical motion of MCS and cumuli, and the large scale vertical transport are excluded, i.e. Term VI is ignored. Jet thermodynamics is mainly forced by horizontal advections rather than the radiative heating and phase change of moisture on large scale. Donner et al. (1993) found that the large scale radiative forcing is dominant in deep convections. However, the contributions are not significant when comparing to the horizontal structure of the jets, and so and Term X is neglected.

The resultant thermodynamic equation of heat and moisture for large scale now are simplified as follow

$$\vec{\nabla} \cdot \overline{\mathbf{v}}_h^L \theta^L = - \frac{\partial(\overline{w^M \theta^M}^L)}{\partial z} - \frac{\partial(\overline{w^S \theta^S}^L)}{\partial z} \quad (4.10)$$

$$\vec{\nabla} \cdot \overline{\mathbf{v}}_h^L q^L = - \frac{\partial(\overline{w^M q^M}^L)}{\partial z} - \frac{\partial(\overline{w^S q^S}^L)}{\partial z} \quad (4.11)$$

II                      VII                      VIII

The equations above state that, in steady state, the heat and moisture on large scale transported by the corresponding horizontal mean flow (jets) fuel the relevant quantities which are transported vertically on smaller scales (i.e. MCS and cumulus) in large area.

#### 4.2.2 Simplification of small scale equation

Unlike the corresponding equations in dynamic issues, cumulus equations in thermodynamic issue [Eq. ( 3.27) and ( 3.33)] cannot be nullified because the heat and moisture transports are associated with precipitation. In order to keep the compatibility to the existing parameterization schemes, the framework of those schemes are integrated to the relevant equations. To do that, it is necessary to transform the equations in the schemes in order to fit the corresponding terms in the small scale equations.

As mentioned in Section 4.1.2, circulation associated with cumulus in steady state shows no tendency. In the existing schemes, the heat and moisture contained in an air mass transported by this steady flow is based on the “quasi-mass-continuity”. In short, it states that the net difference between entrainment and detrainment rate of cumulus contributes to the vertical mass flux divergence within the cumulus boundary [Eq. (1) in Awakara et al. (1974)],

$$E_i - D_i = \frac{\partial M_i}{\partial z}$$

where  $E_i$  and  $D_i$  ( $kg\ m^{-3}\ s^{-1}$ ) are the entrainment and detrainment rates, respectively.  $M_{net,i}$  is mass flux by  $M_{net,i} = \rho w$  with air density  $\rho$  and vertical wind speed  $w$ . Subscript  $i$  represents the  $i$ -th individual cloud.

Meanwhile, in the scheme of Tiedtke (1989), mass flow is represented by the meaning of a bulk cumulus, provided that its size remains the same with time.

$$E_u - D_u = \frac{\partial M_u}{\partial z} \quad \text{and} \quad E_d - D_d = \frac{\partial M_d}{\partial z}$$

where subscripts  $u$  and  $d$  denote updraft and downdraft, respectively.

By summarizing the aforementioned equations, a composite equation can be deduced to depict this mass flow in steady state,

$$E - D = \frac{\partial M}{\partial z} \quad (4.12)$$

This equation describes the motion of mass in a cumulus while keeping the mainframe that the difference between horizontal entrainment and detrainment processes results in the vertical mass flux divergence, regardless of the size of the cumulus. Hence, this equation can be applied on a scale which is able to resolve the associated convection. As the equations above show the interaction between the (bulk) cumulus and its “sole” environment, it is necessary to advance the equation above in order to fit the proposed equations.

Consider the definition of “scale” in the model. For a cumulus itself, the air from on large scale environment (with scale  $Ll$ ) entrains through the boundary to the cumulus by its own flow (with scale  $Hm$ ). However, the entrainment process occurs not only between cumulus and large scale environment, but also between cumulus and MCS ( $HL$ ). Therefore, there must be a term in Eq. ( 3.27 ) and ( 3.33 ) which quantitatively describes the advection between scales  $Hm$  and  $Ll$ , as well as  $Hm$  and  $HL$ .

In the Eq. ( 3.27 ), Term III is the descriptive term for that. Rewrite Term III and it gives

$$-\vec{\nabla} \cdot \mathbf{v}_h^{Hm} \bar{\theta}^{Lm} = -\underbrace{\vec{\nabla}_h \cdot \mathbf{v}_h^M \bar{\theta}^{Ll}}_{E_{Ll}} - \underbrace{\vec{\nabla}_h \cdot \mathbf{v}_h^{Hm} \bar{\theta}^{HL}}_{E_{HL}}$$



It can be seen that Term III is actually referring to the cumulus horizontal transport of heat on 2 scales.  $E_{LL}$  is the horizontal transport of large scale heat by cumulus motion; while  $E_{HL}$  transport of MCS heat by cumulus motion, as shown in Figure 4.3 schematically. The former depicts the entrainment from large scale environment, while the latter from MCS.

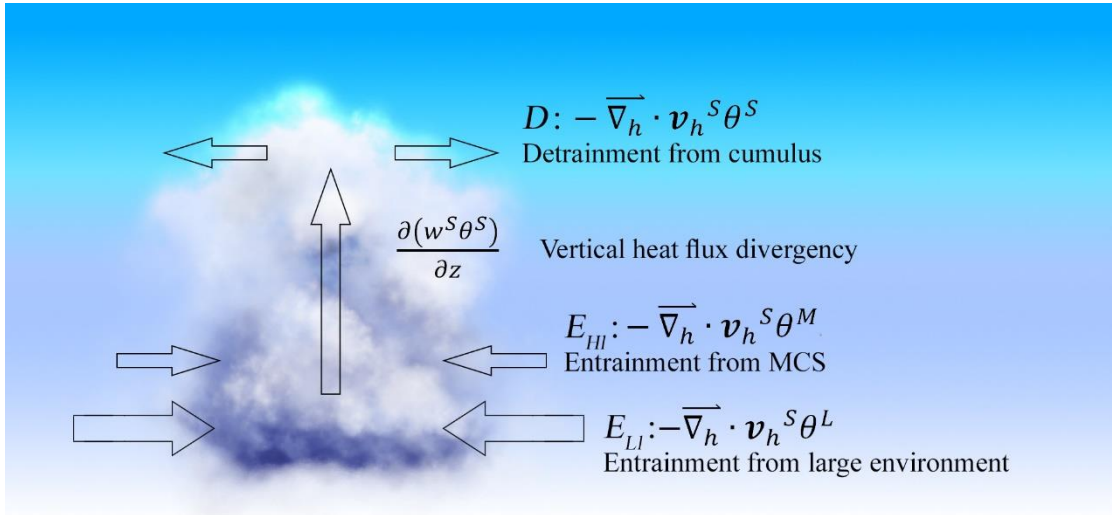


Figure 4.3 Proposed dynamics of a cumulus.  $E$  and  $D$  represent entrainment and detrainment, respectively. In this study, there are two types of entrainment: From large environment and from MCS. Details refer to the discussion of Eq. (4.14) in Section 4.2.3(4). Note that entrainments and detrainment do not occur necessarily at the cloud base and cloud top.

Likewise, the (horizontal) detrainment of cumulus is represented by Term IV, i.e.  $-\bar{\nabla}_h \cdot \mathbf{v}_h^{Hm} \theta^{Hm}$ . This term shows the heat of MCS detrained by the flow of MCS itself to either large scale environment or MCS. The last element which has to be considered is the term corresponds to vertical mass flux. Similar to the detrainment process, vertical heat flux divergence is the result of transport of heat of cumulus by the vertical flow of cumulus itself. It is obvious that this process can be described by Term X only in Eq. (3.27). The contribution of the vertical mass flux divergence to the MCS and large scale will be shown in later section.

Thus, Eq. ( 4.12 ) can be rewritten as follow to describe the cumulus thermodynamics

$$\begin{array}{ccc}
 -\overline{\nabla}_h \cdot \mathbf{v}_h^S (\theta^M + \theta^L) & - \overline{\nabla}_h \cdot \mathbf{v}_h^S \theta^S & = \frac{\partial(w^S \theta^S)}{\partial z} \\
 \text{III} & \text{IV} & \text{X}
 \end{array} \quad (4.13)$$

It is a simplified version of Eq. ( 3.27 ) apparently. Based on observations, cumulus shows a conspicuous life cycle which is associated with the tendency term (Term I). However, as mentioned, cumulus is assumed in steady state, so this term is omitted. Also, radiative heating on small scale favours the genesis of cumulus only, so Term XIV is ignored too.

As mentioned in Section 4.2.1, vertical flux divergence of heat and moisture associated with cumulus affect the large scale forcing. Relative to the cumulus, there should be a feedback to the large scale environment, and also to MCS. These effects are reflected by Term XII in the corresponding equations. However, as the focus of this equation is on the small scale only, these averaged effect will be neglected here. Forcing due to evaporation (Term XV) is omitted as it is not the focus.

In the same way, Eq. ( 3.33 ) regarding the conservation of moisture can be simplified as

$$\begin{array}{ccc}
 -\overline{\nabla}_h \cdot \mathbf{v}_h^S (q^M + q^L) & - \overline{\nabla} \cdot \mathbf{v}_h^S q^S & = \frac{\partial(w^S q^S)}{\partial z} \\
 \text{III} & \text{IV} & \text{X}
 \end{array} \quad (4.14)$$

The two equations above state that the net difference of entrainment and detrainment of heat / moisture in a cumulus contributes to the vertical cumulus heat / moisture flux divergence, provided that the entrainments involve MCS and large scale environment.

### 4.2.3 Simplification of middle scale equation

#### 1 MCS terms

The simplification of Eq. ( 3.29 ) is based on the concept that MCS is an intermediate medium between jets and cumuli. MCS allows transport of momentum, heat and moisture among them in order to maintain the heavy rainfall system through mesoscale convection. In other words, the vertical term related to MCS itself are more important than the horizontal counterpart. As a result, Term XII retained while Term IV is neglected.

Since Eq. ( 3.29 ) describes the thermodynamic motion of MCS only, the corresponding effect on large scale is neglected for simplicity and the effect should be reflected in the corresponding large scale equation. Therefore, Term XV is neglected, as well as its horizontal counterpart Term VII.

## 2 Turbulence terms

In the turbulence aspect, Terms VI, IX, XIV, and XVII, are neglected.

## 3 Terms associated with Jets and MCS

Heat and moisture from large scale environment are transported by the circulation associated with MCS. The phenomenon has been described in Section 2 that moist tongue associated with LLJ often reaches MCSs' vicinity. While LLJ is responsible for horizontal transport, MCS is responsible for the vertical transport of heat and moisture on mesoscale in the vicinity of jet's exit region. It leads to the negligence of Term III and Term XI. On the contrary, the reverse processes, i.e. MCS's heat and moisture transported by large scale flow, are also insignificant though they are possible to exist. As a result, Terms II and X omitted.

## 4 Cumulus terms

It is not a complete picture yet as cumuli also create an identical effect on the MCS scale as what they do on large scale. Analogues to the effect of cumulus in large area, there should be a term like  $-\frac{\overline{\partial_w^{Hm} \theta^{Hm}}^{Hl}}{\partial z}$  in Eq. ( 3.29 ) to represent the effect in middle scale area. However, scale of MCS, i.e.  $Hl$ , is a sub-scale from Scale  $Lm$ . By the definition in Section 3, it is not possible to perform averaging on  $Hl$  scale. Instead, the effect of cumulus heat / moisture flux divergence on mesoscale is shown in an indirect manner.

The effect is presented by eliminating the value over large area (Term XVI) from that over middle area (Term XIII). The former value consists of the information on a large area only, while the latter consists of the information in both large scale area and MCS, hence the difference is the net effect of cumuli on the MCS. Note that  $\overline{\quad}^{Lm}$  is rewritten as  $\overline{\quad}^{(M+L)}$  since  $Lm = Hl + Ll$ . The quantity with this overbar carries the value associated with MCS, and also the large scale mean. The misleading overbar  $\overline{\quad}^M$  is avoided which means "averaged over MCS scale" (It does not exist). In other words, Term XIII and XVI collaborate in order to show the net effect of vertical transport of cumulus heat in MCS. Their horizontal counterparts Term V and VIII are neglected because of their insignificance.

5 Real forcings

Similar to cumulus equation, the forcing due to radiative heating, Term XVIII, is excluded. However, the heat due to phase change of moisture is an important factor because it is related to the heated produced is associated with the enhancement of vertical transport, as mentioned in the previous section.

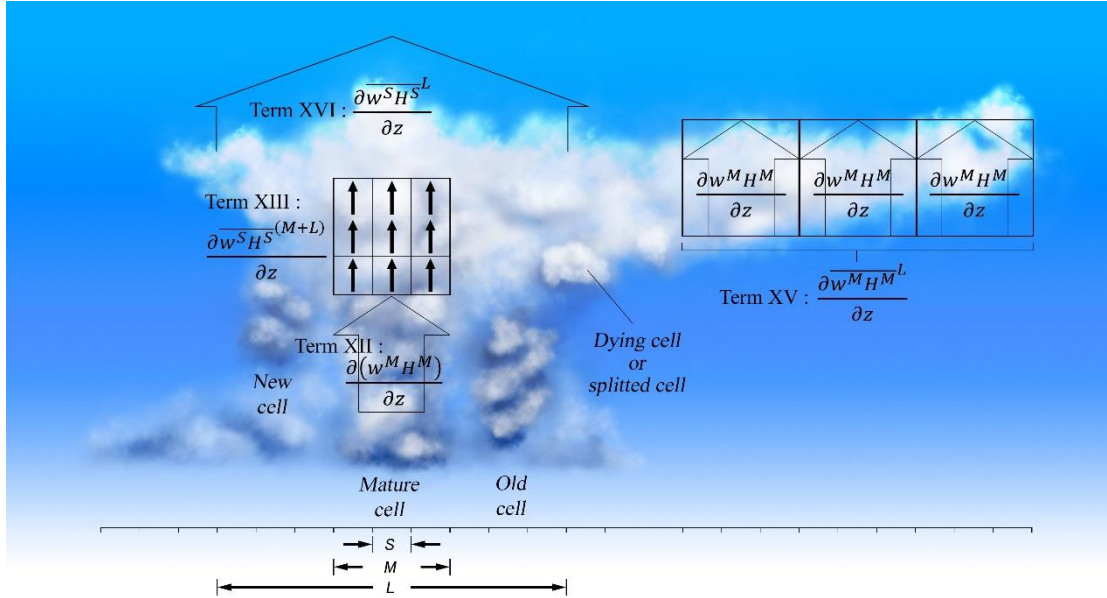


Figure 4.4 Representation of the terms in Eq. ( 4.15 ) and ( 4.16 ). In this case, the ratio of Scale  $S : M : L$  is 1:3:9. Small solid arrow represents flux divergence on Scale  $S$ , open arrow on Scale  $M$ , and the huge arrow on Scale  $L$ . Quantity  $H$  can be either potential temperature  $\theta$  or specific mixing ratio  $q$

The mentioned terms are presented schematically in Figure 4.4, and the resultant equation for MCS's heat conservation is given as follow:

$$\begin{matrix} \frac{\partial(w^M \theta^M)}{\partial z} & = & -\frac{\partial \overline{w^S \theta^S}^{(M+L)}}{\partial z} & - & \left( -\frac{\partial \overline{w^S \theta^S}^L}{\partial z} \right) & - & \frac{L_v e^M}{\rho C_p} \\ \text{XII} & & \text{XIII} & & \text{XVI} & & \text{XIX} \end{matrix} \quad (4.15)$$

It states that the vertical heat flux divergence increases when heat is dissipated by cumuli on mesoscale (net difference of Term XIII and XVI) and when latent heat is released through mesoscale condensation of moisture. Apply to the case of rainfall system, when it is in a steady state, the heat transported in MCS by the ascending motion is supported by the latent heat released on mesoscale, and also by the heat released from

cumuli on mesoscale. However, at the height higher than the base of anvil region, the dissipation from the cumuli becomes weaker, and the former factor dominates.

It is not difficult to see that the corresponding equation for moisture explains the origin of the mesoscale latent heat. Similar to the simplification for Eq. ( 4.15 ), the equation can be written as

$$\frac{e^M}{\rho} = \left[ \frac{\overline{\partial w^S q^S}^{(M+L)}}{\partial z} - \left( \frac{\overline{\partial w^S q^S}^L}{\partial z} \right) \right] + \frac{\partial(w^M q^M)}{\partial z} \quad (4.16)$$

XIX      XIII                  XVI                  XV

It means that the mesoscale condensation process, i.e. negative value of  $E^M$ , is balanced by the moisture which is transported by either cumuli or MCS. It is a process in which the cumulus moisture converts to be on mesoscale by the meaning of condensation. These two factors are comparable to each other at the junction between the MCS's convective and anvil region.

Combining the phenomena described by Eq. ( 4.15 ) and ( 4.16 ), it can be implied that, in an extreme case, all the moisture transported in small cumulus scale is transported upward and condensates on mesoscale. The resultant latent heat flux then contributes to the vertical mesoscale heat flux divergence.

### 4.3 Physical Interpretation of the Multiscale Heavy Rainfall

In this section, the essential interactions *with respect to MCS* are showed and interpreted.

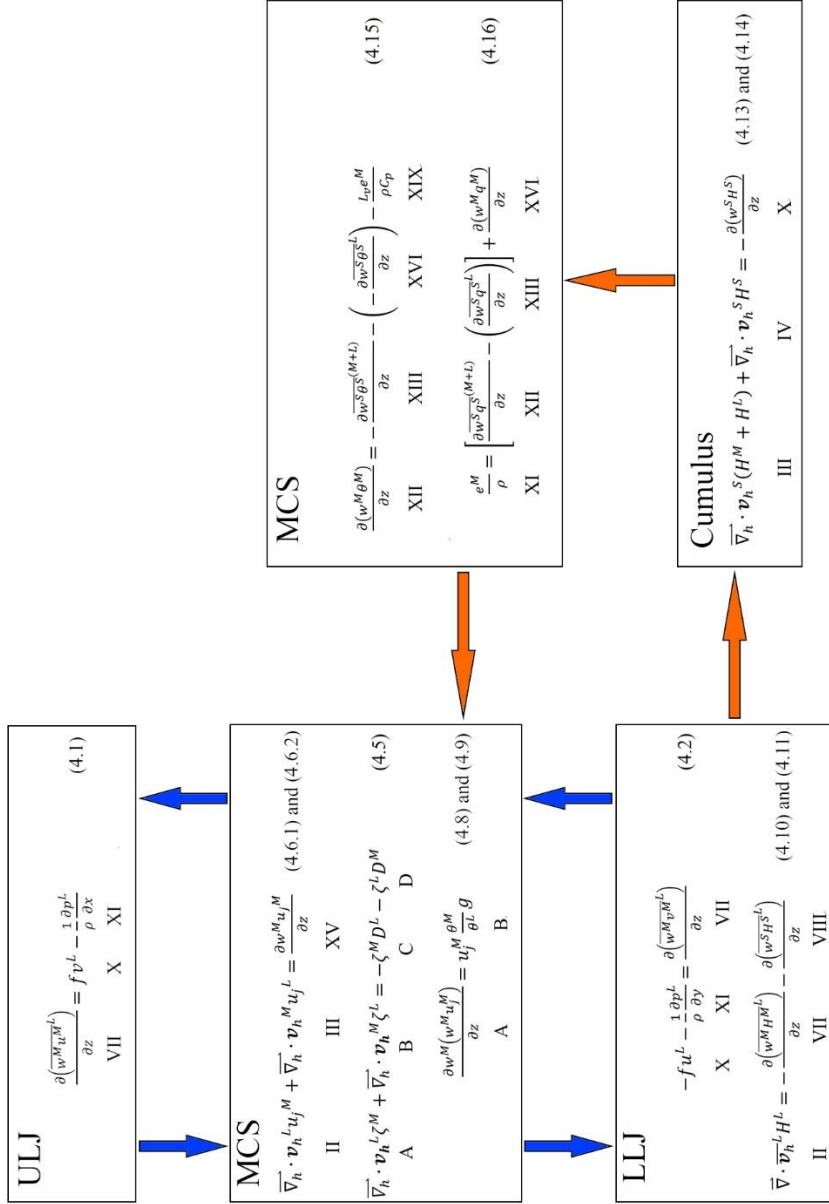


Figure 4.5 MCS-centric flow chart showing the essential interactions of MCS with jets and cumuli. Blue arrows indicate the dynamic circulation between LLJ and ULJ with respect to MCS, while orange arrow indicates the MCS thermodynamic circulation which enhances the ageostrophic circulation.

A mechanism of HRS in term of MCS is proposed. The mechanism is divided to the dynamic and thermodynamic circulations. The relevant MCS-centric flow chart is shown in Figure 4.5, in which crucial interactions in term of MCS can be found.

### 4.3.1 Dynamic circulation

The jet dynamics is ageostrophic, especially in the jets' exit regions. It is the result of the geostrophic balance which is altered by the presence of MCS vertical flux divergences. The vertical flux divergence of MCS's horizontal momentum in large area supports the ageostrophy of the jets. The most important characteristic of Eq. ( 4.1 ) and ( 4.2 ) is that the vertical flux divergence of MSC is related to the jets' ageostrophy of the jets, as these equations can be rewritten as

$$f v_a^L - \frac{1}{\rho} \frac{\partial p_a^L}{\partial x} = \frac{\partial(\overline{w^M u^M})}{\partial z}, \quad \text{and}$$

$$\frac{\partial(\overline{w^M v^M})}{\partial z} = -f u_a^L - \frac{1}{\rho} \frac{\partial p_a^L}{\partial y},$$

respectively.

where subscripts  $a$  and  $g$  indicate the ageostrophic and geostrophic components, respectively.

The first equation states that stronger ageostrophy of ULJ gives larger mesoscale flux divergence, and the second equation larger flux divergence gives stronger ageostrophy of LLJ. Overall, these MCS flux divergences adjust the geostrophic balance associated with ULJ and LLJ in order to sustain the jets in ageostrophic manner. Thus, the flux divergences play a crucial role in the exchange of momentum between the jets.

As it is the linkage between the jets, MCS flux divergence is responsible for the maintenance of the heavy rainfall system. It means that, its associated flux divergence not only weakens the LLJ in the exit region [as mentioned in Section 4.1.1 b)], but also intensifies it in its entrance region.

Here is the mechanism. In the lower troposphere, the ageostrophy of the LLJ in the exit region leads to the dissipation of horizontal momentum through mesoscale vertical transport *in a large area* [Eq. ( 4.2 )], as shown in Figure 4.6 schematically. Respect to mesoscale, the corresponding gradient of MCS flux divergence contributes to the negative advection of positive (negative) mesoscale vorticity on its cyclonic (anti-cyclonic) side [see Eq. ( 4.5 ) and Figure 4.2]. The result is the decrease of mesoscale

vorticity in the exit region and hence the jet decelerates. In steady state, a balance is achieved among the horizontal advection of mesoscale vorticity, the divergence effects, and the gradient of MCS flux divergence, described by Eq. ( 4.6.1 ) and (4.6.2). It states that the MCS flux divergence, i.e. vertical transport of mesoscale horizontal momentum, balances the advections between the middle scale and the large scale mean flows.

In addition, the divergence effect tells that mesoscale vorticity at a point increases by two sources [Eq. ( 4.5 )], 1) The mesoscale vorticity is concentrated by large scale convergence, and 2) a portion of large scale vorticity is concentrated by mesoscale convergence.

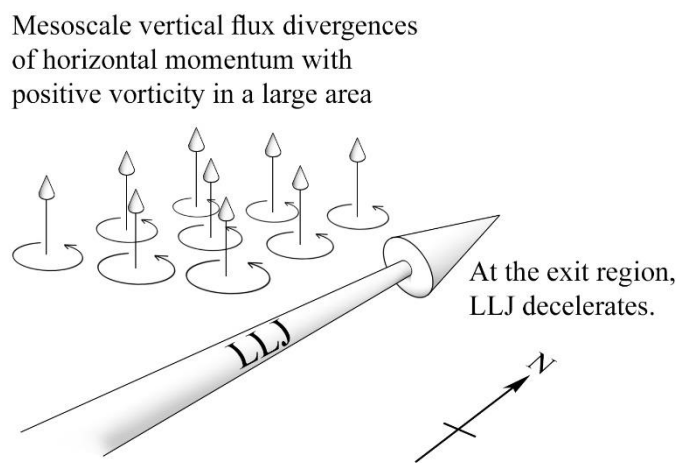


Figure 4.6 Schematic diagram showing the interaction between LLJ and MCS.

The horizontal momentum is transported vertically to the exit region of ULJ, as shown in Figure 4.7, constitutes the upward branch of the ageostrophic circulation. The ageostrophy of ULJ in the region is responsible for those MCS flux divergence transported. The ULJ decelerates as described by Eq. ( 4.1 ) as its geostrophic balance is altered due to the divergence of mesoscale horizontal momentum on its cyclonic side. Reverse process occurs on the anti-cyclonic side of the ULJ, where the mesoscale momentum is transported downward, to the anti-cyclonic side of the LLJ. This downdraft constitutes the downward branch of the circulation. The resultant gradient of the mesoscale flux divergence in the entrance region of the LLJ leads to increase of mesoscale vorticity, enhance the ageostrophy, and so the jet accelerates.

By this ageostrophic circulation, LLJ is intensified (weakened) in its entrance (exit) region, and thus it can be maintained. Maintenance of the LLJ means the maintenance of moisture transport on large scale, which use to fuel the convections of cumuli and MCSs. With this mechanism, the heavy rainfall system can be sustained. On the other



hand, the moisture which is transported vertically in cumuli and MCS plays a role of strengthening the corresponding circulation. The detail will be discussed in the next section.

### 4.3.2 Thermodynamic circulation

Heat and moisture on large scale are carried by the LLJ in the lower atmosphere. Eq. ( 4.10 ) and ( 4.11 ) state that these thermodynamic quantities advected by large scale mean flow contribute to the mesoscale and cumulus scale flux divergences.

Heat and moisture are transported vertically either by MCSs or cumuli, on large scale. For those transported by MCS, they must be transported by the mean of cumulus *first*. Heat is released mainly on small scale in the lower troposphere, while on mesoscale in the middle troposphere. Nevertheless, the mesoscale heat can be the result of the accumulation of small scale heat. No matter by MCS or cumuli, the heat and moisture at last are transported to the upper troposphere, especially the cyclonic regions shared by both jets, and potentially unstablize the region.

#### A Cumulus path:

Respect to cumulus, the flux divergence Term X is contributed by the entrainment and detrainment processes, i.e. Term III and IV, respectively, in Eq. ( 4.13 ) and ( 4.14 ). Cumulus entrains large scale and MCS heat and moisture, and detrains its own to the ambient environment. The net difference of these processes results in the upward transport of heat and moisture, as proposed in numerous cumulus parameterization schemes.

#### B MCS path:

Apart from the “traditional route” of cumulus heat/moisture contributes to large scale, which stated by the existing parameterization schemes, it can also contribute to MCS in concept. The effect of cumulus heat on MCS scale is reflected by Term XIII and XVI in Eq. ( 4.15 ). The cumulus latent heat accumulates and is transported on mesoscale. Another contribution is the mesoscale latent heat flux itself. They originate from mesoscale evaporation rate, which has two sources, as delineated by Eq. ( 4.16 ), 1) cumuli (net effect of Term XIII and XVI), it means that the cumulus moisture flux divergence on the MCS scale contributes to the mesoscale condensation rate and 2) the moisture flux divergence on mesoscale itself (Term XV). It implies that, MCS serves as an intermediate medium for the heat and moisture to convert from small to mesoscale through the condensation process. Hence, cumulus heat contributes to the mesoscale in two ways, by the direct contribution, or by small scale evaporation on MCS scale.

C Enhancement of the ascent

Respect to MCS, the ascending motion is enhanced by the buoyancy of MCS's air itself, as delineated in Eq. ( 4.8 ) and ( 4.9 ). Mesoscale heat flux divergence increases with the latent heat flux in MCS when condensation takes place (negative value of evaporation rate), as described in Eq. ( 4.15 ), and the potential temperature departure from its ambient environment increases with height. The increase in buoyancy is the result, as well as the instability of the region, i.e. the location of the MCS which located on the cyclonic sides of both jets, as shown in Figure 4.7. The instability enhances the ascent in the upward branch of the ageostrophic circulation. Reverse process occurs in the downward branch by the evaporation of the precipitation or water, and so downward motion is enhanced. As a result, the ageostrophic circulation is strengthened by the thermodynamic process. Ideally the mesoscale motion is located in the region where maximum vorticity can be benefited and also the largest flux divergence for the jets' ageostrophy can be produced. Based on the conditions mentioned, an ideal geometry, as shown in Figure 4.7, is established. The ageostrophic circulation is perpendicular to the ULJ's axis while less than 90° to the LLJ's axis.

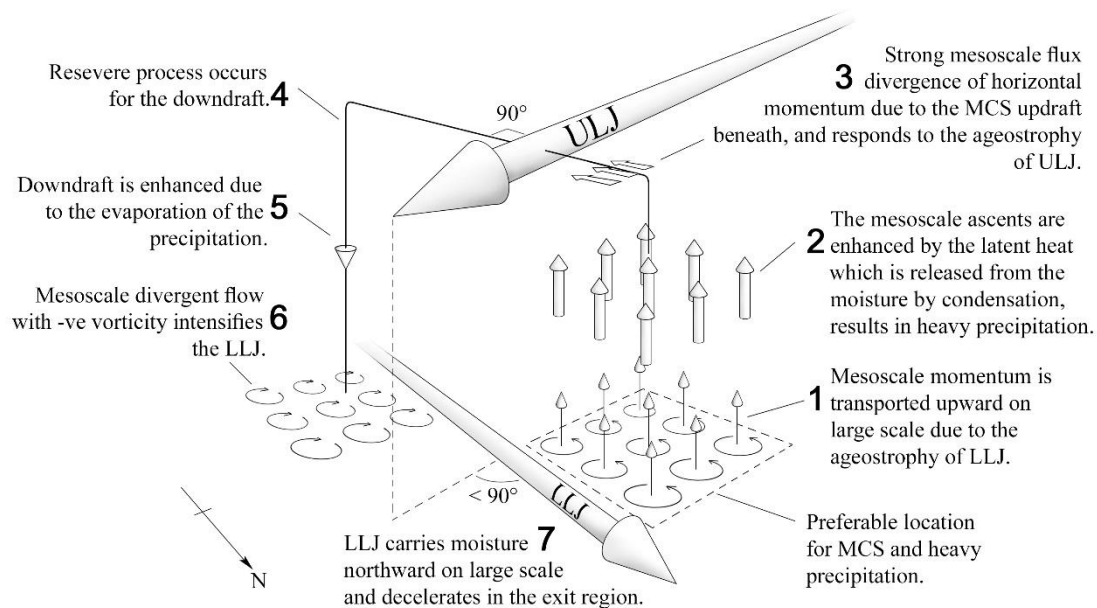


Figure 4.7 Collaboration of dynamic and thermodynamic circulations in a heavy rainfall system, i.e. Ageostrophic circulation between the jets enhanced by the buoyancy associated with MCS.

Overall, the result of the two paths are the same. Heat and moisture are transported vertically in the lower troposphere and latent heat is released through the phase change of the moisture in the middle troposphere. The presence of MCS is the result of vertical mesoscale heat and moisture flux divergence, and also the accumulation of cumulus moisture. Note that that the thermodynamic quantities also can be transported directly from cumulus scale to large scale. The dynamic circulation which associated with the position of LLJ and ULJ, determines a preferable location for these convections.



## 5 Numerical Experiment for MCS Diagnosis

In this chapter, the simplified middle scale equation of MCS will be verified by a numerical experiment. Verification of the equations by using numerical model is necessary since an observation is a quantity at a point which is measured with a specific resolution or on a specific scale. Using the simulated gridded data from numerical models allows us to translate the data on one scale to another upon the demand. The “translation” here refers to the averaging algorithm developed in Chapter 3. A pre-monsoon rainfall event in southeastern China is simulated by WRF on a parent and nested domains. The time period chosen for simulations is roughly the same as Case 2’s studied by Wu et al. (2011). Hence, this numerical experiment can be treated as an extended study based on their work. The results from the domains corresponding to the defined scales are used to visualize the interactions with respect to MCS.

Overall, this chapter is composed of 4 parts,

- 5.1) Background, which includes the aims and description of the experiment.
- 5.2) Experiment design, which is a technical part regarding to the model settings used in the simulation
- 5.3) Result analysis, where the interested terms are plotted and analyzed, and the significance of the interactions are evaluated.
- 5.4) Discussion based on the result, where the circulations will be evaluated and compared to the conceptual model. The deduced circulations and mechanism of the HRS in the event will be visualized.

## 5.1 Background

A pre-monsoon phenomenon in southeastern China was simulated using a numerical model WRF. Five domains, i.e. the parent domain with four nested domains, were introduced to the simulation. The selected case was on 13 June 2008, the beginning of the period when the “rain belt” located at the mid-lower reaches of Yangtze River [Ding (2008)]. In this pre-monsoon period, heavy rainfall has been observed along the coastal region of South China and its mechanism has been studied by Wu et al. (2010). The striking feature are a ULJ and a LLJ beneath. The presence of ULJ, LLJ, MCS (broad rainfall area) and the extent of rainfall fit the definition of HRS in this study. This system in reality therefore can be used as an example to investigate the proposed mechanism of the HRS.

Overall, the aims of this experiment are

- 1) To simulate the HRS with high resolution.
- 2) To estimate the terms in MCS equation.
- 3) To apply the equation for diagnosis.

## 5.2 Experiment Design

The simulation time begins on 12 June 2008 at 1800 UTC, and lasts for 2 days. The simulation was initialized by NCEP FNL reanalysis data with a resolution of  $1^\circ \times 1^\circ$ . After the spinning up for 1 day, the data at 1800 UTC on 13 June is used for the analysis. During this period, corresponding synoptic data shows that the rainfall area is located along the coastal region of southeastern China [see Figure 2(e) in Wu et al. (2011)].

In order to compute the interested terms in MCS equation, which consist of the quantities with different resolutions, the output from three domains corresponds to the representative resolutions have been selected for the computation. Table 5.1 shows the spatial and temporal (timestep) resolution of the domains in the simulation. The data on each domain is equivalent to *the mean* on the respective scales. Note that Domain 2 and 4 were not involved with the computation, since Domain 2 and 4 served as transient domains to keep the nesting ratio in a low value for reliable outcomes and numerical stability. By adding these two domains, nesting ratio of 3 is maintained in the simulation, and the only disadvantage is an extra expenditure of computer resource. The details of the selected domains are summarized in Table 5.2.

In addition, 48 vertical levels were used on all domains. The discretization halted when the model top reached 5 hPa level. For convenience, the outputs with eta coordination were transformed to Cartesian coordination in the analysis. The practical outputs have an identical spatial resolution as the inputs, while the only difference between them is the vertical layers which were interpolated to 42 layers in the outputs.

Figure 5.1 shows the positions of Domain 1, 3, and 5 introduced in the simulation. The nested domains are positioned according to the development of mesoscale disturbances (refer as MCS later) which are located in the exit region of an ULJ and on the cyclonic side of a LLJ.

Domain	Resolution (nesting ratio)			Scale represented
	$dx$	$dy$	$dt$	
1 (Parent)	54 km	54 km	6 sec	$Ll$
2	18 km (3)	18 km (3)	2 sec (3)	–
3	6 km (3)	6 km (3)	1 sec (2)	$Lm$
4	2 km (3)	2 km (3)	.5 sec(2)	–
5	.667 km (3)	.667 km (3)	.25 sec (2)	$Ls$

Table 5.1 Model configuration for the simulation.

Domain	No. of grid		Location in degree	
	$nx$	$ny$	Cen. Lat.	Cen. Lon.
1	175	100	30.0 N	117.5 E
3	508	367	30.7 N	120.7 E
5	1816	1174	28.5 N	119.3 E

Table 5.2 Setting of Domain 1, 3, and 5.

The quantity associated with  $Hl$  and  $Hm$  are computed from the data of Domain 3 and 5 respectively. The existence of Domain 1 is a must for the nesting process. The computation of perturbations from the outputs is based on the definition used when deriving the equations (see details in Chapter 3). The value on Scale  $Lm$  (Domain 3) was computed by averaging 81 values on Scale  $Ls$  (Domain 5), i.e. 9(9) points in  $x(y)$  direction on one single vertical level, while the value on Scale  $Ll$  (Domain 1) by 243 values on Scale  $Lm$  (Domain 3), i.e. 9(9) in  $x(y)$  direction on 3 vertical levels. Then the perturbation at a grid point is evaluated by the subtraction of the averages. For example, the perturbation of  $Hm$  was calculated by subtracting  $Ll$  value from the corresponding  $Lm$  value.

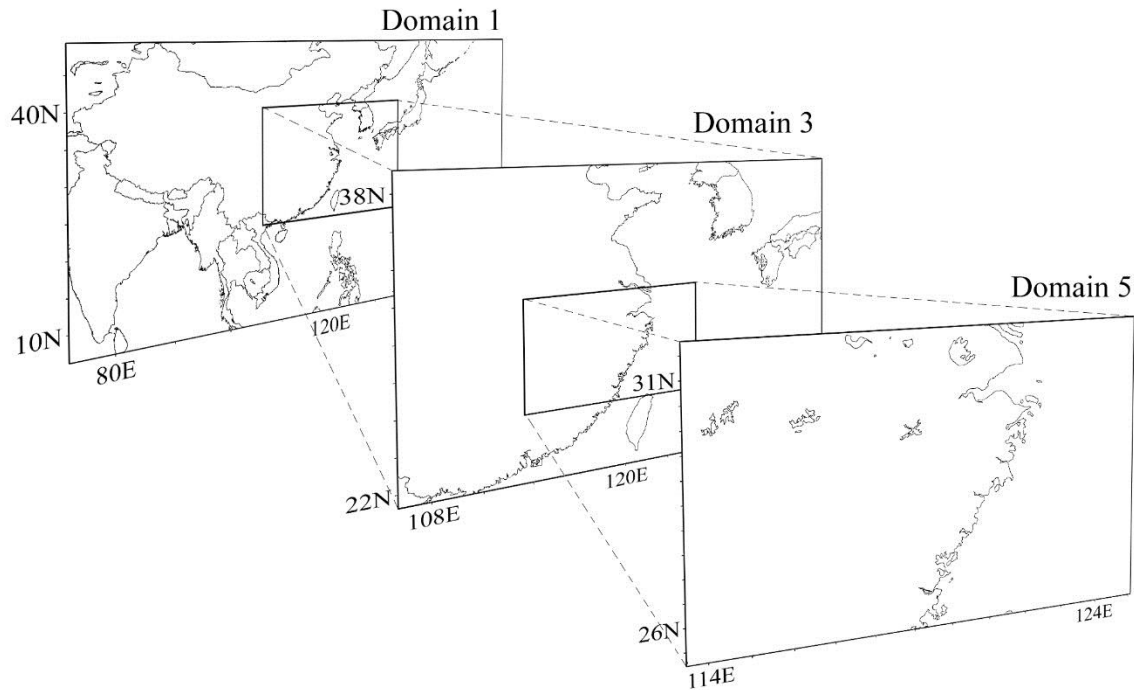


Figure 5.1 Domains of the simulation. Five domains are used in the numerical experiment, and Domain 1 (parent), 3 (nested), and 5 (nested) are used for analysis.

## 5.3 Result Analysis

In this part, the terms of the simplified equations are evaluated to verify the interactions among the three scales with respect to mesoscale. 1800Z 13 June 2008 is selected for the analysis as it is the mature state of the MCS.

### 5.3.1 General pattern

The position of jets in Domain 3 is depicted in Figure 5.2, with the LLJ at 2 km above ground level (AGL) extending from the coast of southeastern China to the southern Japan. The flow decelerates over the South China Sea, eventually a jet streak appears on the southeastern coast of China. The LLJ is southwesterly and its exit region coincided with that of the ULJ (to the west at 12 km AGL), which is consistent to what described in Chapter 2. Moreover, it is also located in the entrance region of the ULJ to the east simultaneously. This phenomenon of LLJ in the entrance region of ULJ has been studied by Chen (1982). The study shows that unstable gravity-inertia wave developed in the entrance region of ULJ has a triggering effect on the LLJ beneath.



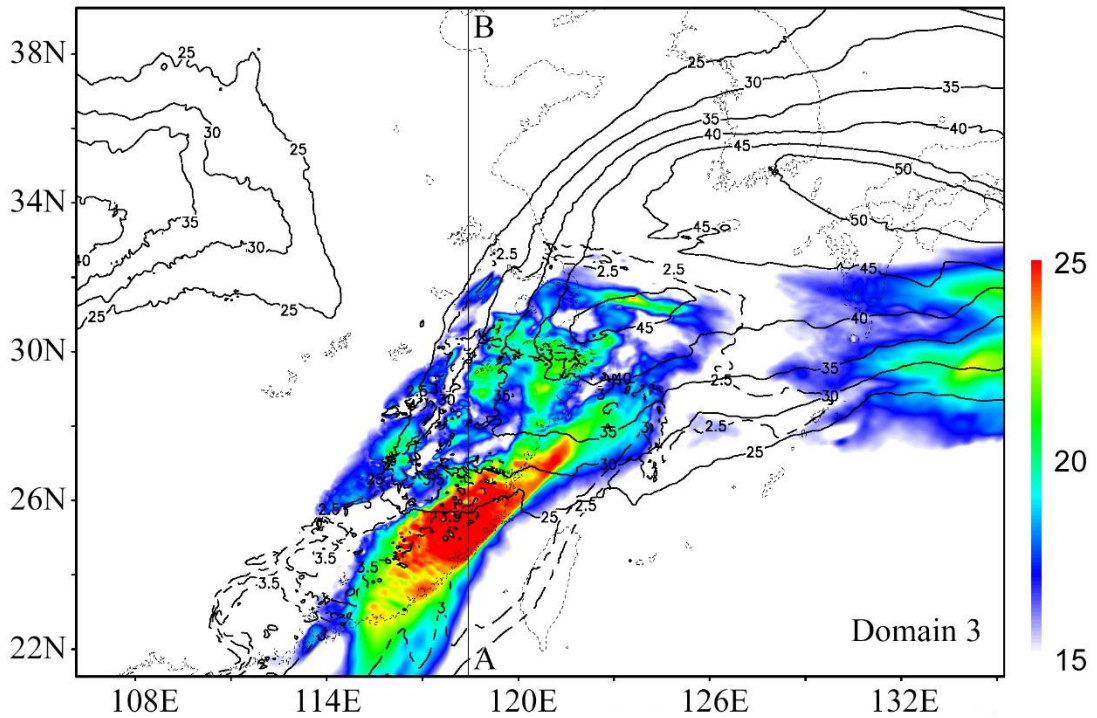


Figure 5.2 LLJ and ULJ in Domain 3. LLJ is in shading, ULJ in solid contour ( $\text{m s}^{-1}$ ), and water vapour mixing ratio at LLJ level ( $> 2.5 \text{ g kg}^{-1}$ ) in long dashed ( $\text{g kg}^{-1}$ ). Line AB at  $118.5\text{E}$  is for the cross section shown in Figure 5.22.

The location of this simulated LLJ is consistent with the synoptic charts in previous studies. The LLJ is often found in the coastal area between South China Sea and southeastern China. This orientation allows moisture transporting from the sea to the continent. This characteristic is represented by a “moist tongue” which coincides to the location of the LLJ, as shown by the mixing ratio contour in Figure 5.2.

In order to examine the mesoscale disturbances associated with the LLJ and ULJ, representative layers for the LLJ and ULJ are determined, the representative levels for the LLJ and ULJ are chosen to be 7 and 12 km AGL in all domains, respectively. Hereafter, “LLJ level” in this work means the representative LLJ level where the associated mesoscale interactions are the most obvious, while the representative ULJ level is same as the simulated.

### 5.3.2 Diagnosis on the event

In this section, the distribution of the interested terms in the simplified middle scale equations will be plotted. The result is used to determine the significance of the terms, and also the reliability of the involved processes.

#### A Dynamic circulation – LLJ and MCS

Recalling Eq. ( 4.2 ), the ageostrophic circulation associated with LLJ is balanced by the vertical flux divergence of mesoscale horizontal momentum in a large area. To examine this process and determine the significance of the terms involved, the distribution of each term is plotted at the LLJ level.

The distribution of ageostrophic zonal wind component  $u_a^L$  at 7 AGL in Domain 3 is computed by the left hand side of Eq. (4.2) divided by the Coriolis parameter which

varies with latitudes, i.e.  $u_a = \frac{-1}{f} \left( -f u^L - \frac{1}{\rho} \frac{\partial p^L}{\partial y} \right)$  (Figure 5.3). It can be obtained that

the jet streak is embedded in the positive value region.  $u_a^L$  reaches the highest value at the jet streak with its maximum extending downstream to the exit region on the right flank. It also indicates that the jet decelerates downstream due to the forcing arisen by  $u_a$ , and the associated ageostrophic circulation only dominates in the rear portion of the LLJ. Meanwhile, Figure 5.4 shows the distribution of Term VII, i.e. the right hand side of Eq. ( 4.2 ). It represents the effect of vertical transport of mesoscale horizontal (meridional) momentum on large scale. The negative region aligns with the LLJ on its cyclonic side, and the high value region coincides with the jet streak location. Accordingly, the mesoscale vertical transport of horizontal momentum is associated with the LLJ. In order to evaluate the relative contribution, the ratio of Term VII to

Term II and III, i.e.  $\frac{\partial(\overline{w^M v^M M^L})}{\partial z} / \left( -f u^L - \frac{1}{\rho} \frac{\partial p^L}{\partial y} \right)$ , is used. As shown in Figure 5.5, the high ratio region (the band in cyan – blue colour) coincides with the negative region in Figure 5.4. It suggests that the vertical flux divergence of the horizontal momentum explains at least 30% (pale cyan) of the ageostrophic circulation in the vicinity of the LLJ. Note that the ratio is *not* an absolute value, and thus the positive value suggests that the divergence flux is positively correlated to the ageostrophy. However, on the anti-cyclonic side, the value decreases though it remains positive correlation.

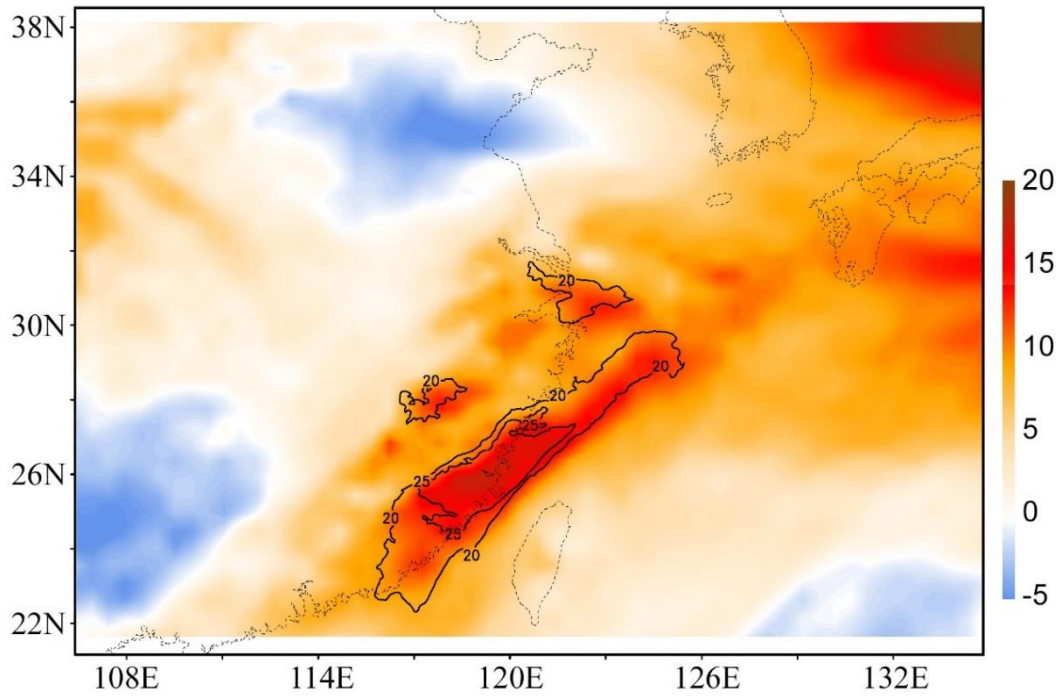


Figure 5.3 The distribution of ageostrophic zonal wind component ( $\text{m s}^{-1}$ ) at 7 km AGL, in Domain 3. Isotachs of LLJ ( $> 20 \text{ m s}^{-1}$ , horizontal wind) at the same level is shown for reference.

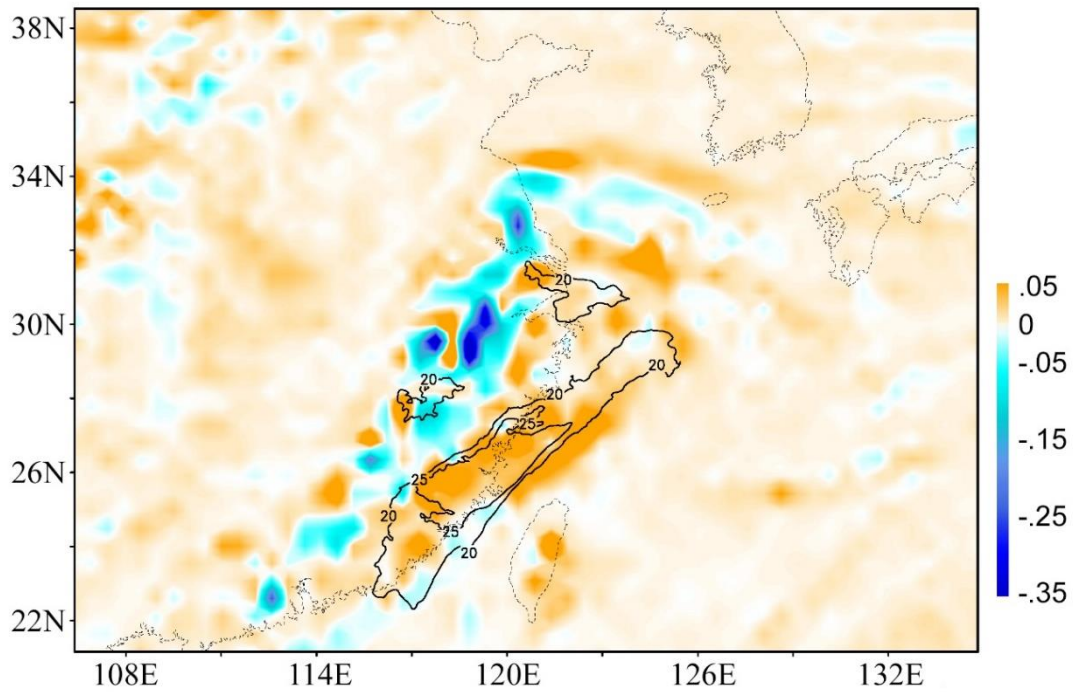


Figure 5.4 The distribution of  $\frac{\partial(\overline{wM_vM^L})}{\partial z}$  ( $\times 10^{-3} \text{ m s}^{-2}$ ), i.e. Term VII in Eq. (4.2).

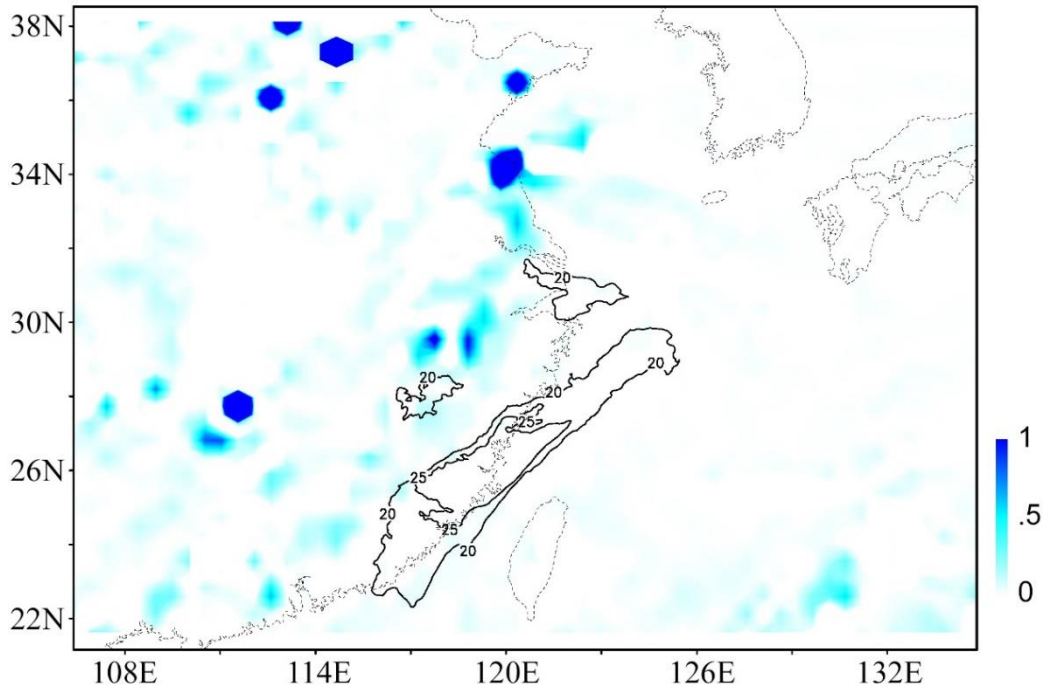


Figure 5.5 Ratio of vertical flux divergence of mesoscale horizontal momentum to the ageostrophic component [(Term VII / Term II + III) in Eq. ( 4.2 )]. Only the region with positive correlation is shown here.

### B Dynamic circulation – ULJ and MCS

Likewise, Eq.(4.1) which links the circulation of ULJ and MCS is verified. Unlike the LLJ, the pattern of ageostrophic meridional component  $v_a = \frac{1}{f} \left( f v^L - \frac{1}{\rho} \frac{\partial p^L}{\partial x} \right)$  at 11.5 km AGL forms a dipole in the region, as shown in Figure 5.6. The maximum (minimum) is located on the ULJ to the east (west) on its left (right) flank. This phenomenon resembles the LLJ's. It indicates that positive (negative)  $v_a$  is needed in order to accelerate (decelerate) the jet. As a result, strong gradient of  $v_a^L$  is generated between the entrance region of the ULJ to the east and the exit region of the ULJ to the west. Similar to LLJ, the distribution of vertical flux divergence of mesoscale zonal momentum [Term VII in Eq. ( 4.1 )] is associated with the ULJs (Figure 5.7). For the ULJ to the east, the positive (negative) region dominates on the left (right) flank and the maximum region coincides with the  $v_a^L$  maximum. Instead of a negative region with a  $v_a^L$  minimum to the west, the positive contribution of Term VII is suppressed, and the suppression coincides with the negative  $v_a$  region (see the middle white band in Figure 5.6 for reference). On the same propose, the relevant ratio is used to weight the significance of the terms (Figure 5.8). Positively correlated region fairly surrounds

the jet streak to the east, but dominates on the cyclonic side of the ULJ to the west. It implies that the forcing on the anti-cyclonic side of the ULJ to the west is affected by the presence of the ULJ to the east. Overall, similar conclusion can be made that the vertical flux divergence of the horizontal momentum explains at least 30% of the ageostrophic circulation on the cyclonic side of the ULJ to the west.

The orientations of the simulated ULJs in fact differ from that in the conceptual model. The flow in the entrance region of ULJ to the east is southwesterly and changes to westerly gradually downstream. In order to examine its southerly characteristic and the associated ageostrophic circulation, the corresponding ratio of Eq. ( 4.2 ) is used. However, the ratio are inconspicuous at 11.5 km AGL. Instead, the distribution at 10 km AGL is shown in Figure 5.9. The orientation of the high ratio region exhibits a similar manner as that of the LLJ. It is located on the left flank in the entrance region and dominates where the flow carries southerly component. Note that the high ratio region aligns in South – North direction.

Based on the finding of Part A and B, the vertical flux divergence of mesoscale horizontal momentum on large scale is associated with:

- 1) The location relative to the jets. The prominent region of the divergence flux is mainly located on the cyclonic side (left flank) of the LLJ and ULJ; while the corresponding region with opposite value on the anti-cyclonic side (right flank). This outcome explains how the large scale momentum converts to be of mesoscale where the LLJ/ULJ decelerates due to its ageostrophy. It can be obtained that the involved divergence flux accounts for at least 30% of the corresponding ageostrophic forcing.
- 2) Wind component of the jets. The mesoscale momentum component is determined by the ageostrophic component of the jet, which is related to the orientation of the jet.
- 3) Height. By comparing the distribution at LLJ level (7 km AGL) and where just below the ULJ (10 km AGL), it can be implied that the estimated vertical flux divergence of mesoscale meridional momentum in Eq. (4.2) decreases with height. One of the possible reasons is due to the stability at upper level and so the ascent is reduced. Another reason is due to the veering of wind associated with the LLJ's warm advection, and the resultant zonal component is responsible for ULJ's ageostrophy.



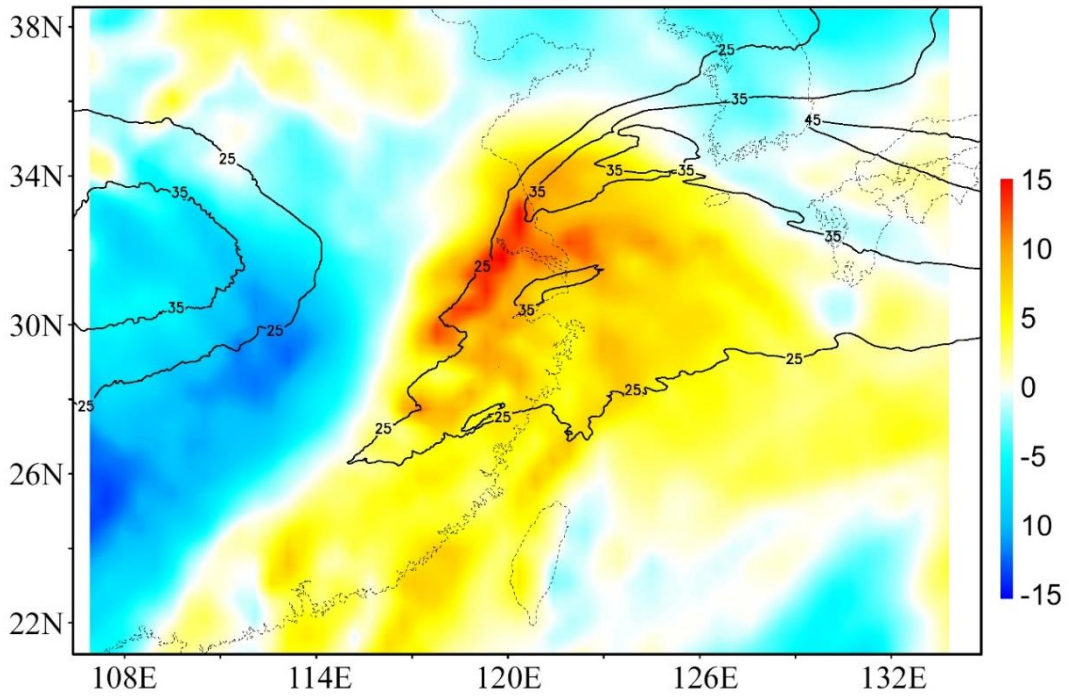


Figure 5.6 Same as Figure 5.3, but for the ageostrophic meridional component  $v_a$  ( $\text{m s}^{-1}$ ) of the ULJs at 11.5 km AGL.

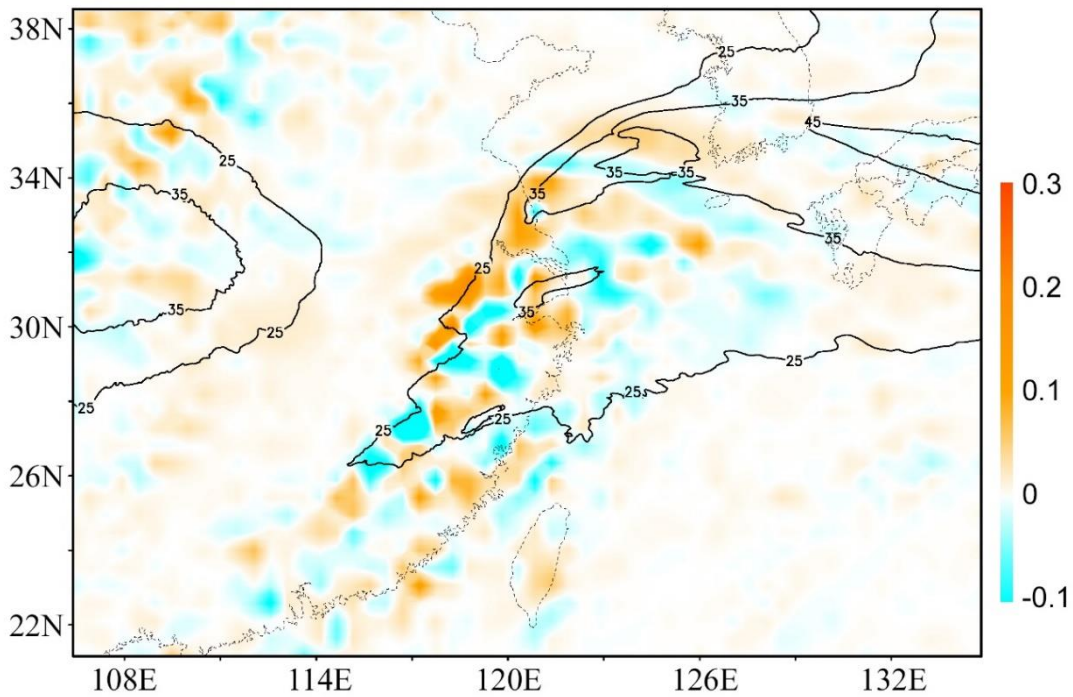


Figure 5.7 Same as Figure 5.4, but for  $\frac{\partial(\overline{w^M u^M L})}{\partial z}$  ( $\times 10^{-3} \text{ m s}^{-2}$ ), Term VII in Eq. (4.1).

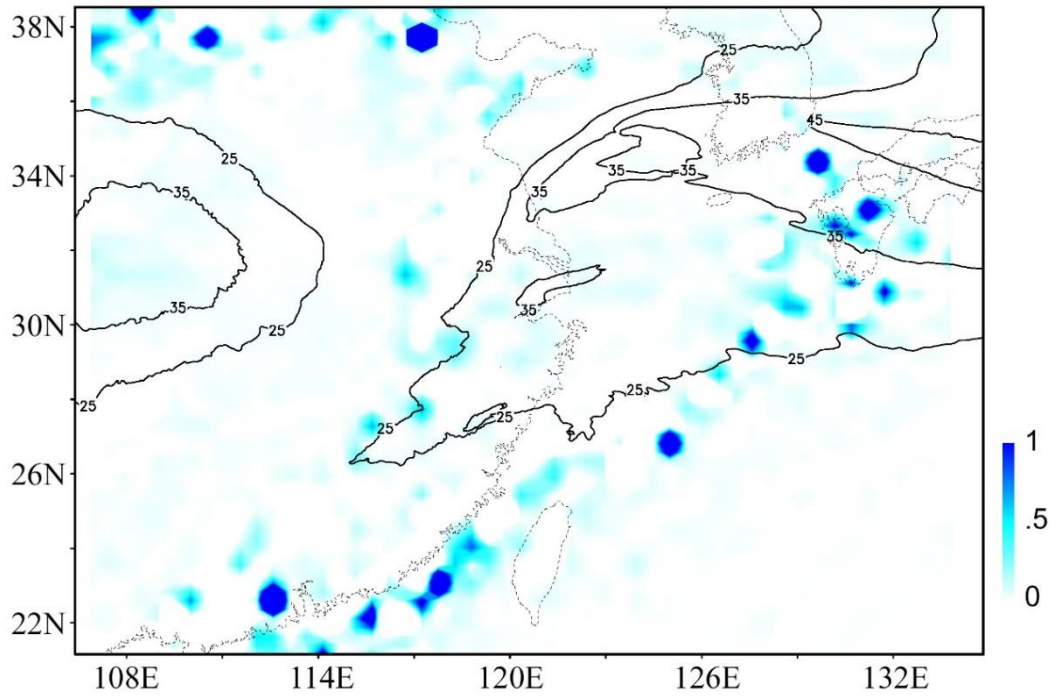


Figure 5.8 Same as Figure 5.5, but for the ratio respect to Eq. ( 4.1 ).

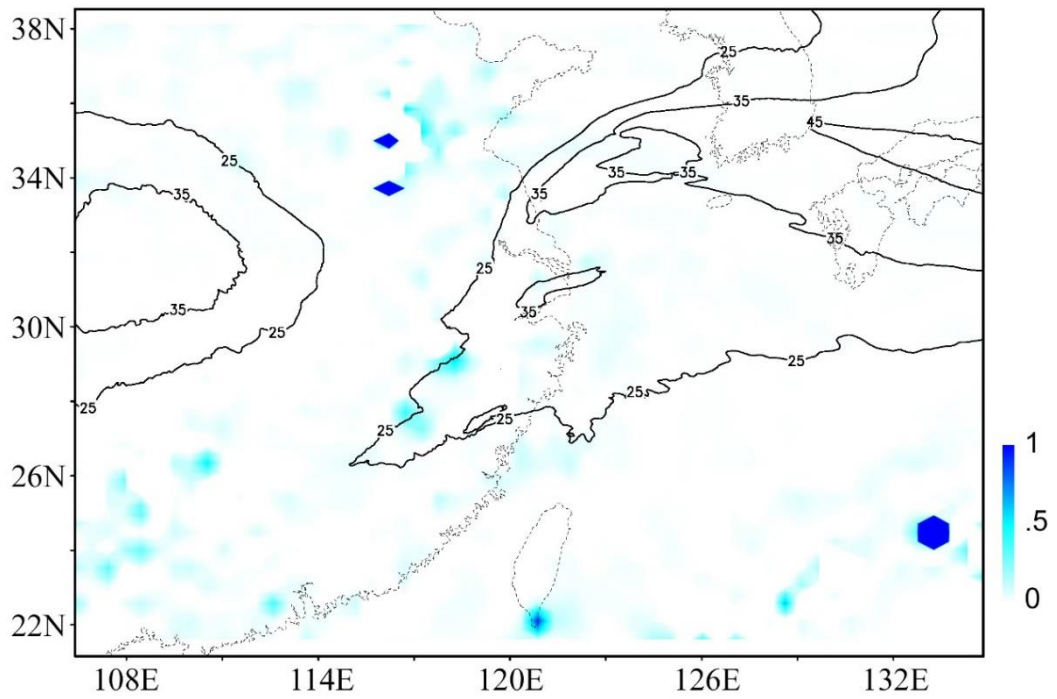


Figure 5.9 Same as Figure 5.5, but at 10 km AGL.

### C Dynamic circulation – MCS and large scale motion

In this part, Eq. (4.6.2) is verified to illustrate the interaction between MCS and large scale motion *with respect to mesoscale*. Figure 5.10 shows the advection process  $\overline{\nabla}_h \cdot \mathbf{v}_h^L \mathbf{v}^M$  (Term II) in Domain 3, at the LLJ level. Positive advection processes dominates on left flank of LLJ only, while negative on the right flank, near the jet streak. The region bounded by dash-dotted lines is dominated by positive mesoscale vorticity (For the detailed vorticity pattern, see Appendix C). As seen in the figure, the relevant positive advection is located in this bounded region, and note that they are in coincidence on the left flank of the LLJ. The dash-dotted line which halves the jet streak fairly splits the negative advection process (indicates in cyan colour) from the region. Likewise, the advection process described by Term III is shown in Figure 5.11. The pattern is similar to that in Figure 5.10, but the amplitude is higher. The positive advection process in the vicinity of LLJ extends northwestward to the dashed-dotted border to the west.

As mentioned in Section 4.1.3(A4), the increase of mesoscale vorticity in space involves both advection processes mentioned above and they can be considered as a whole. Figure 5.12 shows the total contribution of both Term II and III. It can be obtained that negative advection processes dominate the right flank of the LLJ. The dash-dotted border in the middle of the streak fairly keeps these negative processes out of the region. In addition, on the LLJ's left flank, the advection of mesoscale vorticity with a deeper red colour in the rear portion is more intensive in the exit region than that in the entrance region. Overall, the advection process between middle and large scale flows is associated with the LLJ. The positive advection processes is related to the positive mesoscale vorticity.



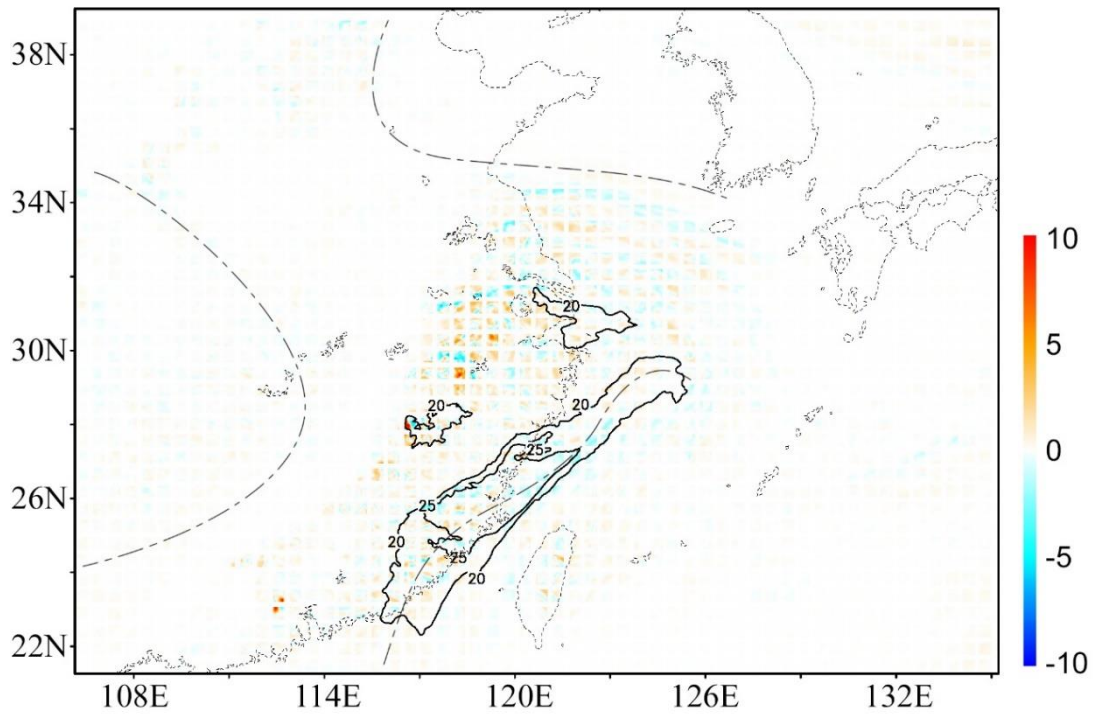


Figure 5.10 The distribution of  $\overline{\nabla_h \cdot \mathbf{v}_h^L v^M}$  ( $\times 10^{-3} m s^{-2}$ ) at 7 km AGL, i.e. Term II in Eq. (4.6.2). LLJ streak is represented by isotach of  $>20 m s^{-1}$  (horizontal wind). The region dominated by positive mesoscale vorticity is bounded by dash-dotted lines. The shading is presented in grids because the advection terms at the edges are undefined as they involve the averaged values of the adjacent averaged areas.

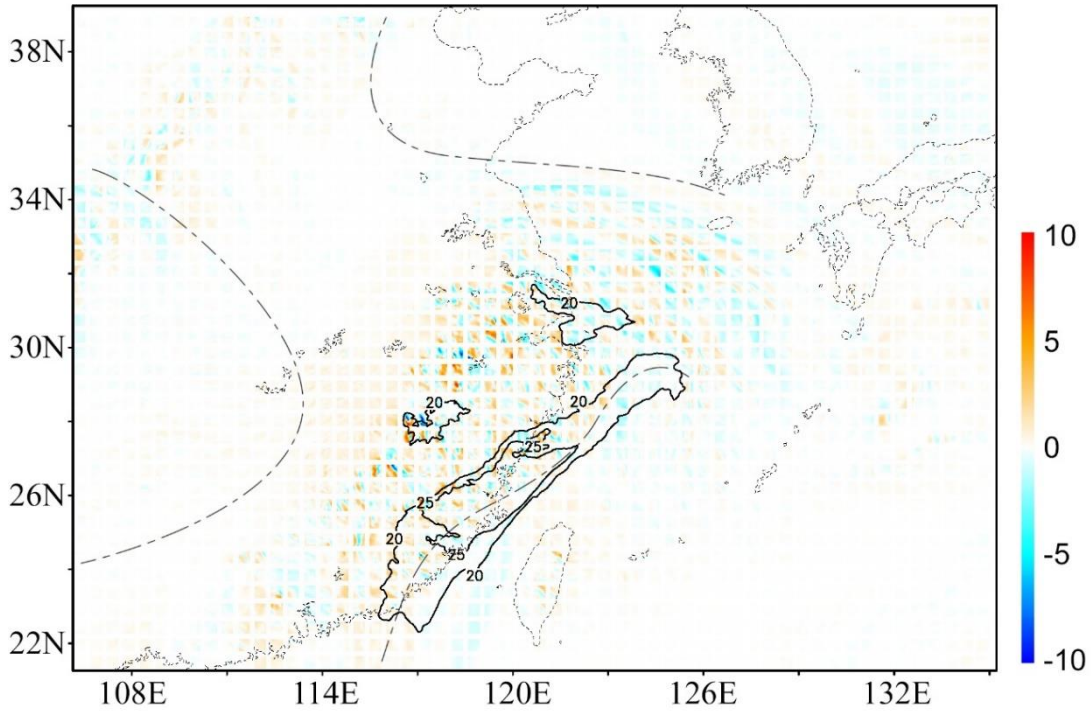


Figure 5.11 Same as Figure 5.10, but for  $\overline{\nabla}_h \cdot \mathbf{v}_h^M v^L$  ( $\times 10^{-3} m s^{-2}$ ), Term III in Eq. (4.6.2)

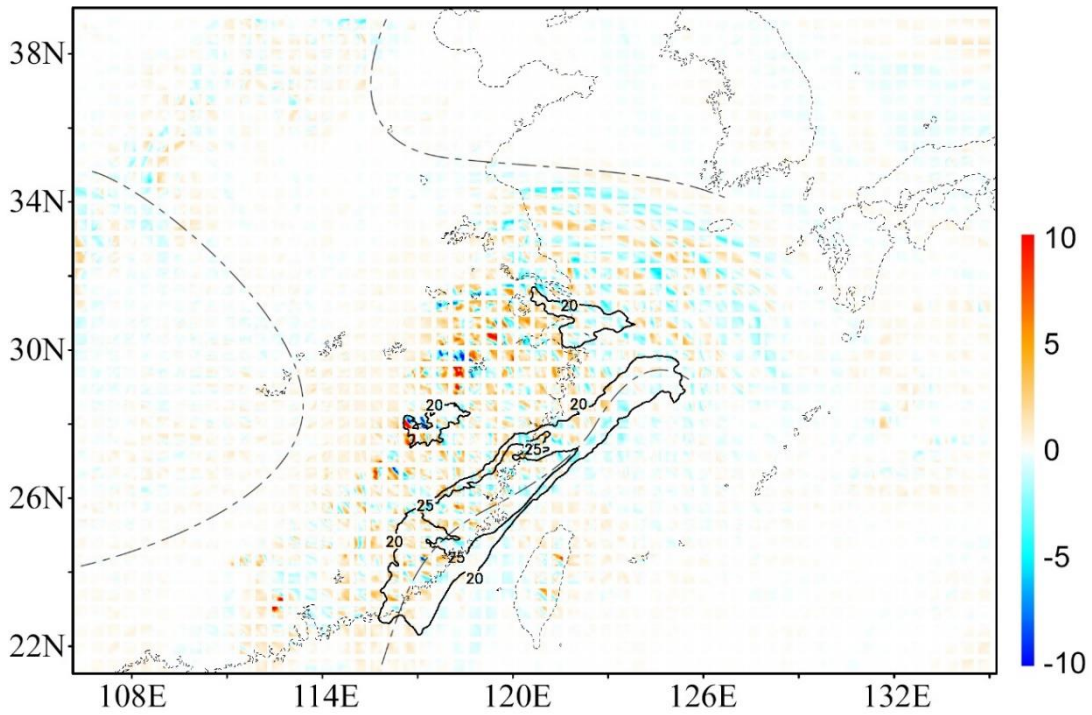


Figure 5.12 The total distribution of Term II and Term III in Eq. (4.6.2)

In Part A and B, the vertical mesoscale divergence flux on large scale has been studied. Respect to MCS, this effect can be analyzed in a resolved scale. Figure 5.13 shows the pattern of the corresponding term,  $\frac{\partial w^M v^M}{\partial z}$  [Term XV in Eq. (4.6.2)], in Domain 3 at the LLJ level. The red region, which represents positive flux divergence, coincides with the orange-red region in Figure 5.12. In addition, the broad red region is located in the positive vorticity region only, in alignment with the LLJ on its cyclonic side.

The counterpart ratio for Eq. (4.6.2) is used to weight the significance of the terms involved. The distribution of the ratio of Term XV/(Term II + Term III) is shown in Figure 5.14. Although the pattern is noisy, it can be obtained that the density of the high value (blue points) is higher in the bounded region and reaches maximum on the cyclonic side of LLJ. This suggests that in general the vertical divergence flux of mesoscale horizontal momentum is positively correlated to the advection processes between middle and large scale motions, especially on the cyclonic side of LLJ. According to the figure, the flux divergence explains about 50% of the advection processes which is associated with the LLJ.

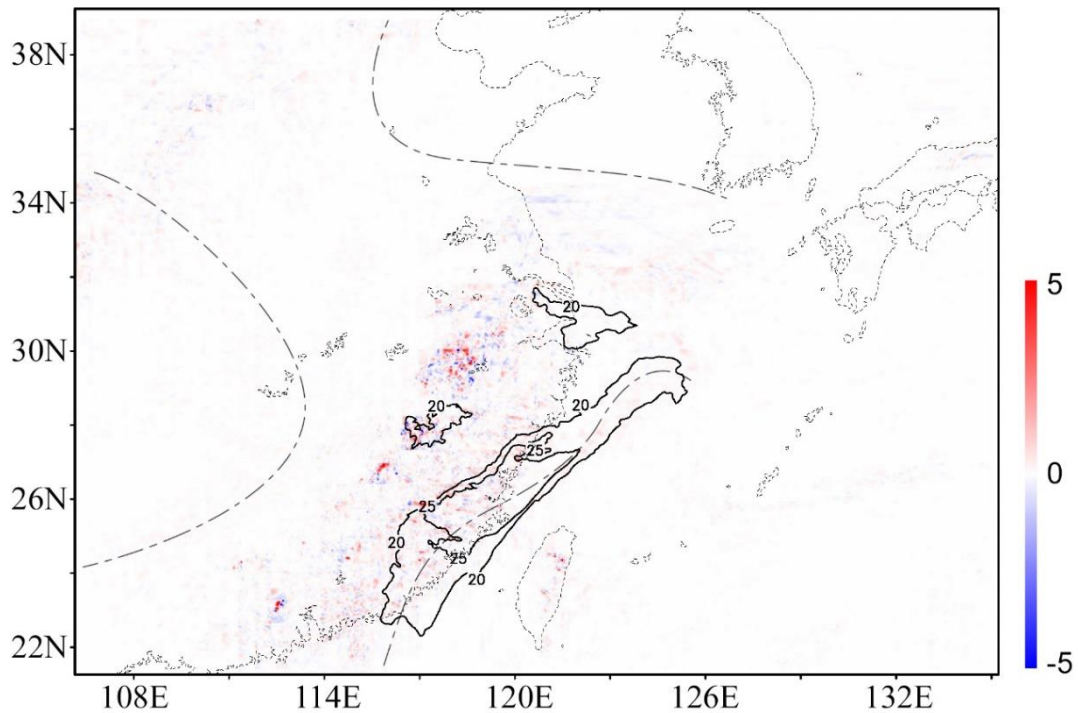


Figure 5.13 Same as Figure 5.4, but for  $\frac{\partial w^M v^M}{\partial z}$  ( $\times 10^{-3} \text{ m s}^{-2}$ ), Term XV in Eq. (4.6.2), at 11.5 km AGL.



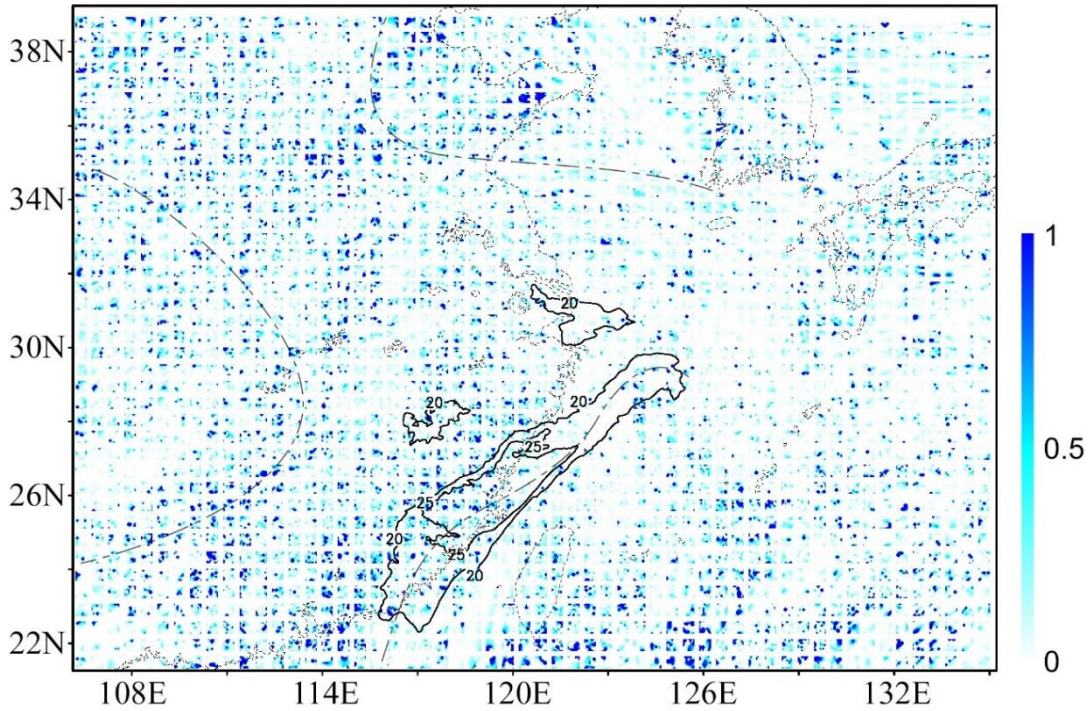


Figure 5.14 Same as Figure 5.5, but for the ratio of Term XV/(Term II + Term III) in Eq. (4.6)

#### D Thermodynamic circulation – MCS and Cumuli

In this part, the Eq. ( 4.15 ) and ( 4.16 ) are examined in order to find out how heat is generated by the condensation of moisture on middle and small scales. As the small cumulus scale is involved, Domain 5 which has the highest resolution is used for the analysis.

Before studying the heat issue, it is better to determine the moisture pattern first as it has been hypothesized that one of the heat sources is the latent heat released from the condensation of moisture. In order to visualize the effect on the moisture distribution, a higher level of 7.5 km AGL is used. This level is one output level higher than the representative LLJ level. Figure 5.15 shows the distribution of  $\frac{\partial(w^M q^M)}{\partial z}$  [Term XV in Eq. ( 4.16 )]. It shows that the vertical mesoscale moisture flux divergence is relatively gentle along the coastal region, but more intensive in the inland region. Two regimes with intensive flux divergence are developed at (29.5N, 118E) and (27.5N, 116.5E). The negative region represents the decrease of moisture flux due to condensation, while positive for evaporation. At this level, the flux divergence due to shallow cumuli are insignificant and it is assumed that any effect from cumulus scale can contribute on

mesoscale. The effect due to cumulus moisture flux divergence *on middle mean scale* [Term XIII in Eq. ( 4.16 )] is shown in Figure 5.16. It is obtained that the decrease of cumulus moisture flux divergence coincides with the location of the two regimes and it means that only condensations in small scale occur in those areas. Furthermore, the order of the magnitude is the same as that of Term XV. This implies that, above the jet level, the cumulus moisture flux divergence on mesoscale is also significant compared to that on mesoscale itself.

Note that the values of Term XVI are in the order of  $-8$ , i.e. 100 times smaller than the two terms mentioned, so it is ignored.

The total contribution of Term XV and XIII gives the total mesoscale condensation rate by MCS and cumuli, i.e. Term XIX in Eq. ( 4.16 ), but it is not shown here because it can be reflected by Term XIX in Eq. ( 4.15 ) which will be discussed later.

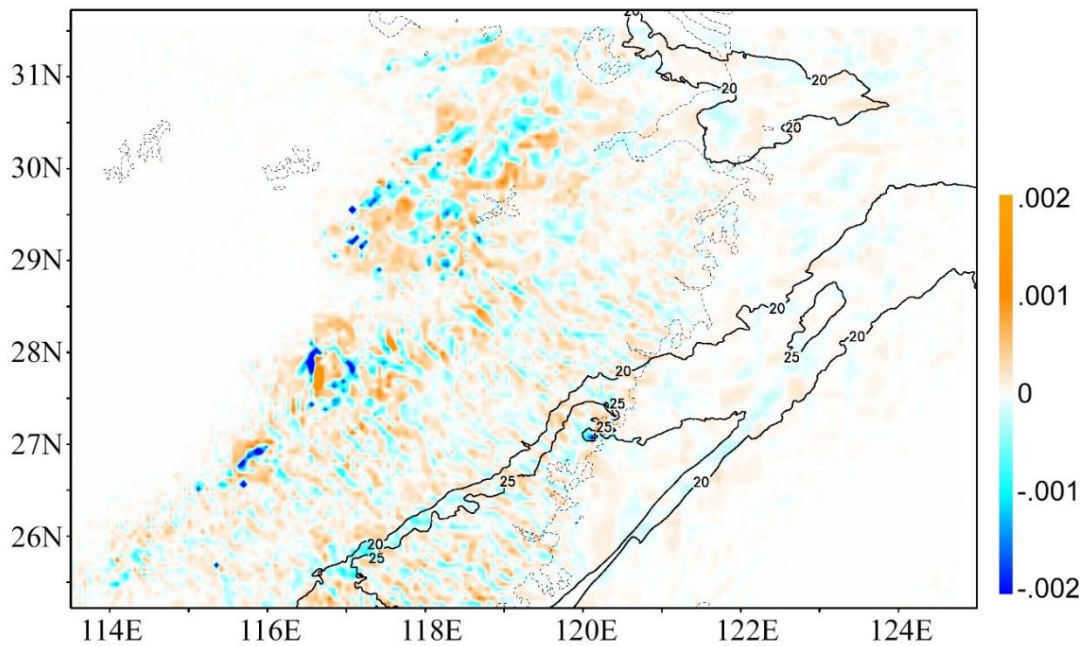


Figure 5.15 The distribution of  $\frac{\partial(w^M q^M)}{\partial z}$  ( $\times 10^{-3} \text{ kg kg}^{-1} \text{ s}^{-1}$ ) [Term XV in Eq. ( 4.16 )] at 7.5 km AGL, in Domain 5. Isotach of LLJ  $> 20 \text{ m s}^{-1}$  at 7 km AGL is shown for reference.

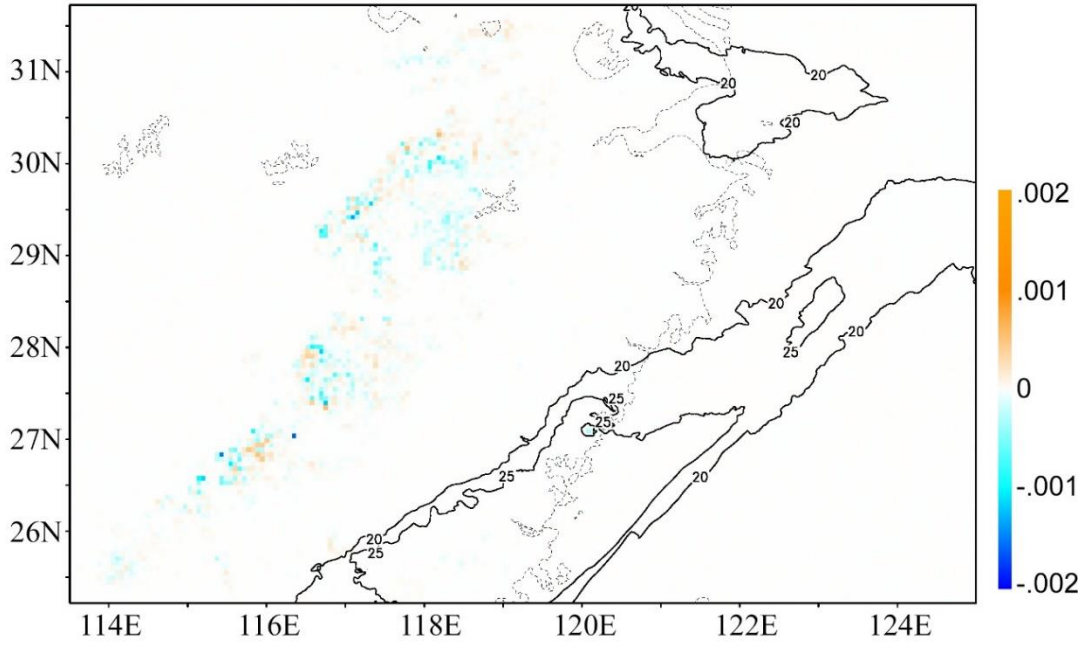


Figure 5.16 The distribution of  $\frac{\partial \overline{w^S q^S}^{(M+L)}}{\partial z}$  ( $\times 10^{-3} \text{ kg kg}^{-1} \text{ s}^{-1}$ ) [Term XIII in Eq. ( 4.16)].

The balance of mesoscale heat is described by Eq. ( 4.15 ). The mesoscale heat flux divergence  $\frac{\partial(w^M \theta^M)}{\partial z}$  is represented by Term XII, as shown in Figure 5.17. It is similar to the pattern in Figure 5.15. Two regimes with intensive flux divergences are developed. Note that this level is still 7.5 km AGL. In each regime, the upward flux divergence region (positive region) is larger than downward flux region (negative). It tends to organize in an irregular shape in one piece, while the regions with downward flux divergence exist individually.

The contributions to Term XII, as mentioned in Eq. ( 4.15 ), are Term XIX, XIII and XVI. Term XIX is a complex term as it involves Term XI in Eq. ( 4.16 ), latent heat of condensation  $L_p$  (function of specific mixing ratio) and heat capacity of vapour  $C_p$  which is a function of temperature.

Values of  $L_v$  and  $C_p$  are given by:

$$L_v = [2.501 - 0.00237T(\text{in deg. cel.})] \times 10^6 \quad (\text{J kg}^{-1})$$

$$C_p = C_{pd}(1 + 0.84q) \quad (\text{m}^2 \text{ s}^{-2} \text{ K}^{-1}) \quad \text{where } C_{pd} = 1004.67 \text{ m}^2 \text{ s}^{-2} \text{ K}^{-1}$$



The value of the latent heat flux divergence  $-\frac{L_v e^M}{\rho C_p}$  (Term XIX) at each point is then computed, with the given specific mixing ratio and temperature from the model output. Its pattern in the vicinity of LLJ is almost identical to that of Term XII, especially on its cyclonic side, as shown in Figure 5.18. The intensive flux divergence also coincides with the locations of those two regimes, so as the location of upward and downward regions. The contribution of cumulus heat on mesoscale is insignificant. As shown in Figure 5.19, the contribution is limited though upward flux divergences is located in the prescribed locations. Overall, it can be deduced that Term XII is mainly contributed by Term XIX. In other words, the mesoscale heat flux divergence can be almost determined by the mesoscale latent heat of condensation, provided that the corresponding evaporation rate originates from cumuli and MCS itself. Overall, it shows that moisture on small cumulus scale tends to evaporate on mesoscale and contributes to the mesoscale evaporation rate, rather than transporting the cumulus heat on mesoscale and contributes to mesoscale heat flux divergence directly.

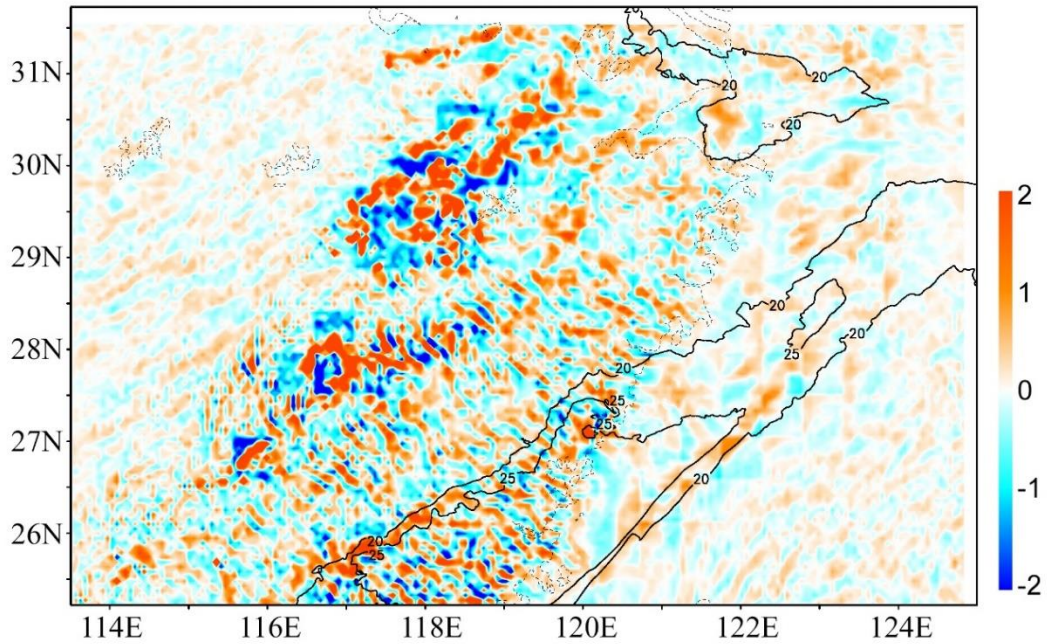


Figure 5.17 Same as Figure 5.15, but for  $\frac{\partial(w^M \theta^M)}{\partial z}$  ( $\times 10^{-3} \text{ K s}^{-1}$ ), Term XII in Eq. (4.15)

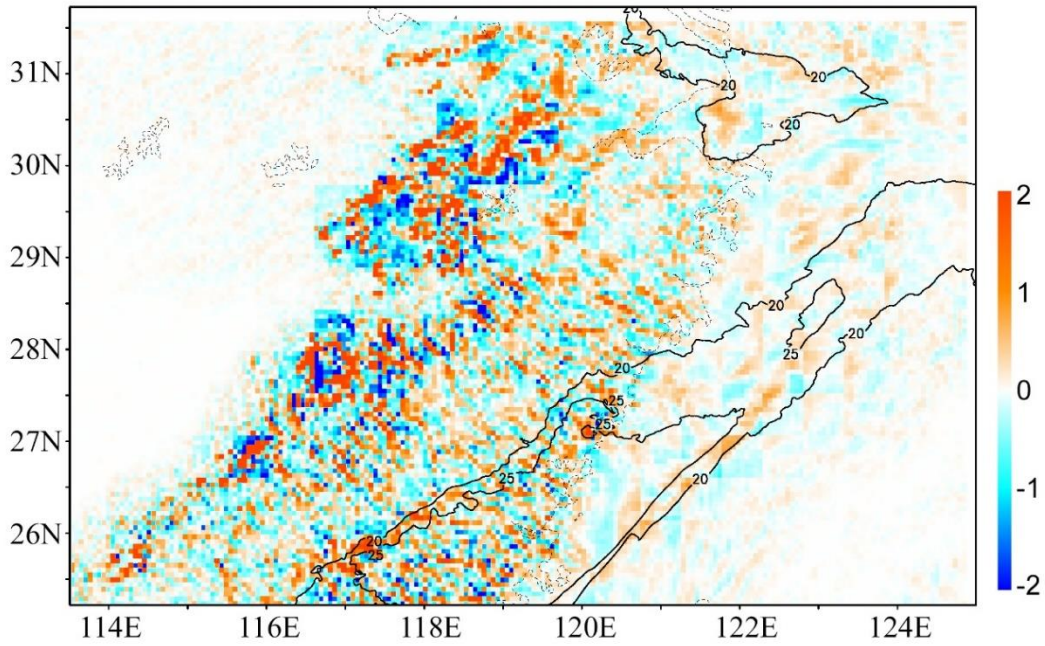


Figure 5.18 Same as Figure 5.17, but for  $-\frac{Lp e^M}{\rho C_p} (\times 10^{-3} \text{ K s}^{-1})$ , Term XIX in Eq. (4.15).

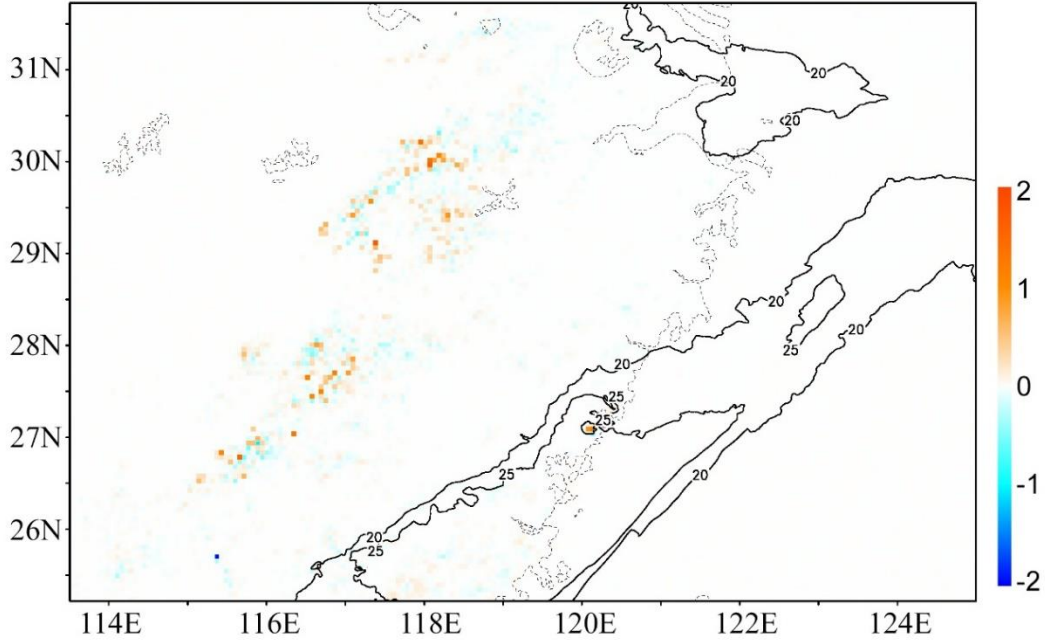


Figure 5.19 Same as Figure 5.17, but for  $-\frac{\overline{\partial w^S \theta^S (M+L)}}{\partial z} (\times 10^{-3} \text{ K s}^{-1})$ , Term XIII in Eq. (4.15).



## E Thermo-driving circulation – Collaboration of MCS dynamics and thermodynamics

So far the large-middle scale dynamics (Part A, B and C), and middle-small scale thermodynamics (Part D) have been analyzed. The key question is arising that how the former and the latter is related, in what form and to what degree. Eq. (4.9) is introduced to describe this linkage in steady state. Hence the terms will be investigated. Figure 5.20 shows the distribution of  $\frac{\partial w^M(w^M v^M)}{\partial z}$  (Term A) at 7.5 km AGL, in Domain 3. It implies that the vertical advection of vertical flux divergence of mesoscale horizontal momentum is significant in the jet region only. The flux is advected upward on the cyclonic side of the LLJ in the rear portion while downward in the front portion and near the entrance region.

The pattern of mesoscale horizontal momentum transported by buoyancy  $v^M \frac{\theta^M}{\theta^L} g$  (Term B) is shown in Figure 5.21. The transport of mesoscale momentum by buoyancy is mostly found on the cyclonic side of the LLJ in the rear portion, extends from the jet streak to the exit region, while by subsidence air in the front portion and on the anti-cyclonic side in the exit region. It is in agreement with the proposed mechanism in Chapter 4. It is noted that the positive region is bounded by the dash-dotted line in the LLJ's exit region. Moreover, these regions coincide to the highly positive vorticity (represented by red shading in Appendix C) because the ascending motion, which contributed by buoyancy, is associated with positive vorticity.

The magnitude of Term XIX is an order higher than that of Term XV. It is suggesting that the Term XV is one of the terms contributed by Term XIX. Other factors, such as the horizontal advection terms on the same scale, have been considered. However, the magnitudes of those horizontal advection terms are small compared to that of Term XV (not shown here), and so the resultant pattern is similar to Figure 5.20. Overall, it shows that the horizontal (meridional) momentum transported by buoyancy explains ~10% of the increase of vertical momentum flux with height. The locations of transport by buoyancy and subsidence are consistent to the proposed mechanism of HRS in Chapter 4.

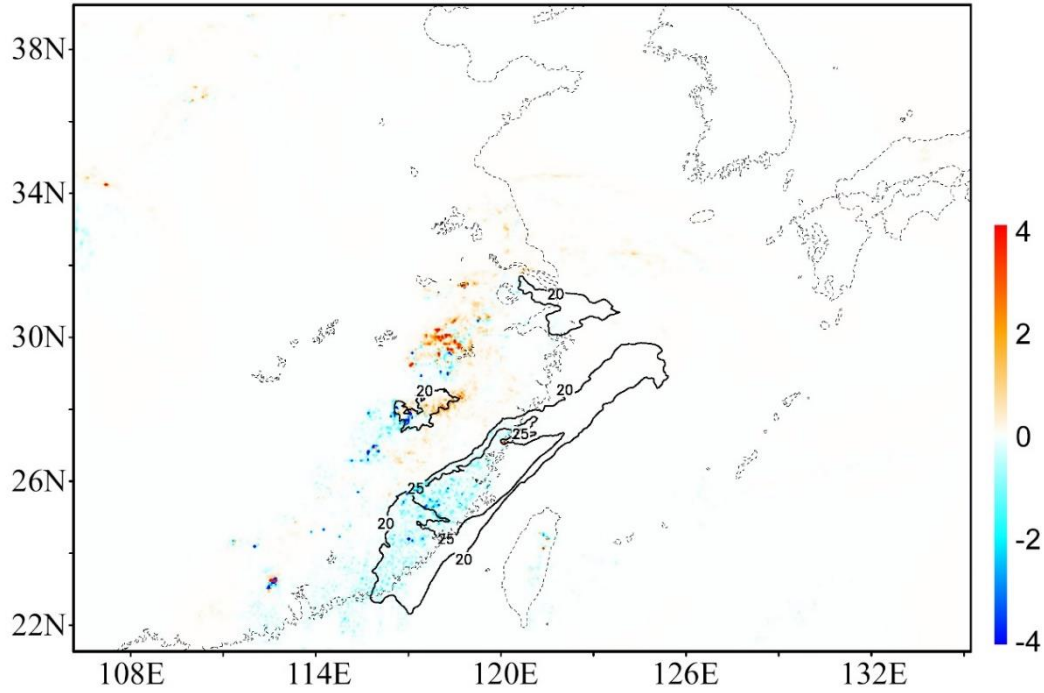


Figure 5.20 The distribution of  $\frac{\partial w^M(w^M v^M)}{\partial z}$  ( $\times 10^{-3} \text{ m}^2 \text{ s}^{-3}$ ) at 7.5 km AGL, i.e. Term A in Eq. (4.9). Isotach of LLJ  $> 20 \text{ m s}^{-1}$  at 7 km AGL is shown for reference.

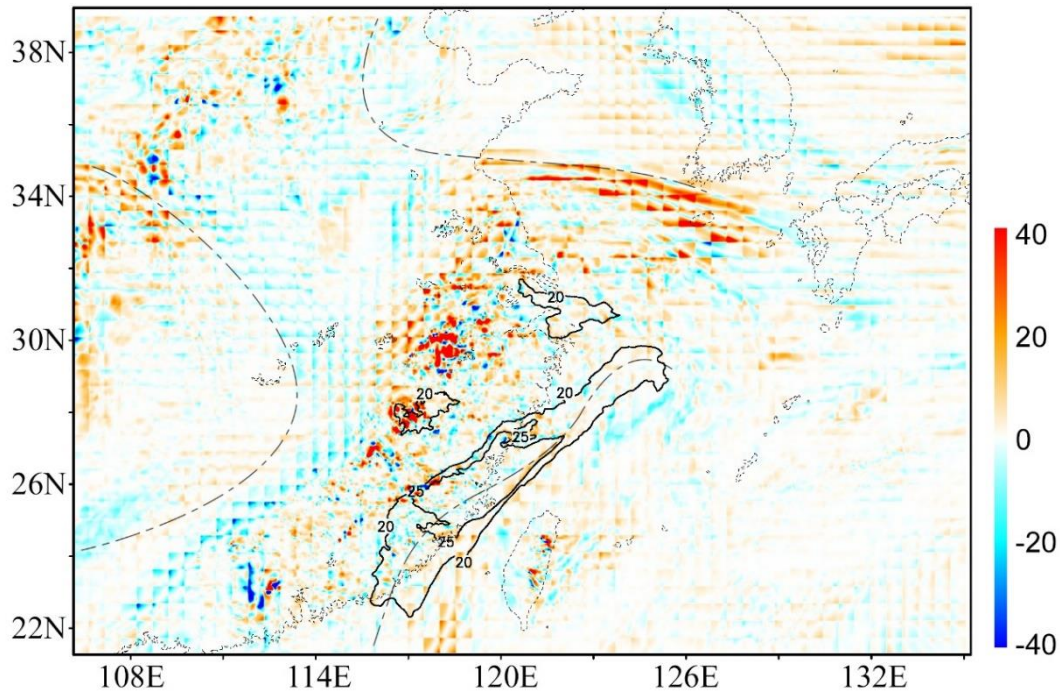


Figure 5.21 Same as Figure 5.20, but for  $v^M \frac{\theta^M}{\theta^L} g$  ( $\times 10^{-3} \text{ m}^2 \text{ s}^{-3}$ ), i.e. Term B in Eq. (4.9). The region bounded by dash-dotted line is dominated by the positive mesoscale vorticity.

## 5.4 Conclusions and Discussion

### 5.4.1 Evaluation of the dynamic circulation

In Section 5.3.2(A) and (B), the circulation between LLJ and ULJ was simulated. The result showed the mesoscale horizontal momentum was vertically transported between the jets due to their ageostrophy, especially in the LLJ's exit region. It means that the upward branch of the circulation was stronger than the downward branch. The horizontal mesoscale flux divergence, i.e. Term III and IV, were also evaluated. Although their magnitudes are in the same order as their vertical counterparts, their patterns (not be shown here) showed that horizontal mesoscale transport on the large scale is somewhat independent of the jet's ageostrophy. Overall, the pattern shown in Figure 5.5 was in agreement with that in Figure 4.2. Highly negative gradient of mesoscale flux divergence was obtained in the exit region, while positive gradient in the entrance region, though the gradient is weaker. The fairly negative value in the entrance region was responsible for the acceleration of the jet, hence the maximum of the jet streak is located ahead of it.

To ensure the existence of the vertical branches, the vertical velocity cross-section of *middle mean scale* along 118.5E (Line AB in Figure 5.2) is plotted, as shown in Figure 5.22. The cross-section lies between the anti-cyclonic side of the entrance region (south) and the cyclonic side of the exit region (north), i.e. it is on the same plane as the ageostrophic circulation illustrated in Figure 4.7. Ascents are obtained at 28N, 29N and 30N, while downdrafts at 22N and 24N. The intensity of the updrafts is stronger than that of downdraft, which is consistent with Figure 5.5. Moreover, it is found that the paths of the vertical motion are tilted toward the ULJ to the west, and the degree of tilting increases with latitude. This implies that the shape of the circulation is affected by the position of the jets.

In Section 5.3.2(C), the balance of advection between middle and large scales and the mesoscale flux divergence was clearly presented. Figure 5.12 shows that positive (negative) horizontal advection occurred on the cyclonic (anti-cyclonic side), contributed to positive (negative) vertical flux divergence. The balance can be fairly achieved, especially on the cyclonic side, as shown in Figure 5.14. The mesoscale vorticity was increased due to the horizontal momentum advection on the cyclonic side of LLJ, in order to sustain the jet itself. At the same time, the gradient of the corresponding flux divergence decreased.

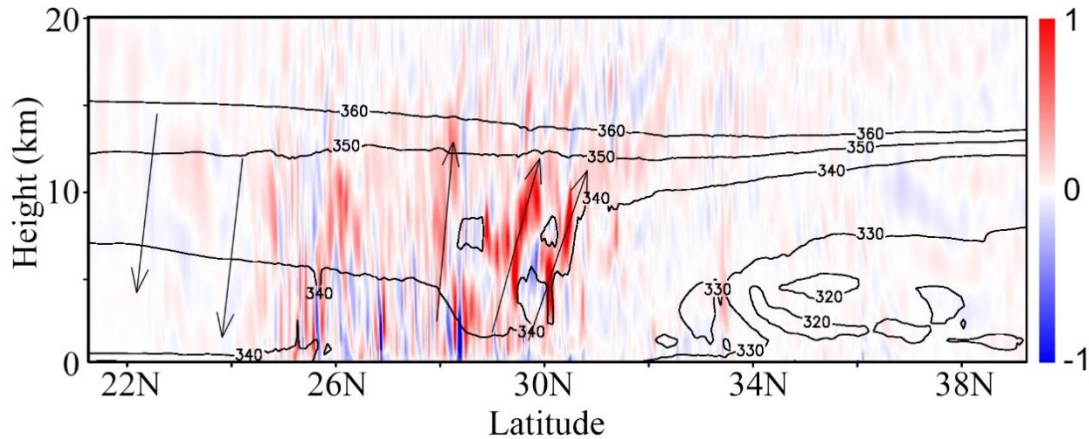


Figure 5.22 The cross section at 118.5E i.e. Line AB in Figure 5.2. Shading represents vertical velocity ( $\text{m s}^{-1}$ ), while arrows indicate the position of updrafts and downdrafts. Contour shows the distribution of equivalent potential temperature (K).

#### 5.4.2 Evaluation of thermodynamic circulation

In Section 5.3.2(D), the enhancement of vertical mesoscale flux divergence was presented. The magnitude of mesoscale moisture flux divergence (Figure 5.15) was comparable to that of cumulus on the corresponding scale (Figure 5.16). The contribution of cumuli dominated in the regions of the mesoscale disturbances only. It means that the mesoscale condensation rate was not only contributed by the corresponding moisture flux divergence, but also by that of cumulus on mesoscale. Meanwhile, the mesoscale heat flux divergence was mainly contributed by the corresponding latent heat flux divergence, i.e. the pattern of Figure 5.17 resembles that of Figure 5.18, rather than by cumulus heat flux divergence. It implies that, moisture tended to evaporate on small cumulus scale, together with the counterpart on mesoscale, contributed to the mesoscale latent heat flux divergence. On the other hand, at the level of the mesoscale disturbance, heat could be transported on small scale and contributed to mesoscale directly. However, this effect was insignificant (Figure 5.19).

The result in Section 5.3.2(E) showed that the vertical transport of mesoscale momentum flux divergence was only one of the factors contributed by the buoyancy transport. The ratio of Term XV / Term XIX in Eq. ( 4.7 ) was also investigated, and it showed the value around 0.1 in the LLJ's vicinity (pattern is not shown here). It implies that the buoyancy of air contributed little to the transport of momentum flux divergence on mesoscale. However, the buoyancy enhanced the ascents in the exit region. Referring to Figure 5.22, the upward motion region dominates at the level higher than 7 km AGL. The two striking updrafts, which corresponding to the maximum of mesoscale heat flux

region (Figure 5.17), extends to the ULJ level. Note that the bright red area of these two updrafts become larger above 7 km AGL. On the contrary, such enhancement is absent in the downward branch of the circulation. Due to the limitation of Domain 5, the subsidence of air corresponding to the downward branch is unable to be investigated deeply.

### 5.4.3 Evaluation of the MCS

As proposed in the conceptual model, the MCS enhances the potential instability. As shown in Figure 5.22, the instability increases at the location of the updrafts, indicated by the increase of (middle scale mean) equivalent potential temperature ( $\theta_e$ ) with height. To the south of the updrafts, the atmosphere is stratified and relatively stable. Figure 5.23 shows the distribution of  $\theta_e$  at 7.5 km AGL in Domain. It shows that in the location of the mesoscale disturbances high  $\theta_e$  is drawn from the “tongue” and so the instability is higher than the ambient region.

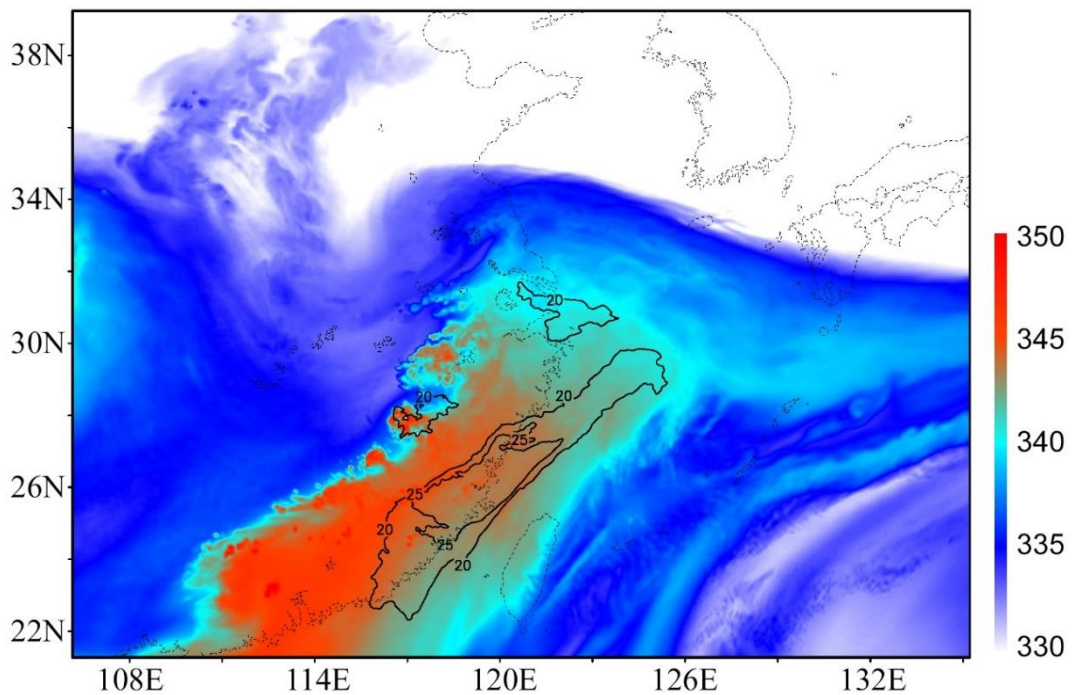


Figure 5.23 Equivalent potential temperature (K) distribution at 7.5 km AGL, in Domain 3.

Note that this  $\theta_e$  tongue is almost identical to the shape of the moist tongue shown in Figure 5.2. Apart from the instability, it has been mentioned that precipitation occurs in the position of MCS. Therefore, rain water mixing ratio is another signature of MCS. The pattern of this quantity is shown in Figure 5.24. It is obtained that the location of the highest rain water mixing ratio region agrees with that of the mesoscale disturbance.



To sum up, in these region, ascents occur and are enhanced at the level about 7 km AGL, with a high rain water content. This outcome is consistent with what proposed in the conceptual model. Hence, it can be confirmed that the mesoscale disturbances with these updrafts are the MCS components of the HRS.

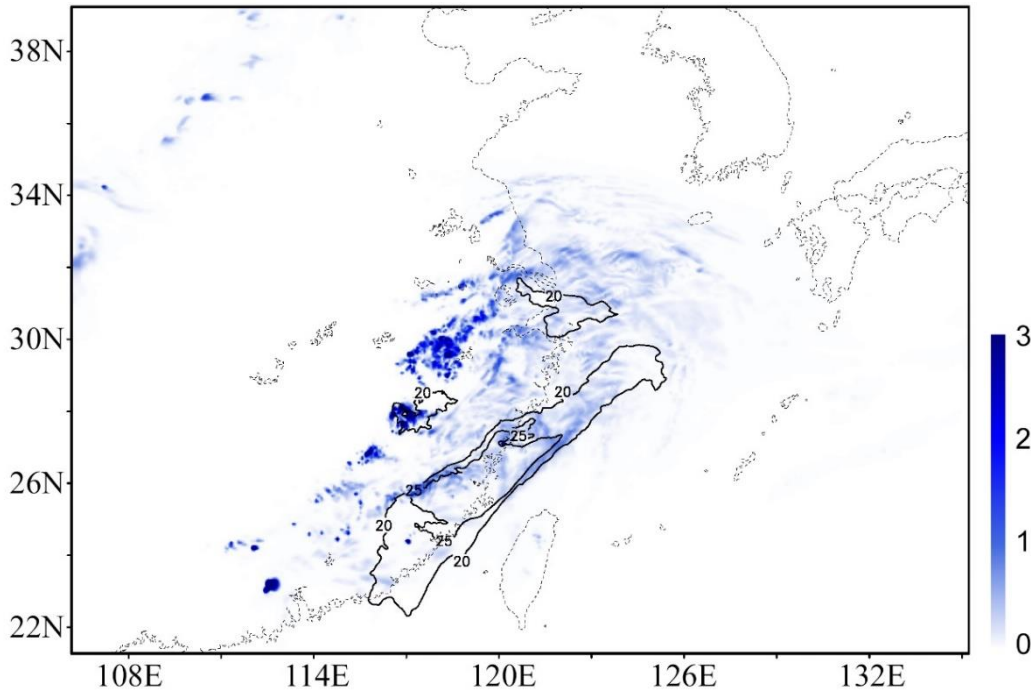


Figure 5.24 Same as Figure 5.23, but for rain water mixing ratio ( $\text{g kg}^{-1}$ ) at 7.5 km AGL.

The thermodynamic relation between MCS and the large scale motion is also investigated. Figure 5.25 shows the horizontal advection of moisture associated with LLJ [Term II in Eq. ( 4.11 )] at 7 km AGL. Negative value here means the advection of moisture from wet to dry region. It can be obtained that the advection extends to the MCS regions. Comparing the pattern with the corresponding averaged mesoscale moisture flux divergence (Term VII) which is shown in Figure 5.26, the horizontal moisture advection explains about 25 – 50% of the mesoscale moisture flux divergence in the MCS regions. Moreover, at the LLJ level, the contribution to the cumulus moisture flux divergence (Term VIII) is not significant (Figure 5.27). However, at the level below the LLJ streak, the contribution of the cumulus moisture flux divergence is higher by an order of 2 (not shown here).

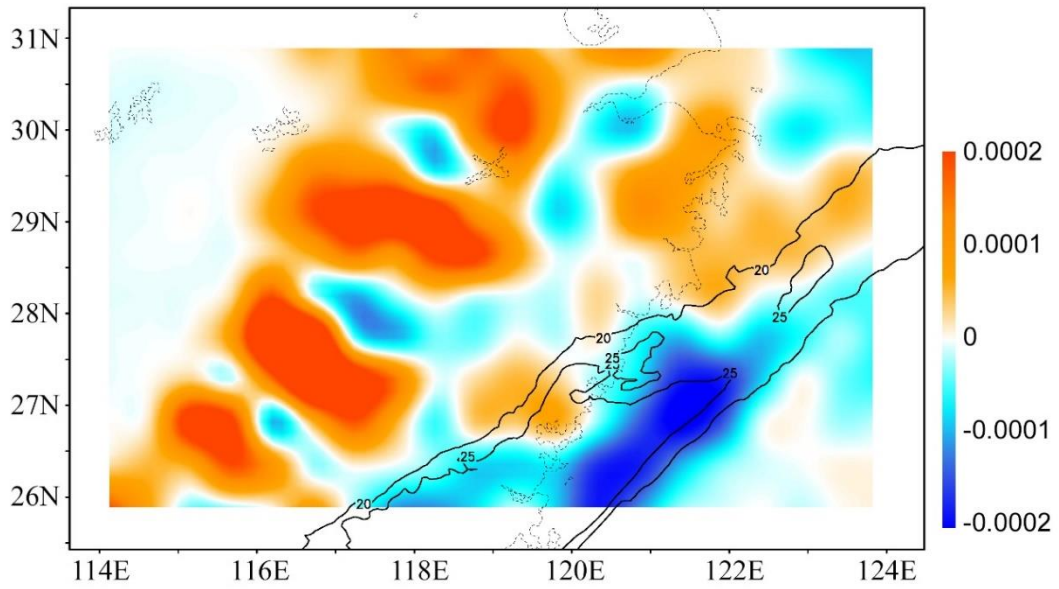


Figure 5.25 The distribution of horizontal moisture advection  $\bar{\nabla} \cdot \bar{\mathbf{v}}_h^L q^L$  ( $\text{g kg}^{-1} \text{s}^{-1}$ ), i.e. Term II in Eq. ( 4.11 ). Note that negative value here is associated with the advection of LLJ. Contour ( $\text{m s}^{-1}$ ) shows the LLJ streak.

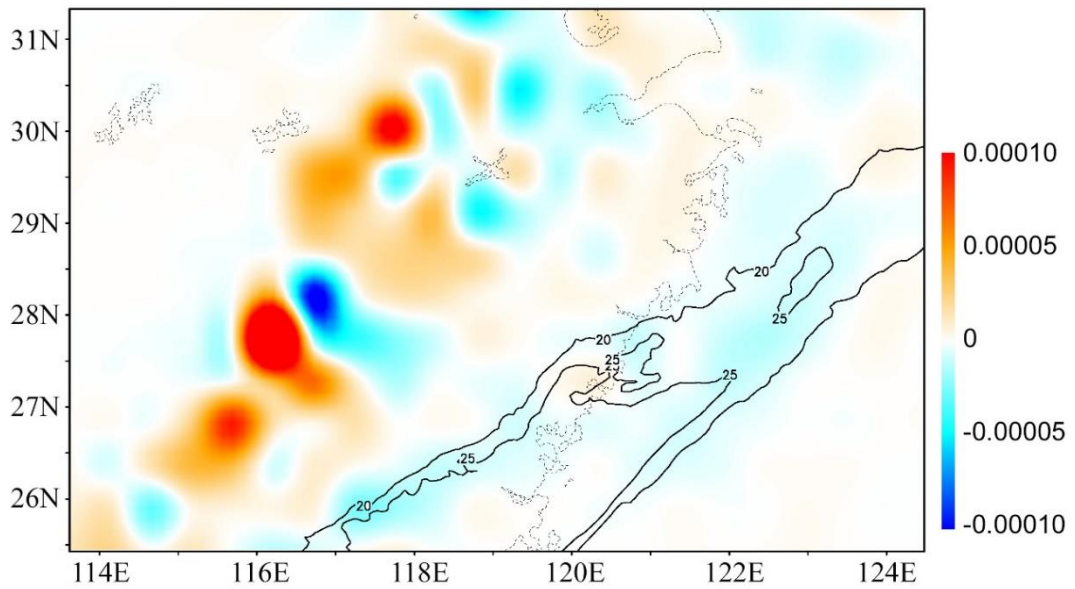


Figure 5.26 Same as Figure 5.25, but for  $-\frac{\partial(\overline{w^M q^{M^L}})}{\partial z}$  ( $\text{g kg}^{-1} \text{s}^{-1}$ ), i.e. Term VII in Eq. ( 4.11 ).

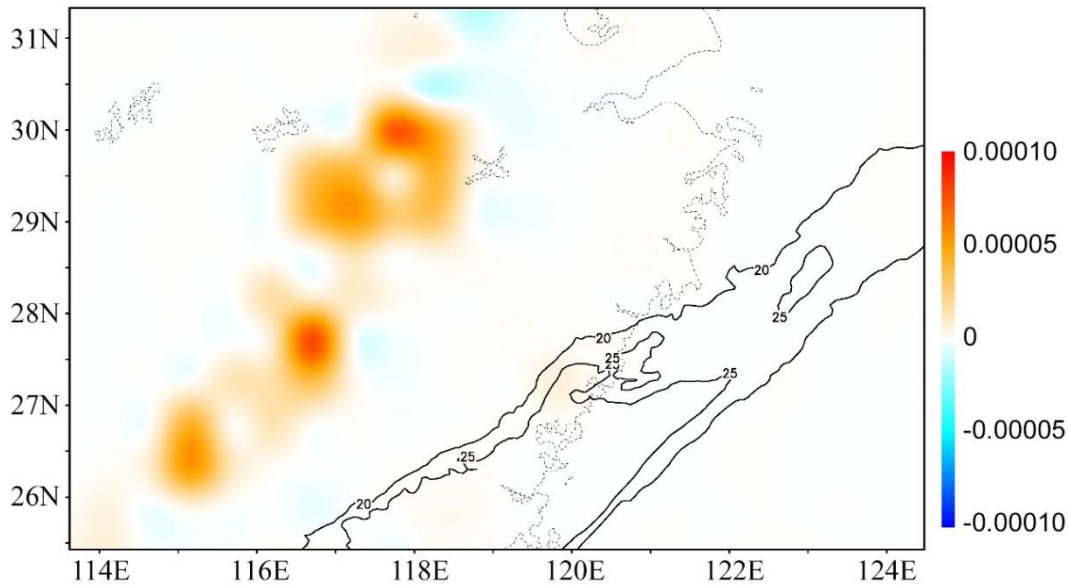


Figure 5.27 Same as Figure 5.25, but for  $-\frac{\partial(\overline{w^s q^s})}{\partial z}$  ( $\text{g kg}^{-1} \text{s}^{-1}$ ), i.e. Term VIII in Eq. ( 4.11 ).

In the heat issue, the horizontal heat advection associated LLJ contributed less to both heat flux divergences on small and mesoscale (the relevant ratios are not shown here). It can be deduced that heat on large scale was converted to smaller scales through the form of moisture, but not in form of heat itself. The large scale mean heat destabilizes the large scale environment, but not in the MCS and cumulus regions. The horizontal moisture advection, accordingly, should contribute to other cross-scale horizontal moist processes. However, this is out of the study syllabus and will not be discussed here.

This finding explains the origin of the heat fluxes above the LLJ level which is discussed in Section 5.3.2(D). Here is the full deduced path. Large scale horizontal moisture advection associated with LLJ supplies moisture to cumulus regions in the lower troposphere, and to the MCS regions above the jet level. However, on the LLJ level, the effective cumulus region decreases, and the contribution to the cumulus moisture flux divergence is unable to be resolved on the large scale. Instead, the corresponding contribution was resolved on mesoscale mentioned in Section 5.3.2(D) and it implied that the cumulus moisture at / above LLJ level is reflected by the mesoscale evaporation rate.



### 5.4.4 Conclusion

On the basis of the conceptual model and the outcomes of analysis above, a feasible mechanism of HRS for the case of 13rd June 2008 can be proposed here, as shown in Figure 5.28.

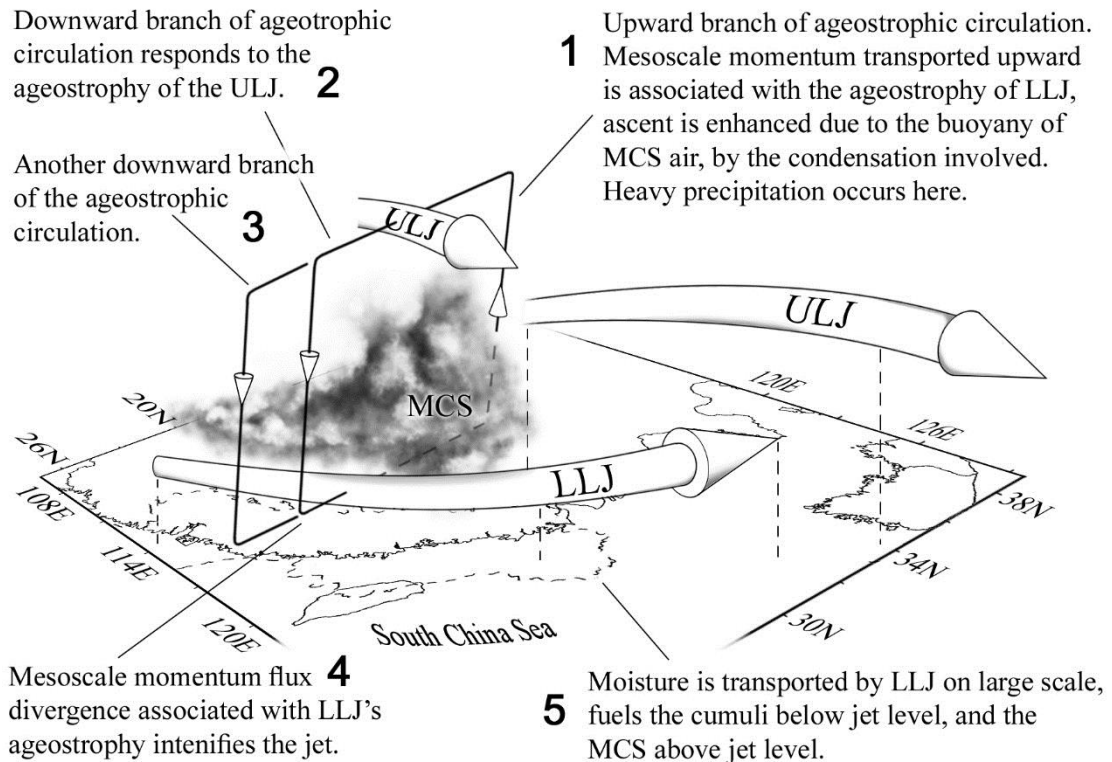


Figure 5.28 HRS over southeastern China for the case of 1800 UTC 13 June 2008. The mechanism is based on the conceptual model. Dashed line on the map indicates the moisture tongue corresponding to specific mixing ratio of  $3 \text{ g kg}^{-1}$  at the jet level.

The HRS over southeastern China was a collaboration of the components with scales from global to micro in a specific geometry. The westerly ULJ over China migrated southward during the summer season. The exit region of the ULJ to the west gets closer to that of the LLJ and the ageostrophic circulation associated with the jets was triggered. Differing from those in the model, the simulated LLJ was southwesterly rather than purely southerly, while the ULJ to the east was also southwesterly rather than pure westerly. The ageostrophic circulation was located between the LLJ (7 km AGL) and the ULJ (12 km AGL) to the west. Mesoscale momentum was transported upward on the cyclonic side of LLJ due to its ageostrophy. The transport was presented by the corresponding flux divergence in the analysis. The analysis also showed that the ascent was tilted toward the ULJ.

There was no sign of coupling of the LLJ and the ULJ as no upper- and surface-fronts were presented in the HRS. In the work of Sortais (1993), convective events is associated with the enhancement in the pre-frontal region. Also, the orientation of the jets was not orthogonal and thus coupling was hardly achieved. In this study, the mesoscale convective activity regarding the MCS was solely explained by the resolved heat and moisture fluxes on meso- and cumulus scales.

MCS was found in the location of the ascent, where the ascent was enhanced due to the increase of buoyancy. The buoyancy was associated with the mesoscale heat flux divergence, and this heat flux divergence was associated with the counterpart of latent heat. Mesoscale condensation rate was contributed by the cumulus moisture flux divergence on mesoscale and MCS's itself. Downward branch of the circulation was found on the anti-cyclonic side of ULJ, responding to the ageostrophy of ULJ. Two downdrafts were found based on the simulation results. The downward mesoscale transport at low level, responds to the LLJ's ageostrophy and intensified the jet. The jet was therefore sustained and moisture was supplied from South China Sea to the continent.

Large scale horizontal moisture advection along the coast of southeastern China was associated with LLJ. The moisture was mainly transported on small cumulus scale below the jet level, and mainly on mesoscale above the jet level.

It implies that when the ULJ retreats in winter seasons, this specific geometry of the components collapses, as well as the collaboration. The ageostrophic circulation and the moisture cycle cannot be established. As a result, the system cannot be triggered.

To sum up, mesoscale was responsible for the transport and enhancement of momentum between large scale motions and the accumulation of latent heat on small cumulus scale. Large scale motions is the origin of the jet's ageostrophy and is important for the transport of moisture required by the HRS. Small cumulus scale provides a foundation for the moisture to transport vertically at the low levels.

## 6 Summary and Outlook

Heavy rainfall events often occur over the central United States and southeastern China during summer seasons. Two cases in the central US and southeastern China have been studied by Wu et al. (1998) and Wu et al. (2011), respectively. Comparing their studies, there are several features in common, 1) both events occurred in summers at the mid-latitudes, 2) ULJs in an almost orthogonal alignment existed above the LLJs, 3) the LLJs are responsible for the moisture transport, 4) topographical conditions of the coastal regions in both cases are similar and they favour the moisture transport of LLJ, and 5) both LLJs were southwesterly.

The mechanism of producing rainfall on mesoscale is still questioned as it involves the dealing of multiscale interactions. The importance of mesoscale convective system (MCS) is concealed in the synoptic analysis charts in large scale studies and hidden when the events are simulated with the effect of convections parameterized. To get a deeper understanding of the mechanism, in this study:

- 1) A conceptual model of heavy rainfall system is established;
- 2) A multiscale analysis method is developed to simplify the equation sets specified to HRS;
- 3) The essential interactions among the scales are evaluated using the simulation results of the case on 18 June 2008 over southeastern China, and the mechanism of the involved system is investigated; and
- 4) The reliability of the proposed mechanism and the role of MCS for the event are evaluated and the HRS is visualized based on the analysis result.

The conceptual model of HRS consists of three components: Jets (ULJ and LLJ), MCS, and cumulus. The positions of these three components trigger the occurrence of heavy rainfall on certain location. The system is assumed to be isolated and in steady state; while the interactions among these three components are in dynamic and thermodynamic equilibrium.

As these components of the HRS are of different scales, a multi-scale analysis method has been developed to explain the HRS. Three representative scales are defined, namely large, middle and small scales. Governing equation sets for these three scales are derived by successive filtering using Reynolds averaging (spatial averaging). The resultant equations consist of cross-scale terms which represent the interactions between each two scales. However, due to their non-linear characteristics and the scale diversity, full equations corresponding to the jets (large scale mean), MCS (large scale perturbation) and cumulus (middle scale perturbation), are simplified with respect to mesoscale and only essential interactions are retained. By using the simplified equations, the model was explained in term of dynamic and thermodynamic circulations with mesoscale interactions.

An ageostrophic circulation is developed between the jets. Vertical mesoscale momentum flux divergence in the LLJ's exit region responds to the LLJ's ageostrophy. Mesoscale momentum is transported upward and the jet decelerates. The momentum is transported on the cyclonic side of the LLJ, and reaches the upper atmosphere on the cyclonic side of the ULJ, constitutes the upward branch of the dynamic circulation. On the anti-cyclonic side of the ULJ, the momentum is transported downward due to its ageostrophy, reaches the anti-cyclonic side of the LLJ and constitutes the downward branch of the circulation. The associated mesoscale momentum flux divergence intensifies the LLJ in its entrance region. As a result, a closed ageostrophic dynamic circulation is formed between the jets and the transport of moisture by the LLJ can be sustained. Stronger the ageostrophy of the jets, larger the mesoscale momentum flux divergences on large scale are involved.

The dynamic circulation is strengthened by thermodynamic circulation. At the LLJ level, in the location of MCS, the ascent is enhanced due to the increase of buoyancy. The buoyancy is associated with the mesoscale heat flux divergence, and this heat flux divergence is associated with the corresponding counterpart of latent heat. The related mesoscale condensation rate is contributed by the cumulus moisture flux divergence on mesoscale and that of MCS itself. Reverse process occurs in the downward branch of the circulation with evaporation.

A numerical experiment by WRF was used to verify the aforementioned hypothesis. A heavy rainfall event on 13 June 2008 over southeastern China was simulated. Model result from the parent, and two nested domains, with resolutions corresponding to large, middle and small scale means were used in this event. The resolutions of the domains, from the parent to the finest nested, were 54000, 6000, and 666.67 m, respectively, were

capable of resolving the structures on the corresponding scales. The parent domain resolved the jet structures, and the two nested domains with 2 different resolutions resolved respectively the structure of MCS and cumulus. The significance of the terms in the simplified equations was investigated. The quantities related to the jets, MCS and cumulus were computed, and the terms related to the essential interactions were evaluated.

A LLJ and two ULJs were simulated. Based on the simulation result, a dynamic circulation is found on the proposed location. At the representative LLJ level of 7 km AGL (exactly located at 2 km AGL), the vertical flux divergence of the mesoscale horizontal momentum explains at least 30% of the LLJ's ageostrophy; at the ULJ level (11.5 km AGL), the corresponding vertical flux divergence explains also at least 30% of the ULJ's ageostrophy, especially on the cyclonic side of the ULJ to the west. Based on the distributions of the mesoscale flux divergences, it is deduced that the flux divergence is associated with the location relative to the jets, wind component of the jets and the vertical level. Based on the vertical velocity distribution, an intensive updraft and two gentle downdrafts are found on the cyclonic and anti-cyclonic sides of the LLJ, respectively. It is also found that the circulation was tilted toward the ULJ to the west, especially the updraft.

The simulated mesoscale circulation associated with MCS is consistent with the proposed model. The simulated results show the existence of the balance between the horizontal advectations of middle and large scales and the vertical flux divergence in the vicinity of the LLJ, especially on the cyclonic side. This finding supports the proposed mechanism that the advection of mesoscale vorticity increases (decreases) when the gradient of the vertical mesoscale flux divergence decreases (increases) in the LLJ's entrance (exit) region (see Figure 4.2), i.e. acceleration (deceleration) of the LLJ in the entrance (exit) region.

Thermodynamic circulation is also found in the simulation. At the LLJ level, the mesoscale heat flux divergence is almost determined by the counterpart of latent heat which was associated with condensation. The mesoscale condensation rate originated from cumuli and MCS itself. Both the cumulus and mesoscale moisture flux divergences contributed to the mesoscale condensation rate and their effects are comparable to each other. It implies that cumulus moisture tends to condense on mesoscale and thus the associated latent heat accumulated on mesoscale. At lower levels, large scale moisture was transported horizontally by LLJ and transported vertically by the mean of vertical cumulus moisture flux divergence. The effect of

cumulus moisture flux divergence at LLJ level was unable to be resolved on large scale, but on mesoscale. Moreover, the large scale horizontal advection of heat contributed less to the vertical flux divergences of small and mesoscale, but destabilized the large / middle scale environment. The result also shows that, moisture from large scale was transported vertically on small scale below the LLJ level. Combining the above findings, it can be deduced that cumuli plays the main role on vertical moisture transport in the lower troposphere, but they condensed on mesoscale in the middle troposphere above the LLJ level, hence the associated latent heat accumulates on mesoscale. Together with the corresponding mesoscale moisture flux divergence, it contributes to the mesoscale latent heat flux divergence. As a result, mesoscale heat is transported upward and the buoyancy is increased, where MCS is located.

The enhancement of the ascent was simulated and its effect on the vertical velocity is shown in Figure 5.22. The enhancement of momentum flux divergence by the buoyancy is fairly shown by the simulation. The ratio of the relevant terms shows that the vertical transport of mesoscale momentum flux divergence can be explained by ~10% of the buoyancy transport. It can be concluded that the ascent was enhanced by the buoyancy above the LLJ level, the vertical transport of momentum flux divergence associated with the circulation was enhanced to some extent by the transport of buoyancy.

Overall, the findings from the simulation are consistent with the proposed mechanism. The simulated circulations agrees well with the proposed mechanism of the HRS. Meanwhile, three main differences were found in the simulation comparing to the proposed HRS.

- 1) Two gentle downdrafts were found on the anti-cyclonic side of the LLJ;
- 2) Two ULJs were obtained; and
- 3) The circulation was tilted.

Note that the coupling of the simulated LLJ and ULJ didn't occur according to their orientations and the absence of upper- and surface fronts.

As a whole, HRS is a collaboration of the jets, MCS, and cumuli, in a specific geometry. The system is triggered when the jets get closer to each other: The ULJ migrates southward while the LLJ is permanent and stationary in the coastal region during summer. Mesoscale motions associated with the MCS are responsible for the transport and enhancement of momentum between the jets and the accumulation of small scale

latent heat. Large scale motions is the origin of the jets' ageostrophy and is important for the horizontal moisture transport which fuels the entire HRS. Small cumulus scale motions provide a foundation for the moisture to transport vertically at the lower levels below the LLJ.

Based on the work done by this study, future work can be focused on:

- 1) *Finer simplification process.* Although the simulation results shows that balances exist between each two scales, the significant ratio is not high enough to show a perfect balance, especially those related to thermodynamic circulation, since the system is assumed to be in steady state and thus the contribution of tendency terms are ignored. Also, the interactions apart from those considered may be significant in the corresponding balance. To get a high ratio to describe the balances, a huge amount of "non-related" terms have to be taken into account, leads to more workload on this.
- 2) *Enlargement of the finest domain.* Due to the limitation of computational resource, the region covered by Domain 5 is just large enough to visualize a part of the cyclonic region of the LLJ, near its exit region (see Figure 5.15 as an example). It is necessary to increase the size of Domain 5 in order to investigate the effects of cumulus and mesoscale moisture in the downdraft branch of the ageostrophic circulation.
- 3) *Application of the proposed mechanism to the case of the central US.* The proposed mechanism have been verified in the case of China. The results show that the conceptual model explains the event well. To further assess the proposed mechanism, the conceptual model should be applied to the case of the US which has a similar synoptic condition to the event in China.





## 7 Appendix

### A Derivation of mesoscale vorticity equation

Differentiate Eq. 3.25.1 with respect to  $y$ , it gives

$$\begin{aligned}
 \frac{\partial}{\partial t} \left( \frac{\partial u^M}{\partial y} \right) = & \\
 & - \frac{\partial u^L}{\partial y} \frac{\partial u^M}{\partial x} - u^L \frac{\partial}{\partial x} \left( \frac{\partial u^M}{\partial y} \right) - \frac{\partial u^M}{\partial y} \frac{\partial u^L}{\partial x} - u^M \frac{\partial}{\partial x} \left( \frac{\partial u^L}{\partial y} \right) \\
 & \quad 1 \qquad \qquad 2 \qquad \qquad 3 \qquad \qquad 4 \\
 & - \frac{\partial v^L}{\partial y} \frac{\partial u^M}{\partial y} - v^L \frac{\partial}{\partial y} \left( \frac{\partial u^M}{\partial y} \right) - \frac{\partial u^M}{\partial y} \frac{\partial v^L}{\partial y} - u^M \frac{\partial}{\partial y} \left( \frac{\partial v^L}{\partial y} \right) \\
 & \quad 5 \qquad \qquad 6 \qquad \qquad 7 \qquad \qquad 8 \\
 & - \frac{\partial u^M}{\partial y} \frac{\partial u^L}{\partial x} - u^M \frac{\partial}{\partial x} \left( \frac{\partial u^L}{\partial y} \right) - \frac{\partial u^L}{\partial y} \frac{\partial u^M}{\partial x} - u^L \frac{\partial}{\partial x} \left( \frac{\partial u^M}{\partial y} \right) \\
 & \quad 9 \qquad \qquad 10 \qquad \qquad 11 \qquad \qquad 12 \\
 & - \frac{\partial v^M}{\partial y} \frac{\partial u^L}{\partial y} - v^M \frac{\partial}{\partial y} \left( \frac{\partial u^L}{\partial y} \right) - \frac{\partial u^L}{\partial y} \frac{\partial v^M}{\partial y} - u^L \frac{\partial}{\partial y} \left( \frac{\partial v^M}{\partial y} \right) \\
 & \quad 13 \qquad \qquad 14 \qquad \qquad 15 \qquad \qquad 16 \\
 & - \frac{\partial u^M}{\partial y} \frac{\partial u^M}{\partial x} - u^M \frac{\partial}{\partial x} \left( \frac{\partial u^M}{\partial y} \right) - \frac{\partial u^M}{\partial y} \frac{\partial u^M}{\partial x} - u^M \frac{\partial}{\partial x} \left( \frac{\partial u^M}{\partial y} \right) \\
 & \quad 17 \qquad \qquad 18 \qquad \qquad 19 \qquad \qquad 20 \\
 & - \frac{\partial v^M}{\partial y} \frac{\partial u^M}{\partial y} - v^M \frac{\partial}{\partial y} \left( \frac{\partial u^M}{\partial y} \right) - \frac{\partial u^M}{\partial y} \frac{\partial v^M}{\partial y} - u^M \frac{\partial}{\partial y} \left( \frac{\partial v^M}{\partial y} \right) \\
 & \quad 21 \qquad \qquad 22 \qquad \qquad 23 \qquad \qquad 24 \\
 & - \frac{\partial w^L}{\partial y} \frac{\partial u^M}{\partial z} - w^L \frac{\partial}{\partial z} \left( \frac{\partial u^M}{\partial y} \right) - \frac{\partial u^M}{\partial y} \frac{\partial w^L}{\partial z} - u^M \frac{\partial}{\partial z} \left( \frac{\partial w^L}{\partial y} \right) \\
 & \quad 25 \qquad \qquad 26 \qquad \qquad 27 \qquad \qquad 28 \\
 & - \frac{\partial w^M}{\partial y} \frac{\partial u^L}{\partial z} - w^M \frac{\partial}{\partial z} \left( \frac{\partial u^L}{\partial y} \right) - \frac{\partial u^L}{\partial y} \frac{\partial w^M}{\partial z} - u^L \frac{\partial}{\partial z} \left( \frac{\partial w^M}{\partial y} \right) \\
 & \quad 29 \qquad \qquad 30 \qquad \qquad 31 \qquad \qquad 32 \\
 & - \frac{\partial}{\partial y} \frac{\partial w^M u^M}{\partial z} \qquad \qquad \qquad \text{Eq. (A)}
 \end{aligned}$$

33

where all the non-linear terms are omitted, note that Term 33 is retained in flux form on propose.

Differentiate Eq. 3.25.2 with respect to  $x$ , it gives

$$\begin{aligned}
& \frac{\partial}{\partial t} \left( \frac{\partial v^M}{\partial x} \right) = \\
& \quad - \frac{\partial u^L}{\partial x} \frac{\partial v^M}{\partial x} - u^L \frac{\partial}{\partial x} \left( \frac{\partial v^M}{\partial x} \right) - \frac{\partial v^M}{\partial x} \frac{\partial u^L}{\partial x} - v^M \frac{\partial}{\partial x} \left( \frac{\partial u^L}{\partial x} \right) \\
& \quad \quad \quad 1 \qquad \quad 2 \qquad \quad 3 \qquad \quad 4 \\
& \quad - \frac{\partial v^L}{\partial x} \frac{\partial v^M}{\partial y} - v^L \frac{\partial}{\partial y} \left( \frac{\partial v^M}{\partial x} \right) - \frac{\partial v^M}{\partial y} \frac{\partial v^L}{\partial y} - v^M \frac{\partial}{\partial y} \left( \frac{\partial v^L}{\partial x} \right) \\
& \quad \quad \quad 5 \qquad \quad 6 \qquad \quad 7 \qquad \quad 8 \\
& \quad - \frac{\partial u^M}{\partial x} \frac{\partial v^L}{\partial x} - u^M \frac{\partial}{\partial x} \left( \frac{\partial v^L}{\partial x} \right) - \frac{\partial v^L}{\partial x} \frac{\partial u^M}{\partial x} - v^L \frac{\partial}{\partial x} \left( \frac{\partial u^M}{\partial x} \right) \\
& \quad \quad \quad 9 \qquad \quad 10 \qquad \quad 11 \qquad \quad 12 \\
& \quad - \frac{\partial v^M}{\partial x} \frac{\partial u^L}{\partial y} - v^M \frac{\partial}{\partial y} \left( \frac{\partial v^L}{\partial x} \right) - \frac{\partial v^L}{\partial x} \frac{\partial v^M}{\partial y} - v^L \frac{\partial}{\partial y} \left( \frac{\partial v^M}{\partial x} \right) \\
& \quad \quad \quad 13 \qquad \quad 14 \qquad \quad 15 \qquad \quad 16 \\
& \quad - \frac{\partial u^M}{\partial y} \frac{\partial v^M}{\partial x} - u^M \frac{\partial}{\partial x} \left( \frac{\partial v^M}{\partial y} \right) - \frac{\partial v^M}{\partial x} \frac{\partial u^M}{\partial x} - v^M \frac{\partial}{\partial x} \left( \frac{\partial u^M}{\partial x} \right) \\
& \quad \quad \quad 17 \qquad \quad 18 \qquad \quad 19 \qquad \quad 20 \\
& \quad - \frac{\partial v^M}{\partial x} \frac{\partial v^M}{\partial y} - v^M \frac{\partial}{\partial x} \left( \frac{\partial v^M}{\partial y} \right) - \frac{\partial v^M}{\partial x} \frac{\partial v^M}{\partial y} - v^M \frac{\partial}{\partial y} \left( \frac{\partial v^M}{\partial x} \right) \\
& \quad \quad \quad 21 \qquad \quad 22 \qquad \quad 23 \qquad \quad 24 \\
& \quad - \frac{\partial w^L}{\partial x} \frac{\partial v^M}{\partial z} - w^L \frac{\partial}{\partial z} \left( \frac{\partial v^M}{\partial x} \right) - \frac{\partial v^M}{\partial x} \frac{\partial w^L}{\partial z} - v^M \frac{\partial}{\partial z} \left( \frac{\partial w^L}{\partial x} \right) \\
& \quad \quad \quad 25 \qquad \quad 26 \qquad \quad 27 \qquad \quad 28 \\
& \quad - \frac{\partial w^M}{\partial x} \frac{\partial v^L}{\partial z} - w^M \frac{\partial}{\partial z} \left( \frac{\partial v^L}{\partial x} \right) - \frac{\partial v^L}{\partial x} \frac{\partial w^M}{\partial z} - v^L \frac{\partial}{\partial z} \left( \frac{\partial w^M}{\partial x} \right) \\
& \quad \quad \quad 29 \qquad \quad 30 \qquad \quad 31 \qquad \quad 32 \\
& \quad - \frac{\partial}{\partial x} \frac{\partial w^M v^M}{\partial z} \qquad \qquad \qquad \text{Eq. (B)} \\
& \quad \quad \quad 33
\end{aligned}$$

where all the non-linear terms are omitted, note that Term 33 is retained in flux form on propose.

Subtract Eq. (A) from Eq. (B), and substitute

$$\zeta^M = \frac{\partial v^M}{\partial x} - \frac{\partial u^M}{\partial y}, \quad D^M = \frac{\partial u^M}{\partial x} + \frac{\partial v^M}{\partial y}, \quad \zeta^L = \frac{\partial v^L}{\partial x} - \frac{\partial u^L}{\partial y}, \quad D^L = \frac{\partial u^L}{\partial x} + \frac{\partial v^L}{\partial y}, \quad \text{we have}$$

$$\begin{aligned} \frac{\partial \zeta^M}{\partial t} = & \\ -\vec{\nabla}_h \cdot \mathbf{v}_h^L \zeta^M & \quad \text{B2} + \text{B6} - \text{A2} - \text{A6} \\ -\vec{\nabla}_h \cdot \mathbf{v}_h^M \zeta^L & \quad \text{B10} + \text{B14} - \text{A4} - \text{A8} \\ -\vec{\nabla}_h \cdot \mathbf{v}_h^M \zeta^M & \quad \text{B18} + \text{B24} - \text{A18} - \text{A24} \\ -2\zeta^M D^L & \quad \text{B1} + \text{B3} + \text{B7} + \text{B13} - \text{A3} - \text{A5} - \text{A7} - \text{A9} \\ -2\zeta^L D^M & \quad \text{B5} + \text{B9} + \text{B11} + \text{B15} - \text{A1} - \text{A11} - \text{A13} - \text{A15} \\ -\left(\frac{\partial}{\partial x} \frac{\partial w^M v^M}{\partial z} + \frac{\partial}{\partial y} \frac{\partial w^M u^M}{\partial z}\right) & \quad \text{B31} - \text{A31} \\ -2\zeta^M D^M & \quad \text{B17} + \text{B19} + \text{B21} + \text{B23} - \text{A17} - \text{A19} - \text{A21} - \text{A23} \\ -w^L \frac{\partial \zeta^M}{\partial z} & \quad \text{B26} - \text{A26} \\ -w^M \frac{\partial \zeta^L}{\partial z} & \quad \text{B30} - \text{A30} \\ -\zeta^M \frac{\partial w^L}{\partial z} & \quad \text{B27} - \text{A27} \\ -\zeta^L \frac{\partial w^M}{\partial z} & \quad \text{B31} - \text{A31} \\ -\left(\frac{\partial w^L}{\partial x} \frac{\partial v^M}{\partial z} - \frac{\partial w^L}{\partial y} \frac{\partial u^M}{\partial z}\right) & \quad \text{B25} - \text{A25} \\ -\left(\frac{\partial w^M}{\partial x} \frac{\partial v^L}{\partial z} - \frac{\partial w^M}{\partial y} \frac{\partial u^L}{\partial z}\right) & \quad \text{B29} - \text{A29} \\ -v^L \frac{\partial}{\partial y} \left(\frac{\partial v^M}{\partial x}\right) + u^L \frac{\partial}{\partial x} \left(\frac{\partial u^M}{\partial y}\right) & \quad \text{B16} - \text{A12} \\ -v^M \frac{\partial}{\partial y} \left(\frac{\partial v^L}{\partial x}\right) + u^M \frac{\partial}{\partial x} \left(\frac{\partial u^L}{\partial y}\right) & \quad \text{B8} - \text{A10} \\ -v^M \frac{\partial}{\partial x} \left(\frac{\partial v^M}{\partial y}\right) + u^M \frac{\partial}{\partial x} \left(\frac{\partial u^M}{\partial y}\right) & \quad \text{B22} - \text{A20} \\ & + \text{other non-linear terms} \end{aligned}$$

## B Derivation of mesoscale momentum flux equation

Multiple Eq. (3.25.1) by  $w^M$ , with only necessary terms retained, it gives

$$\begin{aligned} w^M \frac{\partial v^M}{\partial t} = & -w^M \left( \frac{\partial u^L v^M}{\partial x} + \frac{\partial v^L v^M}{\partial y} \right) - w^M \left( \frac{\partial u^M v^L}{\partial x} + \frac{\partial v^M v^L}{\partial y} \right) - w^M \left( \frac{\partial u^M v^M}{\partial x} + \frac{\partial v^M v^M}{\partial y} \right) \\ & - w^M \frac{\partial (w^L v^M)}{\partial z} - w^M \frac{\partial (w^M v^L)}{\partial z} - w^M \frac{\partial (w^M v^M)}{\partial z} \end{aligned}$$

Likewise, multiple Eq. (3.33) by  $v^M$ , we have

$$\begin{aligned} v^M \frac{\partial w^M}{\partial t} = & -v^M \left( \frac{\partial u^L w^M}{\partial x} + \frac{\partial v^L w^M}{\partial y} \right) - v^M \left( \frac{\partial u^M w^L}{\partial x} + \frac{\partial v^M w^L}{\partial y} \right) - v^M \left( \frac{\partial u^M w^M}{\partial x} + \frac{\partial v^M w^M}{\partial y} \right) \\ & - v^M \frac{\partial (w^L w^M)}{\partial z} - v^M \frac{\partial (w^M w^L)}{\partial z} - v^M \frac{\partial (w^M w^M)}{\partial z} + v^M \frac{\theta^M}{\theta^L} g \end{aligned}$$

Note that buoyancy term is retained here.

Sum the equations up, and rearrange the terms:

$$\begin{aligned} \frac{\partial w^M v^M}{\partial t} = & \left( -w^M \frac{\partial u^L v^M}{\partial x} - v^M \frac{\partial u^L w^M}{\partial x} \right) + \left( -w^M \frac{\partial v^L v^M}{\partial y} - v^M \frac{\partial v^L w^M}{\partial y} \right) \\ & + \left( -w^M \frac{\partial u^M v^M}{\partial x} - v^M \frac{\partial u^M w^M}{\partial x} \right) + \left( -w^M \frac{\partial v^M v^M}{\partial y} - v^M \frac{\partial v^M w^M}{\partial y} \right) \\ & + \left( -w^M \frac{\partial u^M v^L}{\partial x} - v^M \frac{\partial u^M w^L}{\partial x} \right) + \left( -w^M \frac{\partial v^M v^L}{\partial y} - v^M \frac{\partial v^M w^L}{\partial y} \right) \\ & + \left( -w^M \frac{\partial (w^L v^M)}{\partial z} - v^M \frac{\partial (w^L w^M)}{\partial z} \right) \\ & + \left( -w^M \frac{\partial (w^M v^M)}{\partial z} - v^M \frac{\partial (w^M w^M)}{\partial z} \right) \\ & + \left( -w^M \frac{\partial (w^M v^L)}{\partial z} - v^M \frac{\partial (w^M w^L)}{\partial z} \right) \\ & + v^M \frac{\theta^M}{\theta^L} g \end{aligned}$$

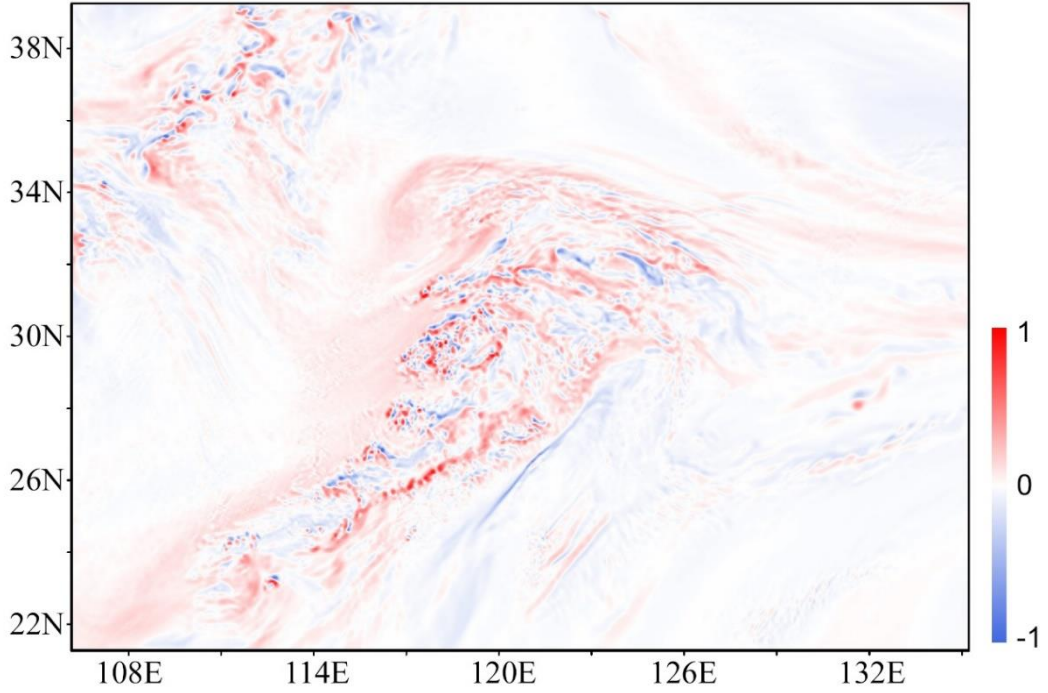
As a result, the equation can be rewritten in vector form

$$\begin{aligned} \frac{\partial w^M v^M}{\partial t} = & -\vec{\nabla}_h \cdot \mathbf{v}_h^L (w^M v^M) - \vec{\nabla}_h \cdot \mathbf{v}_h^M (w^M v^M) - w^M \vec{\nabla}_h \cdot \mathbf{v}_h^M v^L - v^M \vec{\nabla}_h \cdot \mathbf{v}_h^M w^L \\ & - \frac{\partial w^L (w^M v^M)}{\partial z} - \frac{\partial w^M (w^M v^M)}{\partial z} - w^M \frac{\partial (w^M v^L)}{\partial z} - v^M \frac{\partial (w^M w^L)}{\partial z} \\ & + v^M \frac{\theta^M}{\theta^L} g \end{aligned}$$

As it is a vertical flux equation, with all horizontal and  $w^L$ 's terms omitted in steady state, it becomes

$$\frac{\partial w^M (w^M v^M)}{\partial z} = v^M \frac{\theta^M}{\theta^L} g$$

### C Distribution of mesoscale vorticity ( $\times 10^{-3} \text{ s}^{-1}$ ) on LLJ level 7 km AGL



## 8 List of Abbreviations

AGL	about ground level
HRS	heavy rainfall system
LLJ	low-level jet
MCC	mesoscale convective complex
MCS	mesoscale convective system
NCEP FNL	National Centers for Environmental Prediction Final
ULJ	upper-level jet
WRF	The Weather Research & Forecasting Model

## 9 List of Parameters / Constants

$C_p = C_{pd}(1 + 0.84q)$ ( $\text{m}^2 \text{s}^{-2} \text{K}^{-1}$ )	Specific heat capacity for moist air at constant pressure
$C_{pd} = 1004.67$ ( $\text{m}^2 \text{s}^{-2} \text{K}^{-1}$ )	Specific heat capacity for dry air
$f = (1.46 \times 10^{-4})\sin\phi$ ( $\text{s}^{-1}$ )	Coriolis parameter, varies with latitude $\phi$
$g = 9.81$ ( $\text{m s}^{-2}$ )	Acceleration due to gravity
$L_v = [2.501 - 0.00237T(\text{in deg. cel.})] \times 10^6$ ( $\text{J kg}^{-1}$ )	Latent heat of evaporation with temperature $T$
$R = 287.04$ ( $\text{m}^2 \text{s}^{-2} \text{K}^{-1}$ )	Gas constant for dry air

## 10 List of Symbols

### D

$D$	detrainment rate
$D^L$	large scale divergence
$D^M$	mesoscale divergence
$D_d$	detrainment rate due to downdraft of $i$ -th cloud
$D_i$	detrainment rate of $i$ -th cloud
$D_u$	detrainment rate due to updraft of $i$ -th cloud

### E

$e^{Hl}$	condensation / evaporation rate perturbation on large scale
$e^{Hm}$	condensation / evaporation rate perturbation on middle scale
$e^{Hs}$	condensation / evaporation rate perturbation on small scale
$e^{Ll}$	net condensation / evaporation rate on large scale
$e^{Lm}$	net condensation / evaporation rate on middle scale
$e^{Ls}$	net condensation / evaporation rate on small scale
$E$	entrainment rate
$E_d$	entrainment rate due to downdraft of $i$ -th cloud
$E_i$	entrainment rate of $i$ -th cloud
$E_{Hl}$	entrainment from mesoscale convective system
$E_{Ll}$	entrainment from large scale environment
$E_u$	entrainment rate due to updraft of $i$ -th cloud

### H

$H$	superscript for high pass signal, or perturbation
$Hs$	high pass signal on small scale
$Hm$	high pass signal on middle scale
$Hl$	high pass signal on large scale

### L

$l$	superscript for large scale
$L$	superscript for low pass signal, or mean
$Ll$	low pass signal on large scale
$Lm$	low pass signal on middle scale
$Ls$	low pass signal on small scale

**M**

$m$	superscript for middle scale
$M$	vertical mass flux
$M_d$	vertical mass flux due to downdraft in $i$ -th cloud
$M_i$	vertical mass flux in $i$ -th cloud
$M_u$	vertical mass flux due to updraft in $i$ -th cloud

**P**

$p$	pressure
$p^{Hl}$	pressure perturbation on large scale
$p^{Hm}$	pressure perturbation on middle scale
$p^{Hs}$	pressure perturbation on small scale
$p^L$	see $p^{Ll}$
$p_a^L$	pressure due to ageostrophy on large scale
$p_g^L$	pressure in geostrophic balance on large scale
$p^{Ll}$	mean pressure on large scale
$p^{Lm}$	mean pressure on middle scale
$p^{Ls}$	mean pressure on small scale

**Q**

$q^{Hl}$	specific mixing ratio perturbation on large scale
$q^{Hm}$	specific mixing ratio perturbation on middle scale
$q^{Hs}$	specific mixing ratio perturbation on small scale
$q^L$	see $q^{Ll}$
$q^{Lm}$	mean specific mixing ratio on middle scale
$q^{Ll}$	mean specific mixing ratio on large scale
$q^{Ls}$	mean specific mixing ratio on small scale
$q^M$	see $q^{Hl}$
$q^S$	see $q^{Hm}$
$Q^{Hl}$	radiation rate perturbation on large scale
$Q^{Hm}$	radiation rate perturbation on middle scale
$Q^{Hs}$	radiation rate perturbation on small scale
$Q^{Ll}$	net radiation rate on middle scale
$Q^{Lm}$	net radiation rate on middle scale
$Q^{Ls}$	net radiation rate on small scale



**S**

$s$	superscript for small scale
$S^{Hl}$	moisture source perturbation on large scale
$S^{Hm}$	moisture source perturbation on middle scale
$S^{Hs}$	moisture source perturbation on small scale
$S^{Ll}$	mean moisture source on large scale
$S^{Lm}$	mean moisture source on middle scale
$S^{Ls}$	mean moisture source on small scale

**T**

$T_v$	virtual temperature
$T_v^{Hl}$	virtual temperature perturbation on large scale
$T_v^{Hm}$	virtual temperature perturbation on middle scale
$T_v^{Hs}$	virtual temperature perturbation on small scale
$T_v^{Ll}$	mean virtual temperature on large scale
$T_v^{Lm}$	mean virtual temperature on middle scale
$T_v^{Ls}$	mean virtual temperature on small scale

**U**

$u$	zonal wind velocity
$\mathbf{u}$	zonal wind vector
$u^{Hl}$	zonal wind velocity perturbation on large scale
$u^{Hm}$	zonal wind velocity perturbation on middle scale
$u^{Hs}$	perturbation of zonal wind velocity on small scale
$u^L$	see $u^{Ll}$
$u_a^L$	ageostrophic zonal mean component on large scale
$u_g^L$	geostrophic zonal mean component on large scale
$u^{Ll}$	zonal mean wind velocity on large scale
$u^{Lm}$	zonal mean wind velocity on middle scale
$u^{Ls}$	zonal mean wind velocity on small scale
$u^M$	see $u^{Hl}$
$u^S$	see $u^{Hm}$

**V**

$v$	meridional wind velocity
$\mathbf{v}$	meridional wind vector
$v^{Hl}$	meridional wind velocity perturbation on large scale
$v^{Hm}$	meridional wind velocity perturbation on middle scale
$v^{Hs}$	meridional wind velocity perturbation on small scale
$v^L$	see $v^{Ll}$
$v_a^L$	ageostrophic meridional mean component on large scale
$v_g^L$	geostrophic meridional mean component on large scale
$v^{Ll}$	meridional mean wind velocity on large scale
$v^{Lm}$	meridional mean wind velocity on middle scale
$v^{Ls}$	meridional mean wind velocity on small scale
$v^M$	see $v^{Hl}$
$v^S$	see $v^{Hm}$
$\mathbf{v}_h$	horizontal wind vector
$\mathbf{v}_h^{Hl}$	horizontal wind perturbation on large scale
$\mathbf{v}_h^{Hm}$	horizontal wind perturbation on middle scale
$\mathbf{v}_h^{Hn}$	high pass signal of horizontal wind vector on Scale n
$\mathbf{v}_h^{Hs}$	horizontal wind perturbation on small scale
$\mathbf{v}_h^{Ll}$	horizontal mean wind on large scale
$\mathbf{v}_h^{Lm}$	horizontal mean wind on middle scale
$\mathbf{v}_h^{Ln}$	low pass signal of horizontal wind vector on Scale n
$\mathbf{v}_h^{Ls}$	horizontal mean wind on small scale

**W**

$w$	vertical wind velocity
$w^{Hl}$	vertical velocity perturbation on large scale
$w^{Hm}$	vertical velocity perturbation on middle scale
$w^{Hs}$	vertical velocity perturbation on small scale
$w^L$	see $w^{Ll}$
$w^{Ll}$	vertical mean velocity on large scale
$w^{Lm}$	vertical mean velocity on middle scale
$w^{Ls}$	vertical mean velocity on small scale
$w^M$	see $w^{Hl}$
$w^S$	see $w^{Hm}$

**Greek**

$\zeta^M$	Mesoscale vorticity
$\zeta^L$	Large scale vorticity
$\theta$	potential temperature
$\theta^{Hl}$	potential temperature perturbation on large scale
$\theta^{Hm}$	potential temperature perturbation on middle scale
$\theta^{Hs}$	potential temperature perturbation on small scale
$\theta^{Ll}$	mean potential temperature on large scale
$\theta^{Lm}$	mean potential temperature on middle scale
$\theta^{Ls}$	mean potential temperature on small scale
$\theta^L$	see $\theta^{Ll}$
$\theta^M$	see $\theta^{Hl}$
$\theta^S$	see $\theta^{Hm}$
$\nu$	kinematic viscosity
$\rho$	air density
$\rho^{Hl}$	density perturbation on large scale
$\rho^{Hm}$	density perturbation on middle scale
$\rho^{Hs}$	density perturbation on small scale
$\rho^{Ll}$	mean density on large scale
$\rho^{Lm}$	mean density on middle scale
$\rho^{Ls}$	mean density on small scale
$\rho_m$	density of moist air
$\chi$	arbitrary quantity
$\chi^{Hn}$	high pass signal of $\chi$ on Scale n
$\chi^{Ln}$	low pass signal of $\chi$ on Scale n

**Other**

$\nabla$	three dimensional del operator
$\overline{\nabla}_h$	horizontal del operator



## 11 List of Equations

$$\frac{\partial \chi^{Ln}}{\partial t} = \underbrace{-\vec{\nabla}_h \cdot \mathbf{v}_h^{Ln} \chi^{Ln}}_{\text{I}} - \underbrace{\vec{\nabla}_h \cdot \overline{\sum_1^n \mathbf{v}_h^{Hn} \chi^{Hn Ln}}}_{\text{II}} - \underbrace{\frac{\partial (w^{Ln} \chi^{Ln})}{\partial z}}_{\text{III}} - \underbrace{\frac{\partial (\overline{\sum_1^n w^{Hn} \chi^{Hn Ln}})}{\partial z}}_{\text{IV}} \quad (3.8)$$

$$\begin{aligned} \frac{\partial \chi^{Hn}}{\partial t} = & \underbrace{-\vec{\nabla} \cdot \mathbf{v}_h^{Ln} \chi^{Hn}}_{\text{I}} - \underbrace{\vec{\nabla} \cdot \mathbf{v}_h^{Hn} \chi^{Ln}}_{\text{II}} - \underbrace{\vec{\nabla} \cdot \mathbf{v}_h^{Hn} \chi^{Hn}}_{\text{III}} - \underbrace{\vec{\nabla} \cdot \overline{\sum_1^n \mathbf{v}_h^{H(n-1)} \chi^{H(n-1) L(n-1)}}}_{\text{IV}} + \underbrace{\vec{\nabla} \cdot \overline{\sum_1^n \mathbf{v}_h^{Hn} \chi^{Hn Ln}}}_{\text{V}} - \underbrace{\frac{\partial (v_h^{Ln} \chi^{Hn})}{\partial z}}_{\text{VI}} \\ & - \underbrace{\frac{\partial (v_h^{Hn} \chi^{Ln})}{\partial z}}_{\text{VII}} - \underbrace{\frac{\partial (v_h^{Hn} \chi^{Hn})}{\partial z}}_{\text{VIII}} - \underbrace{\frac{\partial \overline{\sum_1^n w^{H(n-1)} \chi^{H(n-1) L(n-1)}}}{\partial z}}_{\text{IX}} + \underbrace{\frac{\partial \overline{\sum_1^n w^{Hn} \chi^{Hn Ln}}}{\partial z}}_{\text{X}} \quad (3.9) \end{aligned}$$

$$\frac{\partial u^{Ls}}{\partial t} = \underbrace{-\vec{\nabla}_h \cdot \mathbf{v}_h^{Ls} u^{Ls}}_{\text{I}} - \underbrace{\vec{\nabla}_h \cdot \overline{\mathbf{v}_h^{Hs} u^{Hs Ls}}}_{\text{II}} - \underbrace{\frac{\partial w^{Ls} u^{Ls}}{\partial z}}_{\text{III}} - \underbrace{\frac{\partial \overline{w^{Hs} u^{Hs Ls}}}{\partial z}}_{\text{IV}} + \underbrace{f v^{Ls}}_{\text{V}} - \underbrace{\frac{1}{\rho^{Ls}} \frac{\partial p^{Ls}}{\partial x}}_{\text{VI}} \quad (3.12.1)$$

$$\frac{\partial v^{Ls}}{\partial t} = \underbrace{-\vec{\nabla}_h \cdot \mathbf{v}_h^{Ls} v^{Ls}}_{\text{I}} - \underbrace{\vec{\nabla}_h \cdot \overline{\mathbf{v}_h^{Hs} v^{Hs Ls}}}_{\text{II}} - \underbrace{\frac{\partial w^{Ls} v^{Ls}}{\partial z}}_{\text{III}} - \underbrace{\frac{\partial \overline{w^{Hs} v^{Hs Ls}}}{\partial z}}_{\text{IV}} - \underbrace{f u^{Ls}}_{\text{V}} - \underbrace{\frac{1}{\rho^{Ls}} \frac{\partial p^{Ls}}{\partial y}}_{\text{VI}} \quad (3.12.2)$$

$$\frac{\partial u^{Hs}}{\partial t} = \underbrace{-\vec{\nabla}_h \cdot \mathbf{v}_h^{Ls} u^{Hs}}_{\text{I}} - \underbrace{\vec{\nabla}_h \cdot \mathbf{v}_h^{Hs} u^{Ls}}_{\text{II}} - \underbrace{\vec{\nabla}_h \cdot \mathbf{v}_h^{Hs} u^{Hs}}_{\text{III}} + \underbrace{\vec{\nabla}_h \cdot \overline{\mathbf{v}_h^{Hs} u^{Hs Ls}}}_{\text{IV}} - \underbrace{\frac{\partial w^{Ls} u^{Hs}}{\partial z}}_{\text{V}} - \underbrace{\frac{\partial w^{Hs} u^{Ls}}{\partial z}}_{\text{VI}} - \underbrace{\frac{\partial w^{Hs} u^{Hs}}{\partial z}}_{\text{VII}} + \underbrace{\frac{\partial \overline{w^{Hs} u^{Hs Ls}}}{\partial z}}_{\text{VIII}} + \underbrace{f v^{Hs}}_{\text{IX}} - \underbrace{\frac{1}{\rho^{Ls}} \frac{\partial p^{Hs}}{\partial x}}_{\text{X}} \quad (3.13.1)$$

$$\frac{\partial v^{Hs}}{\partial t} = \underbrace{-\overline{\nabla}_h \cdot \mathbf{v}_h^{Ls} v^{Hs}}_{\text{I}} - \underbrace{\overline{\nabla}_h \cdot \mathbf{v}_h^{Hs} v^{Ls}}_{\text{II}} - \underbrace{\overline{\nabla}_h \cdot \mathbf{v}_h^{Hs} v^{Hs}}_{\text{III}} + \underbrace{\overline{\nabla}_h \cdot \overline{\mathbf{v}_h^{Hs} v^{Hs} Ls}}_{\text{IV}} - \underbrace{\frac{\partial \overline{w^{Ls} v^{Hs}}}{\partial z}}_{\text{V}} - \underbrace{\frac{\partial \overline{w^{Hs} v^{Ls}}}{\partial z}}_{\text{VI}} - \underbrace{\frac{\partial \overline{w^{Hs} v^{Hs}}}{\partial z}}_{\text{VII}} + \underbrace{\frac{\partial \overline{w^{Hs} v^{Hs} Ls}}}{\partial z}}_{\text{VIII}} - \underbrace{f u^{Hs}}_{\text{IX}} - \underbrace{\frac{1}{\rho^{Ls}} \frac{\partial p^{Hs}}{\partial y}}_{\text{X}} \quad (3.13.2)$$

$$\frac{\partial u^{Lm}}{\partial t} = -\overline{\nabla}_h \cdot \mathbf{v}_h^{Lm} u^{Lm} - \overline{\nabla}_h \cdot \overline{\mathbf{v}_h^{Hm} u^{Hm} Lm} - \overline{\nabla}_h \cdot \overline{\mathbf{v}_h^{Hs} u^{Hs} Lm} - \frac{\partial (\overline{w^{Lm} u^{Lm}})}{\partial z} - \frac{\partial (\overline{w^{Hm} u^{Hm} Lm})}{\partial z} - \frac{\partial (\overline{w^{Hs} u^{Hs} Lm})}{\partial z} + f v^{Lm} - \frac{1}{\rho^{Lm}} \frac{\partial p^{Lm}}{\partial x} \quad (3.14.1)$$

$$\frac{\partial v^{Lm}}{\partial t} = -\overline{\nabla}_h \cdot \mathbf{v}_h^{Lm} v^{Lm} - \overline{\nabla}_h \cdot \overline{\mathbf{v}_h^{Hm} v^{Hm} Lm} - \overline{\nabla}_h \cdot \overline{\mathbf{v}_h^{Hs} v^{Hs} Lm} - \frac{\partial (\overline{w^{Lm} v^{Lm}})}{\partial z} - \frac{\partial (\overline{w^{Hm} v^{Hm} Lm})}{\partial z} - \frac{\partial (\overline{w^{Hs} v^{Hs} Lm})}{\partial z} - f u^{Lm} - \frac{1}{\rho^{Lm}} \frac{\partial p^{Lm}}{\partial y} \quad (3.14.2)$$

$$\frac{\partial u^{Hm}}{\partial t} = -\overline{\nabla}_h \cdot \mathbf{v}_h^{Lm} u^{Hm} - \overline{\nabla}_h \cdot \mathbf{v}_h^{Hm} u^{Lm} - \overline{\nabla}_h \cdot \mathbf{v}_h^{Hm} u^{Hm} - \overline{\nabla}_h \cdot \overline{\mathbf{v}_h^{Hs} u^{Hs} Ls} + \overline{\nabla}_h \cdot \overline{\mathbf{v}_h^{Hm} u^{Hm} Lm} + \overline{\nabla}_h \cdot \overline{\mathbf{v}_h^{Hs} u^{Hs} Lm} - \frac{\partial (\overline{w^{Lm} u^{Hm}})}{\partial z} - \frac{\partial (\overline{w^{Hm} u^{Lm}})}{\partial z} - \frac{\partial (\overline{w^{Hm} u^{Hm}})}{\partial z} - \frac{\partial \overline{w^{Hs} u^{Hs} Ls}}{\partial z} + \frac{\partial \overline{w^{Hm} u^{Hm} Lm}}{\partial z} + \frac{\partial \overline{w^{Hs} u^{Hs} Lm}}{\partial z} + f v^{Hm} - \frac{1}{\rho^{Lm}} \frac{\partial p^{Hm}}{\partial x} \quad (3.15.1)$$

$$\frac{\partial v^{Hm}}{\partial t} = -\overline{\nabla}_h \cdot \mathbf{v}_h^{Lm} v^{Hm} - \overline{\nabla}_h \cdot \mathbf{v}_h^{Hm} v^{Lm} - \overline{\nabla}_h \cdot \mathbf{v}_h^{Hm} v^{Hm} - \overline{\nabla}_h \cdot \overline{\mathbf{v}_h^{Hs} v^{Hs} Ls} + \overline{\nabla}_h \cdot \overline{\mathbf{v}_h^{Hm} v^{Hm} Lm} + \overline{\nabla}_h \cdot \overline{\mathbf{v}_h^{Hs} v^{Hs} Lm} - \frac{\partial (\overline{w^{Lm} v^{Hm}})}{\partial z} - \frac{\partial (\overline{w^{Hm} v^{Lm}})}{\partial z} - \frac{\partial (\overline{w^{Hm} v^{Hm}})}{\partial z} - \frac{\partial \overline{w^{Hs} v^{Hs} Ls}}{\partial z} + \frac{\partial \overline{w^{Hm} v^{Hm} Lm}}{\partial z} + \frac{\partial \overline{w^{Hs} v^{Hs} Lm}}{\partial z} - f u^{Hm} - \frac{1}{\rho^{Lm}} \frac{\partial p^{Hm}}{\partial y} \quad (3.15.2)$$

$$\frac{\partial u^{Ll}}{\partial t} = -\overline{\nabla}_h \cdot \mathbf{v}_h^{Ll} u^{Ll} - \overline{\nabla}_h \cdot \overline{\mathbf{v}_h^{Hl} u^{Hl} Ll} - \overline{\nabla}_h \cdot \overline{\mathbf{v}_h^{Hm} u^{Hm} Ll} - \overline{\nabla}_h \cdot \overline{\mathbf{v}_h^{Hs} u^{Hs} Ll} - \frac{\partial (\overline{w^{Ll} u^{Ll}})}{\partial z} - \frac{\partial (\overline{w^{Hl} u^{Hl} Ll})}{\partial z} - \frac{\partial (\overline{w^{Hm} u^{Hm} Ll})}{\partial z} - \frac{\partial (\overline{w^{Hs} u^{Hs} Ll})}{\partial z} + f v^{Ll} - \frac{1}{\rho^{Ll}} \frac{\partial p^{Ll}}{\partial x} \quad (3.16.1)$$

$$\frac{\partial v^{Ll}}{\partial t} = -\overline{\nabla}_h \cdot \mathbf{v}_h^{Ll} v^{Ll} - \overline{\nabla}_h \cdot \overline{\mathbf{v}_h^{Hl} v^{Hl} Ll} - \overline{\nabla}_h \cdot \overline{\mathbf{v}_h^{Hm} v^{Hm} Ll} - \overline{\nabla}_h \cdot \overline{\mathbf{v}_h^{Hs} v^{Hs} Ll} - \frac{\partial (\overline{w^{Ll} v^{Ll}})}{\partial z} - \frac{\partial (\overline{w^{Hl} v^{Hl} Ll})}{\partial z} - \frac{\partial (\overline{w^{Hm} v^{Hm} Ll})}{\partial z} - \frac{\partial (\overline{w^{Hs} v^{Hs} Ll})}{\partial z} - f u^{Ll} - \frac{1}{\rho^{Ll}} \frac{\partial p^{Ll}}{\partial y} \quad (3.16.2)$$

I II III IV V VI VII VIII IX X XI

✂

$$\begin{aligned}
\frac{\partial u^{Hl}}{\partial t} = & -\overline{\nabla}_h \cdot \overline{\mathbf{v}}_h^{Ll} u^{Hl} - \overline{\nabla}_h \cdot \mathbf{v}_h^{Hl} \overline{u}^{Ll} - \overline{\nabla}_h \cdot \mathbf{v}_h^{Hl} u^{Hl} - \overline{\nabla}_h \cdot \overline{\mathbf{v}}_h^{Hm} u^{HmLm} - \overline{\nabla}_h \cdot \overline{\mathbf{v}}_h^{Hs} u^{HsLm} + \overline{\nabla}_h \cdot \overline{\mathbf{v}}_h^{Hl} u^{HlLl} + \overline{\nabla}_h \cdot \overline{\mathbf{v}}_h^{Hm} u^{HmLl} + \overline{\nabla}_h \cdot \overline{\mathbf{v}}_h^{Hs} u^{HsLl} \\
& - \frac{\partial(w^{Ll}u^{Hl})}{\partial z} - \frac{\partial(w^{Hl}u^{Ll})}{\partial z} - \frac{\partial(w^{Hl}u^{Hl})}{\partial z} - \frac{\partial(\overline{w}^{Hm}u^{HmLm})}{\partial z} - \frac{\partial(\overline{w}^{Hs}u^{HsLm})}{\partial z} + \frac{\partial(w^{Hl}u^{HlLl})}{\partial z} + \frac{\partial(\overline{w}^{Hm}u^{HmLl})}{\partial z} + \frac{\partial(\overline{w}^{Hs}u^{HsLl})}{\partial z} + f v^{Hl} - \frac{1}{\rho^{Ll}} \frac{\partial p^{Hl}}{\partial x}
\end{aligned} \tag{3.17.1}$$

$$\begin{aligned}
\frac{\partial v^{Hl}}{\partial t} = & -\overline{\nabla}_h \cdot \mathbf{v}_h^{Ll} v^{Hl} - \overline{\nabla}_h \cdot \mathbf{v}_h^{Hl} v^{Ll} - \overline{\nabla}_h \cdot \mathbf{v}_h^{Hl} v^{Hl} - \overline{\nabla}_h \cdot \overline{\mathbf{v}}_h^{Hm} v^{HmLm} - \overline{\nabla}_h \cdot \overline{\mathbf{v}}_h^{Hs} v^{HsLm} + \overline{\nabla}_h \cdot \overline{\mathbf{v}}_h^{Hl} v^{HlLl} + \overline{\nabla}_h \cdot \overline{\mathbf{v}}_h^{Hm} v^{HmLl} + \overline{\nabla}_h \cdot \overline{\mathbf{v}}_h^{Hs} v^{HsLl} \\
\text{I} \quad & \text{II} \quad \text{III} \quad \text{IV} \quad \text{V} \quad \text{VI} \quad \text{VII} \quad \text{VIII} \quad \text{IX} \\
& - \frac{\partial(w^{Ll}v^{Hl})}{\partial z} - \frac{\partial(w^{Hl}v^{Ll})}{\partial z} - \frac{\partial(w^{Hl}v^{Hl})}{\partial z} - \frac{\partial(\overline{w}^{Hm}v^{HmLm})}{\partial z} - \frac{\partial(\overline{w}^{Hs}v^{HsLm})}{\partial z} + \frac{\partial(w^{Hl}v^{HlLl})}{\partial z} + \frac{\partial(\overline{w}^{Hm}v^{HmLl})}{\partial z} + \frac{\partial(\overline{w}^{Hs}v^{HsLl})}{\partial z} - f u^{Hl} - \frac{1}{\rho^{Ll}} \frac{\partial p^{Hl}}{\partial y} \\
& \text{X} \quad \text{XI} \quad \text{XII} \quad \text{XIII} \quad \text{XIV} \quad \text{XV} \quad \text{XVI} \quad \text{XVII} \quad \text{XVIII} \quad \text{XIX}
\end{aligned} \tag{3.17.2}$$

$$\begin{aligned}
\frac{\partial w^{Hs}}{\partial t} = & -\overline{\nabla}_h \cdot \overline{\mathbf{v}}_h^{Ls} w^{Hs} - \overline{\nabla}_h \cdot \mathbf{v}_h^{Hs} \overline{w}^{Ls} - \overline{\nabla}_h \cdot \mathbf{v}_h^{Hs} w^{Hs} + \overline{\nabla}_h \cdot \overline{\mathbf{v}}_h^{Hs} w^{HsLs} - \frac{\partial w^{Ls} w^{Hs}}{\partial z} - \frac{\partial w^{Hs} w^{Ls}}{\partial z} - \frac{\partial w^{Hs} w^{Hs}}{\partial z} + \frac{\partial(\overline{w}^{Hs} w^{HsLs})}{\partial z} - \frac{1}{\rho^{Ls}} \frac{\partial p^{Hs}}{\partial z} - \frac{\rho^{Hs}}{\rho^{Ls}} g \\
\text{I} \quad & \text{II} \quad \text{III} \quad \text{IV} \quad \text{V} \quad \text{VI} \quad \text{VII} \quad \text{VIII} \quad \text{IX} \quad \text{X} \quad \text{XI}
\end{aligned} \tag{3.20}$$

$$\begin{aligned}
\frac{\partial w^{Hm}}{\partial t} = & -\overline{\nabla}_h \cdot \overline{\mathbf{v}}_h^{Lm} w^{Hm} - \overline{\nabla}_h \cdot \mathbf{v}_h^{Hm} \overline{w}^{Lm} - \overline{\nabla}_h \cdot \mathbf{v}_h^{Hm} w^{Hm} - \overline{\nabla}_h \cdot \overline{\mathbf{v}}_h^{Hs} w^{HsLs} + \overline{\nabla}_h \cdot \overline{\mathbf{v}}_h^{Hm} w^{HmLm} + \overline{\nabla}_h \cdot \overline{\mathbf{v}}_h^{Hs} w^{HsLm} \\
\text{I} \quad & \text{II} \quad \text{III} \quad \text{IV} \quad \text{V} \quad \text{VI} \quad \text{VII} \\
& - \frac{\partial(w^{Lm}w^{Hm})}{\partial z} - \frac{\partial(w^{Hm}w^{Lm})}{\partial z} - \frac{\partial(w^{Hm}w^{Hm})}{\partial z} - \frac{\partial(\overline{w}^{Hs}w^{HsLs})}{\partial z} + \frac{\partial(\overline{w}^{Hm}w^{HmLm})}{\partial z} + \frac{\partial(\overline{w}^{Hs}w^{HsLm})}{\partial z} - \frac{1}{\rho^{Lm}} \frac{\partial p^{Hm}}{\partial z} - \frac{\rho^{Hm}}{\rho^{Lm}} g \\
& \text{VIII} \quad \text{IX} \quad \text{X} \quad \text{XI} \quad \text{XII} \quad \text{XIII} \quad \text{XIV} \quad \text{XV}
\end{aligned} \tag{3.21}$$

$$\frac{\partial w^{Ll}}{\partial t} = \underbrace{-\vec{\nabla}_h \cdot \mathbf{v}_h^{Ll} w^{Ll}}_{\text{I}} - \underbrace{\vec{\nabla}_h \cdot \overline{\mathbf{v}_h^{Hl} w^{HlLl}}}_{\text{II}} - \underbrace{\vec{\nabla}_h \cdot \overline{\mathbf{v}_h^{Hm} w^{HmLl}}}_{\text{III}} - \underbrace{\vec{\nabla}_h \cdot \overline{\mathbf{v}_h^{Hs} w^{HsLl}}}_{\text{IV}} - \underbrace{\frac{\partial(\overline{w^{Ll} w^{Ll}})}{\partial z}}_{\text{V}} - \underbrace{\frac{\partial(\overline{w^{Hl} w^{HlLl}})}{\partial z}}_{\text{VI}} - \underbrace{\frac{\partial(\overline{w^{Hm} w^{HmLl}})}{\partial z}}_{\text{VII}} - \underbrace{\frac{\partial(\overline{w^{Hs} w^{HsLl}})}{\partial z}}_{\text{VIII}} - \underbrace{\frac{1}{\rho^{Ll}} \frac{\partial p^{Ll}}{\partial z}}_{\text{IX}} - \underbrace{g}_{\text{X}} \quad (3.22)$$

$$\frac{\partial w^{Hl}}{\partial t} = \underbrace{-\vec{\nabla}_h \cdot \mathbf{v}_h^{Ll} w^{Hl}}_{\text{I}} - \underbrace{\vec{\nabla}_h \cdot \mathbf{v}_h^{Hl} w^{Ll}}_{\text{II}} - \underbrace{\vec{\nabla}_h \cdot \mathbf{v}_h^{Hl} w^{Hl}}_{\text{III}} - \underbrace{\vec{\nabla}_h \cdot \overline{\mathbf{v}_h^{Hm} w^{HmLm}}}_{\text{IV}} - \underbrace{\vec{\nabla}_h \cdot \overline{\mathbf{v}_h^{Hs} w^{HsLm}}}_{\text{V}} + \underbrace{\vec{\nabla}_h \cdot \overline{\mathbf{v}_h^{Hl} w^{HlLl}}}_{\text{VI}} + \underbrace{\vec{\nabla}_h \cdot \overline{\mathbf{v}_h^{Hm} w^{HmLl}}}_{\text{VII}} + \underbrace{\vec{\nabla}_h \cdot \overline{\mathbf{v}_h^{Hs} w^{HsLl}}}_{\text{VIII}} - \underbrace{\frac{\partial(\overline{w^{Ll} w^{Hl}})}{\partial z}}_{\text{X}} - \underbrace{\frac{\partial(\overline{w^{Hl} w^{Ll}})}{\partial z}}_{\text{XI}} - \underbrace{\frac{\partial(\overline{w^{Hl} w^{Hl}})}{\partial z}}_{\text{XII}} - \underbrace{\frac{\partial(\overline{w^{Hm} w^{HmLm}})}{\partial z}}_{\text{XIII}} - \underbrace{\frac{\partial(\overline{w^{Hs} w^{HsLm}})}{\partial z}}_{\text{XIV}} + \underbrace{\frac{\partial(\overline{w^{Hl} w^{HlLl}})}{\partial z}}_{\text{XV}} + \underbrace{\frac{\partial(\overline{w^{Hm} w^{HmLl}})}{\partial z}}_{\text{XVI}} + \underbrace{\frac{\partial(\overline{w^{Hs} w^{HsLl}})}{\partial z}}_{\text{XVII}} - \underbrace{\frac{1}{\rho^{Ll}} \frac{\partial p^{Hl}}{\partial z}}_{\text{XVIII}} - \underbrace{\frac{\rho^{Hl}}{\rho^{Ll}} g}_{\text{XIX}} \quad (3.23)$$

$$\frac{\partial \theta^{Hs}}{\partial t} = \underbrace{-\vec{\nabla}_h \cdot \mathbf{v}_h^{Ls} \theta^{Hs}}_{\text{I}} - \underbrace{\vec{\nabla}_h \cdot \mathbf{v}_h^{Hs} \theta^{Ls}}_{\text{II}} - \underbrace{\vec{\nabla}_h \cdot \mathbf{v}_h^{Hs} \theta^{Hs}}_{\text{III}} + \underbrace{\vec{\nabla}_h \cdot \overline{\mathbf{v}_h^{Hs} \theta^{HsLs}}}_{\text{IV}} - \underbrace{\frac{\partial(\overline{w^{Ls} \theta^{Hs}})}{\partial z}}_{\text{V}} - \underbrace{\frac{\partial(\overline{w^{Hs} \theta^{Ls}})}{\partial z}}_{\text{VI}} - \underbrace{\frac{\partial(\overline{w^{Hs} \theta^{Hs}})}{\partial z}}_{\text{VII}} + \underbrace{\frac{\partial(\overline{w^{Hs} \theta^{HsLs}})}{\partial z}}_{\text{VIII}} - \underbrace{\frac{1}{\rho^{Ls} C_p} (\nabla \cdot Q^{Hs})}_{\text{IX}} - \underbrace{\frac{L_v e^{Hs}}{\rho^{Ls} C_p}}_{\text{X}} \quad (3.25)$$

$$\frac{\partial \theta^{Lm}}{\partial t} = \underbrace{-\vec{\nabla}_h \cdot \mathbf{v}_h^{Lm} \theta^{Lm}}_{\text{I}} - \underbrace{\vec{\nabla}_h \cdot \overline{\mathbf{v}_h^{Hm} \theta^{HmLm}}}_{\text{II}} - \underbrace{\vec{\nabla}_h \cdot \overline{\mathbf{v}_h^{Hs} \theta^{HsLm}}}_{\text{III}} - \underbrace{\frac{\partial(\overline{w^{Lm} \theta^{Lm}})}{\partial z}}_{\text{IV}} - \underbrace{\frac{\partial(\overline{w^{Hm} \theta^{HmLm}})}{\partial z}}_{\text{V}} - \underbrace{\frac{\partial(\overline{w^{Hs} \theta^{HsLm}})}{\partial z}}_{\text{VI}} - \underbrace{\frac{1}{\rho^{Lm} C_p} (\nabla \cdot Q^{Lm})}_{\text{VII}} - \underbrace{\frac{L_v e^{Lm}}{\rho^{Lm} C_p}}_{\text{VIII}} \quad (3.26)$$

$$\frac{\partial \theta^{Hm}}{\partial t} = \underbrace{-\vec{\nabla}_h \cdot \mathbf{v}_h^{Lm} \theta^{Hm}}_{\text{I}} - \underbrace{\vec{\nabla}_h \cdot \mathbf{v}_h^{Hm} \theta^{Lm}}_{\text{II}} - \underbrace{\vec{\nabla}_h \cdot \mathbf{v}_h^{Hm} \theta^{Hm}}_{\text{III}} - \underbrace{\vec{\nabla}_h \cdot \overline{\mathbf{v}_h^{Hs} \theta^{HsLs}}}_{\text{IV}} + \underbrace{\vec{\nabla}_h \cdot \overline{\mathbf{v}_h^{Hm} \theta^{HmLm}}}_{\text{V}} + \underbrace{\vec{\nabla}_h \cdot \overline{\mathbf{v}_h^{Hs} \theta^{HsLm}}}_{\text{VI}} - \underbrace{\frac{\partial(\overline{w^{Lm} \theta^{Hm}})}{\partial z}}_{\text{VII}} - \underbrace{\frac{\partial(\overline{w^{Hm} \theta^{Lm}})}{\partial z}}_{\text{VIII}} - \underbrace{\frac{\partial(\overline{w^{Hm} \theta^{Hm}})}{\partial z}}_{\text{IX}} - \underbrace{\frac{\partial(\overline{w^{Hs} \theta^{HsLs}})}{\partial z}}_{\text{X}} + \underbrace{\frac{\partial(\overline{w^{Hm} \theta^{HmLm}})}{\partial z}}_{\text{XI}} + \underbrace{\frac{\partial(\overline{w^{Hs} \theta^{HsLm}})}{\partial z}}_{\text{XII}} - \underbrace{\frac{1}{\rho^{Lm} C_p} (\nabla \cdot Q^{Hm})}_{\text{XIII}} - \underbrace{\frac{L_v e^{Hm}}{\rho^{Lm} C_p}}_{\text{XIV}} \quad (3.27)$$



$$\begin{aligned}
\frac{\partial \theta^{Ll}}{\partial t} = & \underbrace{-\vec{\nabla}_h \cdot \mathbf{v}_h^{Ll} \theta^{Ll}}_{\text{I}} - \underbrace{\vec{\nabla}_h \cdot \overline{\mathbf{v}_h^{Hl} \theta^{HlLl}}}_{\text{II}} - \underbrace{\vec{\nabla}_h \cdot \overline{\mathbf{v}_h^{Hm} \theta^{HmLl}}}_{\text{III}} - \underbrace{\vec{\nabla}_h \cdot \overline{\mathbf{v}_h^{Hs} \theta^{HsLl}}}_{\text{IV}} \\
& - \underbrace{\frac{\partial (w^{Ll} \theta^{Ll})}{\partial z}}_{\text{V}} - \underbrace{\frac{\partial (\overline{w^{Hl} \theta^{HlLl}})}{\partial z}}_{\text{VI}} - \underbrace{\frac{\partial (\overline{w^{Hm} \theta^{HmLl}})}{\partial z}}_{\text{VII}} - \underbrace{\frac{\partial (\overline{w^{Hs} \theta^{HsLl}})}{\partial z}}_{\text{VIII}} - \underbrace{\frac{1}{\rho^{Ll} C_p} (\nabla \cdot Q^{Ll})}_{\text{IX}} - \underbrace{\frac{L_v e^{Ll}}{\rho^{Ll} C_p}}_{\text{XI}}
\end{aligned} \tag{3.28}$$

$$\begin{aligned}
\frac{\partial \theta^{Hl}}{\partial t} = & \underbrace{-\vec{\nabla}_h \cdot \mathbf{v}_h^{Ll} \theta^{Hl}}_{\text{I}} - \underbrace{\vec{\nabla}_h \cdot \mathbf{v}_h^{Hl} v^{Ll}}_{\text{II}} - \underbrace{\vec{\nabla}_h \cdot \mathbf{v}_h^{Hl} \theta^{Hl}}_{\text{III}} - \underbrace{\vec{\nabla}_h \cdot \overline{\mathbf{v}_h^{Hm} \theta^{HmLm}}}_{\text{IV}} - \underbrace{\vec{\nabla}_h \cdot \overline{\mathbf{v}_h^{Hs} \theta^{HsLm}}}_{\text{V}} + \underbrace{\vec{\nabla}_h \cdot \overline{\mathbf{v}_h^{Hl} \theta^{HlLl}}}_{\text{VI}} + \underbrace{\vec{\nabla}_h \cdot \overline{\mathbf{v}_h^{Hm} \theta^{HmLl}}}_{\text{VII}} + \underbrace{\vec{\nabla}_h \cdot \overline{\mathbf{v}_h^{Hs} \theta^{HsLl}}}_{\text{VIII}} \\
& - \underbrace{\frac{\partial (w^{Ll} \theta^{Hl})}{\partial z}}_{\text{IX}} - \underbrace{\frac{\partial (w^{Hl} \theta^{Ll})}{\partial z}}_{\text{X}} - \underbrace{\frac{\partial (w^{Hl} \theta^{Hl})}{\partial z}}_{\text{XI}} - \underbrace{\frac{\partial \overline{w^{Hm} \theta^{HmLm}}}{\partial z}}_{\text{XII}} - \underbrace{\frac{\partial \overline{w^{Hs} \theta^{HsLm}}}{\partial z}}_{\text{XIII}} + \underbrace{\frac{\partial \overline{w^{Hl} \theta^{HlLl}}}{\partial z}}_{\text{XIV}} + \underbrace{\frac{\partial \overline{w^{Hm} \theta^{HmLl}}}{\partial z}}_{\text{XV}} + \underbrace{\frac{\partial \overline{w^{Hs} \theta^{HsLl}}}{\partial z}}_{\text{XVI}} - \underbrace{\frac{1}{\rho^{Ll} C_p} (\nabla \cdot Q^{Hl})}_{\text{XVII}} - \underbrace{\frac{L_v e^{Hl}}{\rho^{Ll} C_p}}_{\text{XVIII}}
\end{aligned} \tag{3.29}$$

$$\begin{aligned}
\frac{\partial q^{Ls}}{\partial t} = & \underbrace{-\vec{\nabla}_h \cdot \mathbf{v}_h^{Ls} q^{Ls}}_{\text{I}} - \underbrace{\vec{\nabla}_h \cdot \overline{\mathbf{v}_h^{Hs} q^{HsLs}}}_{\text{II}} - \underbrace{\frac{\partial w^{Ls} q^{Ls}}{\partial z}}_{\text{III}} - \underbrace{\frac{\partial \overline{w^{Hs} q^{HsLs}}}{\partial z}}_{\text{IV}} - \underbrace{\frac{S^{Ls}}{\rho^{Ls}}}_{\text{V}} - \underbrace{\frac{e^{Ls}}{\rho^{Ls}}}_{\text{VI}}
\end{aligned} \tag{3.30}$$

$$\begin{aligned}
\frac{\partial q^{Hs}}{\partial t} = & \underbrace{-\vec{\nabla}_h \cdot \mathbf{v}_h^{Ls} q^{Hs}}_{\text{I}} - \underbrace{\vec{\nabla}_h \cdot \mathbf{v}_h^{Hs} q^{Ls}}_{\text{II}} - \underbrace{\vec{\nabla}_h \cdot \mathbf{v}_h^{Hs} q^{Hs}}_{\text{III}} + \underbrace{\vec{\nabla}_h \cdot \overline{\mathbf{v}_h^{Hs} q^{HsLs}}}_{\text{IV}} - \underbrace{\frac{\partial \overline{w^{Ls} q^{Hs}}}{\partial z}}_{\text{V}} - \underbrace{\frac{\partial w^{Hs} q^{Ls}}{\partial z}}_{\text{VI}} - \underbrace{\frac{\partial w^{Hs} q^{Hs}}{\partial z}}_{\text{VII}} + \underbrace{\frac{\partial \overline{w^{Hs} q^{HsLs}}}{\partial z}}_{\text{VIII}} - \underbrace{\frac{S^{Hs}}{\rho^{Ls}}}_{\text{IX}} - \underbrace{\frac{e^{Hs}}{\rho^{Ls}}}_{\text{X}}
\end{aligned} \tag{3.31}$$

$$\begin{aligned}
\frac{\partial q^{Lm}}{\partial t} = & \underbrace{-\vec{\nabla}_h \cdot \mathbf{v}_h^{Lm} q^{Lm}}_{\text{I}} - \underbrace{\vec{\nabla}_h \cdot \overline{\mathbf{v}_h^{Hm} q^{HmLm}}}_{\text{II}} - \underbrace{\vec{\nabla}_h \cdot \overline{\mathbf{v}_h^{Hs} q^{HsLm}}}_{\text{III}} - \underbrace{\frac{\partial (w^{Lm} q^{Lm})}{\partial z}}_{\text{IV}} - \underbrace{\frac{\partial (\overline{w^{Hm} q^{HmLm}})}{\partial z}}_{\text{V}} - \underbrace{\frac{\partial (\overline{w^{Hs} q^{HsLm}})}{\partial z}}_{\text{VI}} - \underbrace{\frac{S^{Lm}}{\rho^{Lm}}}_{\text{VII}} - \underbrace{\frac{e^{Lm}}{\rho^{Lm}}}_{\text{VIII}}
\end{aligned} \tag{3.32}$$

$$\begin{aligned}
\frac{\partial q^{Hm}}{\partial t} = & \underbrace{-\vec{\nabla}_h \cdot \mathbf{v}_h^{Lm} q^{Hm}}_{\text{I}} - \underbrace{\vec{\nabla}_h \cdot \mathbf{v}_h^{Hm} q^{Lm}}_{\text{II}} - \underbrace{\vec{\nabla}_h \cdot \mathbf{v}_h^{Hm} q^{Hm}}_{\text{III}} - \underbrace{\vec{\nabla}_h \cdot \mathbf{v}_h^{Hs} q^{Hs^{Ls}}}_{\text{IV}} + \underbrace{\vec{\nabla}_h \cdot \mathbf{v}_h^{Hm} q^{Hm^{Lm}}}_{\text{V}} + \underbrace{\vec{\nabla}_h \cdot \mathbf{v}_h^{Hs} q^{Hs^{Lm}}}_{\text{VI}} \\
& - \underbrace{\frac{\partial(\bar{w}^{Lm} q^{Hm})}{\partial z}}_{\text{VII}} - \underbrace{\frac{\partial(w^{Hm} q^{Lm})}{\partial z}}_{\text{VIII}} - \underbrace{\frac{\partial(w^{Hm} q^{Hm})}{\partial z}}_{\text{IX}} - \underbrace{\frac{\partial\bar{w}^{Hs} q^{Hs^{Ls}}}{\partial z}}_{\text{X}} + \underbrace{\frac{\partial\bar{w}^{Hm} q^{Hm^{Lm}}}{\partial z}}_{\text{XI}} + \underbrace{\frac{\partial\bar{w}^{Hs} q^{Hs^{Lm}}}{\partial z}}_{\text{XII}} - \underbrace{\frac{S^{Hm}}{\rho^{Ls}}}_{\text{XIII}} - \underbrace{\frac{e^{Hm}}{\rho^{Lm}}}_{\text{XIV}}
\end{aligned} \tag{3.33}$$

$$\begin{aligned}
\frac{\partial q^{Ll}}{\partial t} = & \underbrace{-\vec{\nabla}_h \cdot \mathbf{v}_h^{Ll} q^{Ll}}_{\text{I}} - \underbrace{\vec{\nabla}_h \cdot \mathbf{v}_h^{Hl} q^{Hl^{Ll}}}_{\text{II}} - \underbrace{\vec{\nabla}_h \cdot \mathbf{v}_h^{Hm} q^{Hm^{Ll}}}_{\text{III}} - \underbrace{\vec{\nabla}_h \cdot \mathbf{v}_h^{Hs} q^{Hs^{Ll}}}_{\text{IV}} - \underbrace{\frac{\partial(w^{Ll} q^{Ll})}{\partial z}}_{\text{V}} - \underbrace{\frac{\partial(w^{Hl} q^{Hl^{Ll}})}{\partial z}}_{\text{VI}} - \underbrace{\frac{\partial(w^{Hm} q^{Hm^{Ll}})}{\partial z}}_{\text{VII}} - \underbrace{\frac{\partial(w^{Hs} q^{Hs^{Ll}})}{\partial z}}_{\text{VIII}} - \underbrace{\frac{S^{Ll}}{\rho^{Ll}}}_{\text{IX}} - \underbrace{\frac{e^{Ll}}{\rho^{Ll}}}_{\text{X}}
\end{aligned} \tag{3.34}$$

$$\begin{aligned}
\frac{\partial q^{Hl}}{\partial t} = & \underbrace{-\vec{\nabla}_h \cdot \mathbf{v}_h^{Ll} q^{Hl}}_{\text{I}} - \underbrace{\vec{\nabla}_h \cdot \mathbf{v}_h^{Hl} q^{Ll}}_{\text{II}} - \underbrace{\vec{\nabla}_h \cdot \mathbf{v}_h^{Hl} q^{Hl}}_{\text{III}} - \underbrace{\vec{\nabla}_h \cdot \mathbf{v}_h^{Hm} q^{Hm^{Lm}}}_{\text{IV}} - \underbrace{\vec{\nabla}_h \cdot \mathbf{v}_h^{Hs} q^{Hs^{Lm}}}_{\text{V}} + \underbrace{\vec{\nabla}_h \cdot \mathbf{v}_h^{Hl} q^{Hl^{Ll}}}_{\text{VI}} + \underbrace{\vec{\nabla}_h \cdot \mathbf{v}_h^{Hm} q^{Hm^{Ll}}}_{\text{VII}} + \underbrace{\vec{\nabla}_h \cdot \mathbf{v}_h^{Hs} q^{Hs^{Ll}}}_{\text{VIII}} \\
& - \underbrace{\frac{\partial(w^{Ll} q^{Hl})}{\partial z}}_{\text{IX}} - \underbrace{\frac{\partial(w^{Hl} q^{Ll})}{\partial z}}_{\text{X}} - \underbrace{\frac{\partial(w^{Hl} q^{Hl})}{\partial z}}_{\text{XI}} - \underbrace{\frac{\partial\bar{w}^{Hm} q^{Hm^{Lm}}}{\partial z}}_{\text{XII}} - \underbrace{\frac{\partial\bar{w}^{Hs} q^{Hs^{Lm}}}{\partial z}}_{\text{XIII}} + \underbrace{\frac{\partial\bar{w}^{Hl} q^{Hl^{Ll}}}{\partial z}}_{\text{XIV}} + \underbrace{\frac{\partial\bar{w}^{Hm} q^{Hm^{Ll}}}{\partial z}}_{\text{XV}} + \underbrace{\frac{\partial\bar{w}^{Hs} q^{Hs^{Ll}}}{\partial z}}_{\text{XVI}} - \underbrace{\frac{S^{Hl}}{\rho^{Ls}}}_{\text{XVII}} - \underbrace{\frac{e^{Hl}}{\rho^{Ll}}}_{\text{XVIII}}
\end{aligned} \tag{3.35}$$

$$\begin{aligned}
\frac{\partial(\bar{w}^M u^M)}{\partial z} = f v^L - \frac{1}{\rho} \frac{\partial p^L}{\partial x} & \tag{4.1} & -f u^L - \frac{1}{\rho} \frac{\partial p^L}{\partial y} = \frac{\partial(\bar{w}^M v^M)}{\partial z} & \tag{4.2} & \frac{1}{\rho} \frac{\partial p^L}{\partial z} = -g & \tag{4.3} \\
\text{VII} \quad \text{X} \quad \text{XI} & & \text{X} \quad \text{XI} \quad \text{VII} & & \text{X} \quad \text{XI} &
\end{aligned}$$

$$\begin{aligned}
\vec{\nabla}_h \cdot \mathbf{v}_h^L \zeta^M + \vec{\nabla}_h \cdot \mathbf{v}_h^M \zeta^L = & -2\zeta^M D^L - 2\zeta^L D^M - \frac{\partial}{\partial x} \frac{\partial w^M v^M}{\partial z} - \frac{\partial}{\partial y} \frac{\partial w^M u^M}{\partial z} & \tag{4.5} \\
\text{A} \quad \text{B} \quad \text{C} \quad \text{D} & \quad \text{E} \quad \text{F} &
\end{aligned}$$

11 List of Equations

$$\overline{\nabla}_h \cdot \mathbf{v}_h^L u^M + \overline{\nabla}_h \cdot \mathbf{v}_h^M u^L = \frac{\partial w^M u^M}{\partial z} \quad (4.6.1)$$

$$\overline{\nabla}_h \cdot \mathbf{v}_h^L v^M + \overline{\nabla}_h \cdot \mathbf{v}_h^M v^L = \frac{\partial w^M v^M}{\partial z} \quad (4.6.2)$$

II III XII

$$\frac{\partial w^M w^M}{\partial z} = \frac{\theta^M}{\theta^L} g \quad (4.7)$$

XV XIX

$$\frac{\partial w^M (w^M u^M)}{\partial z} = u^M \frac{\theta^M}{\theta^L} g \quad (4.8)$$

$$\frac{\partial w^M (w^M v^M)}{\partial z} = v^M \frac{\theta^M}{\theta^L} g \quad (4.9)$$

A B

$$\overline{\nabla} \cdot \mathbf{v}_h^L \theta^L = -\frac{\partial (\overline{w^M \theta^M})}{\partial z} - \frac{\partial (\overline{w^S \theta^S})}{\partial z} \quad (4.10)$$

$$\overline{\nabla} \cdot \mathbf{v}_h^L q^L = -\frac{\partial (\overline{w^M q^M})}{\partial z} - \frac{\partial (\overline{w^S q^S})}{\partial z} \quad (4.11)$$

II VII VIII

$$-\overline{\nabla}_h \cdot \mathbf{v}_h^S (\theta^M + \theta^L) - \overline{\nabla}_h \cdot \mathbf{v}_h^S \theta^S = \frac{\partial (w^S \theta^S)}{\partial z} \quad (4.13)$$

$$-\overline{\nabla}_h \cdot \mathbf{v}_h^S (q^M + q^L) - \overline{\nabla}_h \cdot \mathbf{v}_h^S q^S = \frac{\partial (w^S q^S)}{\partial z} \quad (4.14)$$

III IV X

$$\frac{\partial (w^M \theta^M)}{\partial z} = -\frac{\partial \overline{w^S \theta^S}^{(M+L)}}{\partial z} - \left( -\frac{\partial \overline{w^S \theta^S}^L}{\partial z} \right) - \frac{L_p E^M}{\rho C_p} \quad (4.15)$$

XII XIII XVI XIX

$$\frac{E^M}{\rho} = \left[ \frac{\partial \overline{w^S q^S}^{(M+L)}}{\partial z} - \left( \frac{\partial \overline{w^S q^S}^L}{\partial z} \right) \right] + \frac{\partial (w^M q^M)}{\partial z} \quad (4.16)$$

XIX XIII XVI XV



## 12 Reference

Akiyama, T., 1973: Ageostrophic Low-Level Jet Stream in the Baiu Season Associated with Heavy Rainfalls over the Sea Area. *J. Meteorol. Soc. Jpn.*, **51**, 205 – 208

Anthes, R. A., 1977: A Cumulus Parameterization Scheme Utilizing a One-Dimensional Cloud Model. *Mon. Wea. Rev.*, **105**, 270 – 286

Arakawa, A., and W. H. Schubert, 1974: Interaction of a cumulus cloud ensemble with the large-scale environment, Part 1. *J. Atmos. Sci.*, **31**, 674 – 701

———, 2004: Review Article. The Cumulus Parameterization Problem: Past, Present and Future. *J. Climate*, **17**, 2493 – 2525

Atkinson, B.W., 1981: Mesoscale Atmospheric Circulations. *Academic Press*. p.3 – 12

Augustine, J. A., K. W. Howard, 1991: Mesoscale Convective Complexes over the United States during 1986 and 1987. *Mon. Wea. Rev.*, **119**, 1575 – 1589

Biggerstaff, M. I., and R. A. Houze, Jr., 1991 Kinematic and Precipitation Structure of the 10-11 June 1985 Squall Line. *Mon. Wea. Rev.*, **119**, 3034 – 3065

Blackmon, M. L., 1977: An Observational Study of the Northern Hemisphere Wintertime Circulation. *J. Atmos. Sci.*, **34**, 1040 – 1053

Bonner, W. D., S. Esbensen and R. Greenberg, 1968: Kinetics of the Low-Level Jet. *J. Appl. Meteorol.*, **7**, 339 – 347

Chen, T. C., J. A. Kpaeyeh, 1993: The Synoptic-Scale Environment Associated with the Low-level Jet of the Great Plains. *Mon. Wea. Rev.*, **121**, 416 – 420

Chen, G., R. Yoshida, W. Sha, T. Iwasaki, 2014: Convective Instability Associated with the Eastward-Propagating Rainfall Episodes over Eastern China during the Warm Season. *J. Climate*, **27**, 2331 – 2339

Chen, G. T. C., and R. Y. Tzeng, 1988a: A study on the maintenance of the winter subtropical jet streams in the northern hemisphere. *Tellus*, **40A**, 392 – 397

———, and CC Yu, 1988b: Study of Low-Level Jet and Extremely Heavy Rainfall over Northern Taiwan in the Mei-Yu Season. *Mon. Wea. Rev.*, **116**, 884 – 891

———, and YS Hsu, 1997: Composite Structure of a Low-Level Jet over Southern China Observed during the TAMEX period. *J. Meteorol. Soc. Jpn.*, **75**, 1003 – 1018

Chen, C., W. K. Tao, P. L. Lin, G. S. Lai, S. F. Tseng and T. C. Chen Wang, 1998: The Intensification of the Low-Level Jet during the Development of Mesoscale Convective Systems on a Mei-Yu Front. *Mon. Wea. Rev.*, **126**, 349 – 371

———, C. C. Wang, and D. T. W. Lin, 2004: Characteristics of Low-Level Jets over Northern Taiwan in Mei-Yu Season and Their relationship to Heavy Rain Events, *Mon. Wea. Rev.*, **133**, 20 – 43

Chen, Q., 1982: The Instability of the Gravity-inertia Wave and its Relation to Low-level Jet and Heavy Rainfall. *J. Meteorol. Soc. Jpn.*, **60**, 1041 – 1057

Ding, Y.H., Z.Y. Wang, 2008: A Study of rainy seasons in China. *Meteorol. Atmos. Phys.*, **100**, 121 – 138

Emanuel, K.A., 1994: Atmospheric Convection. *Oxford University Press*. p.266 – 270

Hamilton. K., Y. O. Takahashi, W. Ohfuchi, 2008: Mesoscale spectrum of Atmospheric Motions Investigated in a Very Fine Resolution Global General Circulation Model. *J. Geophys. Res.*, **113**, D18110

Hawkins Jr, H. F., 1952: The weather and Circulation of August 1952. *Mon. Wea. Rev.*, **80**, 134 – 137

Holopainen, E., 1984: Statistical Local Effect of Synoptic-Scale Transient Eddies on the Time-Mean Flow in the Northern Extratropics in Winter. *J. Atmos. Sci.*, **41**, 2505 – 2515

Houze, R. A., Jr., S. A. Rutledge, M. I. Biggerstaff, and B. F. Smull, 1989: Interpretation of Doppler Weather Radar Displays in Midlatitude Mesoscale Convective Systems. *Bull. Amer. Meteor. Soc.*, **70**, 608 – 619

Grotjahn, R., 1993: Global Atmospheric Circulation. Observations and Theories. *Oxford University Press*, p. 103 – 111

Klein, W. H., 1952: The weather and Circulation of July 1952. A Month with Drought. *Mon. Wea. Rev.*, **80**, 118 – 122

Kuang, X., Y. Zhang, and J. Liu, 2007: Seasonal Variation of the East Asian Subtropical Westerly Jet and the Thermal Mechanism. *Acta Meteorol. Sin.*, **21**, 192 – 203

Kuo, Y.H., and R. A. Anthes, 1984: mesoscale Budgets of Heat and Moisture in a convective system over the Central United States. *Mon. We. Rev.*, **112**, 1482 – 1497

Lenry, C. A., and R. A. Houze Jr, 1980: The Contribution of Mesoscale Motions to the Mass and Heat Fluxes of an Intense Tropical Convective System. *J. Atmos. Sci.*, **37**, 784 – 796

Machado, L. A. T., W. B. Rossow, R. L. Guedes, and A. W. Walker, 1998: Life Cycle Variations of Mesoscale Convective Systems over the Americas. *Mon. We. Rev.*, **126**, 1630 – 1654

Maddox, R.A., 1980: Mesoscale Convective Complexes. *Bull. Amer. Meteor. Soc.*, **61**, 1374 – 1387

Matsumoto S., K. Ninomiya and S. Yoshizumi, 1971: Characteristic Features of “Baiu” Front Associated with Heavy Rainfall. *J. Meteorol. Soc. Jpn.*, **49**, 267 – 281

Matsmoto, S., 1972: Unbalanced Low-Level jet and Solenoidal Circulation Associated with heavy Rainfalls. *J. Meteorol. Soc. Jpn.*, **50**, 194 – 203

———, K. Ninmiya, S. Yoshizumi, 1971: Characteristic Features of “Baiu” Front Associated with Heavy Rainfall. *J. Meteorol. Soc. Jpn.*, **49**, 267 – 281

Orlanski, I. 1975: A rational subdivision of scales for atmospheric processes. *Bull. Am. Met. Soc.*, **56**, 527 – 530

Redelsperger, J. –L., D. B. Parsons, F. Guichard, 2002: Recovery Processes and Factors Limiting Cloud-Top Height following the Arrival of a Dry Intrusion Observed during TOGA COARE. *J. Atmos. Sci.*, **59**, 2438 – 2457

Sortais, J. L., 1993: A Case Study of Coupling between Low- and Upper-level Jet-Front Systems: Investigation of Dynamical and Diabatic Processes. *Mon. Wea. Rev.*, **121**, 2239 – 2253

Stensrud, D. J., 1996: Importance of Low-Level Jets to Climate: A Review. *J. Climate*, **9**, 1698 – 1711

Tiedtke, M., 1989: A comprehensive mass flux scheme for cumulus parameterization in large-scale models. *Mon. Wea. Rev.*, **117**, 1779 – 1800

Ucellini, L. W., and D. R. Johnson, 1979: The coupling of Upper and Lower Tropospheric Jet Streaks and Implications for the Development of Severe Convective Storms. *Mon. Wea. Rev.*, **107**, 682 – 703

van der Hoven, I. (1957): Power Spectrum of Horizontal Wind Speed in the Frequency Range from 0.0007 to 900 cycles per hour. *J. Met.*, **14**, 56 – 72

Wu, L., Y. Shao, and Andrew Y.S. Cheng, 2011: A diagnostic Study of Two Heavy Rainfall Events in South China. *Meteorol. Atmos. Phys.*, **111**, 13 – 25

Wu, Y., S. Raman, 1998: The Summertime Great Plains Low Level Jet and the Effect of its Origin on Moisture Transport. *Bound-Lay. Meteorol.*, **88**, 445 – 466

Zipser, E. J., 1969: The Role of Organized Unsaturated Convective Downdrafts in the Structure and Rapid Decay of an Equatorial Disturbance. *J. Appl. Meteorol.*, **8**, 799 – 814

———, 1977: Mesoscale and Convective-scale Downdrafts as Distinct Components of Squall-Line Structure. *Mon. Wea. Rev.*, **105**, 1568 – 1589



## 13 Acknowledgements

I would like to express my gratitude to my supervisor Prof. Dr. Yaping Shao, who has inspired, motivated and guided me on this challenging research topic. My horizons have been broadened under his guidance and encouragement. I am grateful to him for saving me such a frog which was trapped in a deep well 4 years ago.

This work was granted by Deutscher Akademischer Austausch Dienst (DAAD). I would like to thank Dr. Sylvia Brandt in DAAD Information Centre Hong Kong, and my DAAD consultants in Germany, Miss Anna Brzezinka, Miss Katharina Knoth (former), and Mr. David Hildebrand (former), for their helps and supports. I thank Prof. Dr. Michael Kerschgens and Prof. Dr. Roel Neggers for being my second referees in the extensions of my DAAD scholarship.

I would like to thank Dr. Xinxin Xie, Dr. Shaofeng Liu for their proof-readings, Dr. Sabine Lennartz-Sassinek and Martina Klose for their help of the Zusammenfassung. I also wish to thank other group members, Dr. Jie Zhang, Micheal Hintz, Zhuoqun Li, Dr. Patrick Ludwig, Stefanie Neske, Qian Xia, Zahra Parsakhoo, Katja Künemund and Dr. Claudia Frick, for the discussion of my work in group meetings. I thank them all for the joys they have brought to me during the time I have spent in Germany.

Very special thanks go to my best friend Benny Wing Hin Ng for his technical supports and instructions on Fortran programming, I also thank Escky Ying Ying Chan, Ivan Kai Ming Leung and Winnie She Mei Wong. Without their supports and encouragements this work would not be accomplished. Last but not least, I appreciate the understanding and support of my beloved family throughout these years and I dedicate this work to my eldest uncle.

Especially, I wish to express my gratitude and respect to Mr. Kin Yee Yam. He was my physics teacher in Wong Shiu Chi Secondary school. He led me to the world of Physics and he is still giving me lessons even I left the high school. This PhD thesis doesn't exist without him.



## **14 Erklärung**

Ich versichere, dass ich die von mir vorgelegte Dissertation selbständig angefertigt, die benutzten Quellen und Hilfsmittel vollständig angegeben und die Stellen der Arbeit – einschließlich Tabellen, Karten und Abbildungen –, die anderen Werken im Wortlaut oder dem Sinn nach entnommen sind, in jedem Einzelfall als Entlehnung kenntlich gemacht habe; dass diese Dissertation noch keiner anderen Fakultät oder Universität zur Prüfung vorgelegen hat; dass sie - abgesehen von unten angegebenen Teilpublikationen - noch nicht veröffentlicht worden ist sowie, dass ich eine solche Veröffentlichung vor Abschluss des Promotionsverfahrens nicht vornehmen werde. Die Bestimmungen dieser Promotionsordnung sind mir bekannt. Die von mir vorgelegte Dissertation ist von Prof. Dr. Y. Shao betreut worden.

Köln, den 18.08.2014

Chi Yan Tsui



# 15 Lebenslauf

## Angabe zur Person

---

Name, Vorname:	Chi Yan Tsui
Anschrift:	Kratzweg 126 D-51109, Köln
Geburtsdatum, -ort:	23.09.1981, Hong Kong
Staatsangehörigkeit:	Chinese

## Ausbildung

---

1988 - 1994	C.C.C. Kei Tsun Primary School, Hong Kong
1994 - 1999	Wong Shiu Chi Secondary School, Hong Kong
1999 - 2001	Tai Po Sam Yuk Secondary School, Hong Kong
2002 - 2005	Bachelorsstudium der Applied Physics City University of Hong Kong, Hong Kong
2005 - 2008	Mastersstudium der Applied Physics City University of Hong Kong Hong Kong
2010.04 – 2010.09	Deutsche Sprache Lernen Carl Duisberg Centren Köln, Deutschland
2010 - 2014	Promotionsstudium Meteorologie Universität zu Köln Köln, Deutschland

## Berufliche Tätigkeiten

---

2005 – 2008	Wissenschaftlicher Mitarbeiter City University of Hong Kong, Hong Kong
2008 – 2010	Lehrassistent City University of Hong Kong, Hong Kong
2010 – 2014	Stipendium des “Deutscher Akademischer Austausch Dienst” (DAAD) am Institut für Geophysik und Meteorologie der Universität zu Köln, Deutschland
2012 - 2014	Wissenschaftliche Hilfskraft Universität Bonn, Deutschland
Seit 2014	Wissenschaftliche Hilfskraft Universität zu Köln, Deutschland

Köln, den 25.01.2015

Unterschrift: